skb.se

SKB P-23-21

ISSN 1651-4416
ID 2034552
June 2024

Exploring bentonite sedimentation dynamics 2019–2021

Macarena Leal Olloqui, Patrik Sellin, Hanna Kronberg, Terese Bladström
Svensk Kärnbränslehantering AB

Abstract

Bentonite, renowned for its high montmorillonite clay content, is a crucial geomaterial designated for the primary buffer and backfill in spent nuclear fuel (SNF) disposal. Its unique properties, including water absorption capacity and shear strength, make it ideal for ensuring safety in the KBS-3 design, where waste containers are to be stored in drilled boreholes within granite host rock, surrounded by compacted bentonite blocks. However, the presence of fractures in the surrounding environment could potentially lead to unfettered bentonite swelling, causing dispersion and transport via groundwater. SKB initiated a pilot programme to investigate the flocculation phenomenon across various clay materials, essential for understanding sedimentation rates and clay behaviour in the context of the KBS-3 system. Using artificial fractures to simulate real-world conditions, SKB's experimental work aims to assess sedimentation rates and clay behavioural differences, crucial for future assessments of bentonite erosion and safety in nuclear waste disposal.

This study presents preliminary findings from calculated data and post-mortem analyses conducted on various clay materials. The research focuses on aspects such as initial water content, mass loss rate, surface area, area-specific mass loss rate, expansion volume, dry density of the halo, x-ray fluorescence (XRF) analysis, and electrical conductivity (EC). The study reveals that the initial water content estimation per dialysed material may introduce potential errors due to variability within samples. Mass loss rate calculations indicate significant sedimentation occurs rapidly in the initial weeks of experimentation, followed by a slowdown or cessation. Surface area calculations face challenges due to non-uniform expansion, impacting total surface estimation. Area-specific mass loss rates vary among clay types, with Ca-dominated bentonites exhibiting higher rates compared to Na-dominated bentonites and synthetic saponites. The volume of expansion varies significantly among different clay materials, with Na-dominated bentonites showing the most substantial expansion. The dry density of the halo also varies across clay types, influenced by class mass and mineral phases. XRF analysis reveals elemental composition changes, particularly in Na-dominated bentonites and synthetic saponites. Electrical conductivity measurements reflect variations influenced by factors such as moisture retention, dissolved salts present, and temperature changes. While Na concentration generally correlates with increased EC, exceptions occur, suggesting complex interactions between ions and the interlayer space.

Moreover, based on the results presented in this report, the clays exhibit the following relative order of average sedimentation mass loss rate (wt%), listed from highest to lowest:
Westerwald (4.605 wt% ± 3.380) – MX80 (4.223 wt% ± 0.000) – Sumecton (3.721 wt% ± 0.172) – Sardinian (3.118 wt% ± 2.118) – Moroccan (2.929 wt% ± 1.720) – Asha 505 (2.042 wt% ± 1.366) – Bara-kade (1.687 wt% ± 0.349) – CaBen FLB (1.656 wt% ± 0.000) – Turkish (1.458 wt% ± 0.796) – Kiruna (0.083 wt% ± 0.000).

Owing to the ongoing development of the methodology, these figures should be interpreted with caution as they are indicative at this stage.

Sammanfattning

Bentonit, känd för sitt höga innehåll av montmorillonitlera, är ett viktigt geomaterial som används som buffert och återfyllning vid deponering av använt kärnbränsle (SNF). Dess unika egenskaper, inklusive vattenabsorptionskapacitet och skjuvhållfasthet, gör det idealiskt för att säkerställa säkerheten i ett KBS-3-förvar, där avfallsbehållare ska förvaras i borrade hål i granitberggrund, omgivna av kompakterade bentonitblock. Närvaron av sprickor i den omgivande miljön kan dock potentiellt leda till obehindrad svällning av bentonit, vilket kan orsaka spridning och transport via grundvattnet. SKB inledde ett pilotprogram för att undersöka flockulationsfenomenet för olika lermaterial, vilket är nödvändigt för att förstå sedimentationshastigheter och lerors beteende i KBS-3-systemet. Genom att använda artificiella sprickor för att simulera verkliga förhållanden syftar SKB:s experimentella arbete till att bedöma sedimentationshastigheter och lerors beteendeskillnader, vilket är avgörande för framtida bedömningar av bentoniterosion och säkerhet för slutförvar.

Denna studie presenterar preliminära resultat från beräknade data och efteranalyser utförda på olika lermaterial. Forskningen har fokuserat på aspekter som initial vattenhalt, massförlusthastighet, yta, ytspecifik massförlusthastighet, expansionsvolym, torrdensitet av den utsvällda halon, elementsammansättning med röntgenfluorescensanalys (XRF) och elektrisk konduktivitet (EC). Studien visar att uppskattningen av initial vattenhalt per dialyserat material kan introducera potentiella fel på grund av variationer inom proverna. Beräkningar av massförlusthastighet indikerar att betydande sedimentation sker snabbt under de första veckorna av experimentet, följt av en avmattning eller upphörande. Beräkningar av yta är utmanande på grund av oregelbunden expansion, vilket påverkar den totala ytan. Ytspecifika massförlusthastigheter varierar mellan lertyper, där ursprungliga Ca-dominerade bentoniter uppvisar högre hastigheter jämfört med Na-dominerade bentoniter och syntetiska saponiter. Expansionsvolymen varierar avsevärt mellan olika lermaterial, där Na-dominerade bentoniter visar den mest betydande expansionen. Torrdensiteten av den utsvällda halon varierar också mellan lertyper, påverkad av lermassan och mineralfaser. XRF-analys har avslöjat förändringar i elementsämnessammansättning, särskilt i Na-dominerade bentoniter och syntetiska saponiter. Mätningar av elektrisk konduktivitet återspeglar variationer påverkade av faktorer som fuktighetsretention, upplösta salter och temperaturförändringar. Även om Na-koncentration generellt korrelerar med ökad EC, förekommer undantag som tyder på komplexa interaktioner mellan joner och mellanlagerutrymme.

Dessutom, baserat på resultaten som presenteras i denna rapport, uppvisar lerorna följande relativa ordning av genomsnittlig sedimentationsmassaförlust (wt%), listade från högst till lägst: Westerwald (4,605 wt% ± 3,380) – MX80 (4,223 wt% ± 0,000) – Sumecton (3,721 wt% ± 0,172) – Sardinian (3,118 wt% ± 2,118) – Moroccan (2,929 wt% ± 1,720) – Asha 505 (2,042 wt% ± 1,366) – Bara-kade (1,687 wt% ± 0,349) – CaBen FLB (1,656 wt% ± 0,000) – Turkish (1,458 wt% ± 0,796) – Kiruna (0,083 wt% ± 0,000).

På grund av den pågående utvecklingen av metodologin bör dessa siffror tolkas med försiktighet då de är indikativa i detta skede.

Contents

1 Background

In a spent nuclear fuel repository, groundwaters are responsible for bentonite swelling. Nevertheless, if such swelling is limited by the walls of the deposition holes, resulting in the development of swelling pressure in the bentonite buffer. If fractures intersect with the deposition holes or disposal vaults, the swelling is not rigidly constrained at the intersection surfaces. Consequently, the swelling continues across the fractures until it reaches an equilibrium or steady-state condition. The free swelling of bentonite may cause the montmorillonite layers to separate, leading to the transport of some of the buffer with the groundwaters. The maximum free swelling of bentonite strongly depends on the ions' charge and concentration in the interlayer space. Therefore, suppose the concentration of solutes in groundwater is too low. In that case, the distance between the individual layers of montmorillonite clay may increase significantly, causing the clay-water system to exhibit sol-like behaviour, in which individual or small groups of montmorillonite layers act as colloidal particles.

The potential formation of colloids in a repository is influenced by the local salt concentration in the pore water and the ratio of mono- to di-valent ions in montmorillonite exposed to groundwater. The controlling processes are ion exchange of the original montmorillonite counterions with ions stemming from the extra minerals and surrounding groundwater.

In the SR-Site post-closure safety assessment (SKB 2022), colloid release and erosion could not be disregarded. The significant calculated mass loss in some deposition holes led to the conclusion that advective conditions could not be ruled out. A more exhaustive analysis revealed a previously unknown phenomenon that significantly contributed to the increase in erosion rate. Once released from the clay, the eroded particles promptly form flocs, which are rapidly transported with the flow. Furthermore, flocculation also causes flocs to sediment in sloping fractures, resulting in even more severe erosion than that caused by the inflowing water. In fractures with an aperture larger than 0.10 mm, the rate at which flocs are released from the clay appears to determine the degree of erosion loss.

The major remaining issue concerning colloid formation and erosion is the significance of flocculation. Once clay colloids are exposed to a force, such as a flow in a fracture or gravitation in a vertical or sloping fracture, they can form a new phase or a 'secondary gel'. In the event of a flow in a horizontal fracture, releasing particles from the clay rim into the flowing water is the limiting factor, with flocculation being of secondary importance. However, for sloping fractures, the formation of a 'secondary gel' is the critical parameter that controls the mass loss. At present, there is yet to be a conceptual model that can fully explain this process.

1.1 Objectives

An experimental programme was initiated at SKB's research laboratory in Äspö HRL to verify the findings presented by Alonso et al. (2019) and collect additional data. The primary focus of these experiments was to investigate the flocculation behaviour of various clay types in artificial vertical fractures under no-flow conditions. The primary reasons behind these tests are to: (*i*) determine the empirical sedimentation rates to be used in future assessments of bentonite erosion; and (*ii*) screen differences in behaviour between the different clay materials examined.

2 Experimental set-up

2.1 Clay materials investigated

One of the fundamental aims of the sedimentation tests is to identify behavioural differences among clay types; thus, Na- and Ca-dominated bentonites and a synthetic saponite were considered. The clay materials investigated are gathered in Table 2-1.

Table 2-1: Clay materials examined.

Name	Clay type	SKB ID	Description
Asha 505	Bentonite	c65e89	Asha 505, or Indian bentonite, is a Na-dominated bentonite produced and supplied by Ashapura Minechem Co (Svensson et al. 2011).
Bara-kade	Bentonite	c65e3b	Bara-kade bentonite is a Wyoming Na-dominated bentonite produced and supplied by Bentonite Performance Minerals LLC (Bentonite Performance Minerals LLC 1928).
MX80	Bentonite	c65e9e	MX80 bentonite is a Wyoming Na-dominated type of bentonite produced by American Colloid Co (Svensson et al. 2011).
Moroccan	Bentonite	c65e24	Moroccan bentonite is a Ca, K, Na-bentonite characterised by a low Fe content (Svensson et al. 2019).
Turkish	Bentonite	c65e26	Turkish bentonite is a Ca-dominated bentonite mined in Tokat/Reşadiye Güvendik and supplied by Karben Group Inc. (Svensson et al. 2019).
Sardinian	Bentonite	c65e6f	Sardinian bentonite is a Ca-Mg-dominated bentonite supplied by Laviosa MPC (Svensson et al. 2019).
CaBen FLB	Bentonite	c65e20	CaBen FLB is a Ca-Mg-dominated bentonite from Bulgari (Lundgren and Johanesssson 2020).
Kiruna	Bentonite	c65ef8	Kiruna bentonite is a Ca-dominated bentonite mined in Kiruna, Sweden (IGD-TP 2019).
Westerwald	Bentonite	c65fe3	Westerwald bentonite is a Ca-dominated bentonite produced and supplied by Marx Bergbau GmbH & Co (Fontaine et al. 2020).
Sumecton	Synthetic saponite	c65e85	Sumecton is a synthetic saponite, chemically synthesised by hydrothermal treatment, produced by Kunimine Industries (KI 1943).

2.2 Clay materials specimens' preparation

2.2.1 Dialysis and removal of excess soluble salts

Specimens for this study were prepared using granular clays consisting of poorly sorted grains ranging from micrometres to millimetres in size. To provide better control over the testing conditions, the coarse clays were subjected to a two-step purification process or dialysis: (*i*) to promote ion exchange reactions in favour of a greater Na^+ concentration at the exchange complex; and (*ii*) to remove excess soluble salts.

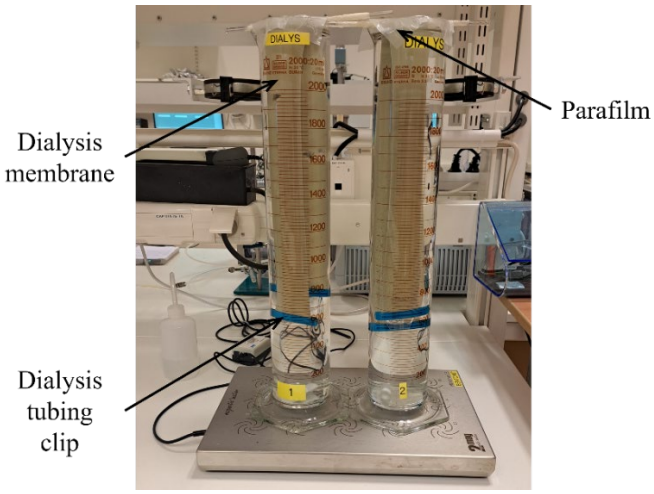

Figure 2-1: *Graduated cylinders containing the membranes with the clay material.*

The clay materials were dialysed using 1M NaCl solution to alter the cations at the exchange complex. To this effect, 300 g of clay material was equally divided into two glass graduated beakers and mixed with 500 ml of 1M NaCl solution each. Thereupon, the resulting slurries were poured within two separated dialysis tubing cellulose membranes (spectra standard RC tubing MWCO: 3.5 kD) of approximately 780 mm length, previously soaked in Milli-Q water for 30 minutes and clamped at one end with a dialysis tubing clip designed to withstand the swelling of the clay materials. Once the slurries were poured within the membranes utilising a plastic funnel, the open ends were sealed by an extra dialysis tubing clip. The dialysis membranes containing the clay materials were placed into two 2,000 ml glass graduated cylinders (Figure 2-1), which in turn were filled with a dialysate solution (1M NaCl) and continuously stirred with a magnetic stirrer.

Furthermore, the glass cylinders were tightly sealed with parafilm to prevent evaporation (Figure 2-1). The exposure to the dialysate solution was carried out over 48 hours for the Na-dominated bentonites and synthetic saponite, whilst the Ca-dominated bentonites were conducted for 96 hours. The dialysate solution was replaced every 24 hours for all clay materials to expedite the exchange process.

Immediately after sodium homoionisation, the clay materials underwent reverse dialysis using Milli-Q water as a dialyser to remove excess soluble salts. Excess dissolved salts diffuse from the clay material throughout reverse dialysis into the Milli-Q water, increasing its EC. To uphold a high concentration gradient, the dialyser was replaced daily, and changes in EC were recorded. Once changes in EC reached values less than 10.00 µS/cm, the reverse dialysis was considered to be completed. The dialysis time required for the different clay materials varied from a few weeks up to three months. Upon reverse dialysis termination, the slurried clay materials were removed from the dialysis membranes and placed in plastic containers to be oven-dried at 40 ºC for five consecutive days.

Notably, the dialysis process followed for Kiruna bentonite was different from the previously described. Kiruna is characterised as being ~100 % Ca-dominated bentonite. Therefore, a 3M NaCl solution was used to promote exchange into a sodium form. The homoionisation process started by mixing 150 g of Kiruna with 500 ml of 3M NaCl solution, leaving the slurry to settle in the beaker for 24 hours, and then, the supernatant was removed. The remaining slurry was placed in a dialysis tubing cellulose membrane, clamped at both ends, and the membrane containing the Kiruna slurry was again exposed to a 3M NaCl solution for 72 hours. Hereon, the reverse dialysis process is identical to that already described.

2.2.2 Samples crushing and compaction

After drying, the dialysed clay materials tend to agglomerate into several centimetre-sized 'chunks'. To manufacture suitable samples for this experimental program, the 'chunky' clay materials must be crushed into small pieces of a few millimetres in size, ranging from 0.20 to 0.50 mm. Thus, an agate mortar was utilised to crush the samples into an adequate size.

Once samples were crushed, the following was to determine the **initial water content**. Thus, a few milligrams per clay material were separated and oven-dried at 105 ºC for 24 hours, and the initial water content was determined following Equation (2-1).

$$\omega\ (\%) = ((W_2 - W_3) / (W_3 - W_1)) \cdot 100 \qquad \text{Equation (2-1)}$$

ω = initial water content (%)
W_1 = weight of the container (g)
W_2 = weight of the clay material at room temperature (g)
W_3 = weight of the container with the dried clay material (g)

Information about the initial water content per each clay material is compiled in Table 2-2.

Table 2-2: Initial water content per each clay material.

Clay materials	ω (%)
Asha 505	3.90
Bara-kade	3.10
Moroccan	7.90
MX80	6.00
Turkish	5.20
Sardinian	10.30
Kiruna	8.00
Westerwald	9.10
Sumecton	6.50

To initially calculate the **amount of dry clay material** to be used, the inner volume of the compaction mould (~7.649 cm^3) and a target dry density of 1.45 g/cm^3 were considered (Equation (2-2)).

$$m = \rho \cdot v \qquad \text{Equation (2-2)}$$

m = mass (g)
ρ = dry density (1.45 g/cm^3)
v = inner volume of the compaction mould (~7.649 cm^3)

However, to calculate the **mass of clay material** to be used per experiment, it is crucial to contemplate that the clay materials were at their hygroscopic water content when weighed (Table 2-2), following Equation (2-3).

$$m_{dry,\ I} = m / (1 - \omega) \qquad \text{Equation (2-3)}$$

$m_{dry,\ I}$ = mass of clay material (g)
m = mass (g)
ω = initial water content (%)

To strengthen the control over the conditions of sample preparation, a target water content of 20 % was considered for all clay samples. Thus, the **clay material's mass at 20 % water content** was calculated taking into account Equation (2-4).

$$m_{20\%} = m / (1 - \omega_d) \qquad \text{Equation (2-4)}$$

$m_{20\%}$ = mass of clay material at 20 % water content (g)
m = dry mass (g)
ω_d = desired water content (20 %)

Finally, to calculate the **mass of Milli-Q water** needed to achieve a 20 % water content, the mass of the clay materials ($m_{dry, I}$) was subtracted from the calculated mass of clay material at 20 % water content ($m_{20\%}$), ensuing Equation (2-5).

$$m_{Milli\text{-}Q} = m_{20\%} - m_{dry, I} \qquad \text{Equation (2-5)}$$

$m_{Milli\text{-}Q}$ = mass of Milli-Q water (g)
$m_{20\%}$ = mass of clay material at 20% water content (g)
$m_{dry, I}$ = mass of clay material (g)

Once known the mass of Milli-Q water to achieve 20 % of water content per sample, the respective amount of Milli-Q water was added to the already weighed mass of clay material. Samples within plastic containers were covered with parafilm and left to stabilise for 24 hours.

After sample stabilisation, the next step was to compact them into a ring-shaped form to be fitted within the artificial fractures. This involved the stabilised samples being subjected to a compaction process to manufacture a ring-shaped sample with the dimensions of the inner volume of the compaction mould. The compaction mould (manufactured in AISI 4340 steel) encompasses (Figure 2-2 (b)): (*i*) an auxiliary base; (*ii*) an external body; (*iii*) an internal body; and (*iv*) a cylindrical press. The external body consists of a cylinder of 70.00 mm in diameter and 50.00 mm in length, with an internal bore of 35.20 mm in diameter and an inner total length of 50.00 mm (Figure 2-2 (a)). Besides, the compaction mould incorporates an auxiliary cylindrical base piece with an inner diameter of 35.20 mm and a 20.00 mm length (Figure 2-2). The auxiliary base piece was necessary to increase the inner volume of the external body to subtract the compacted samples from the compaction mould. Moreover, the compaction mould is also equipped with an internal body composed of a cylindrical base of 35.10 mm and 50.00 mm long, welded to a rod of 15.10 mm in diameter and 44.00 mm in length (Figure 2-2).

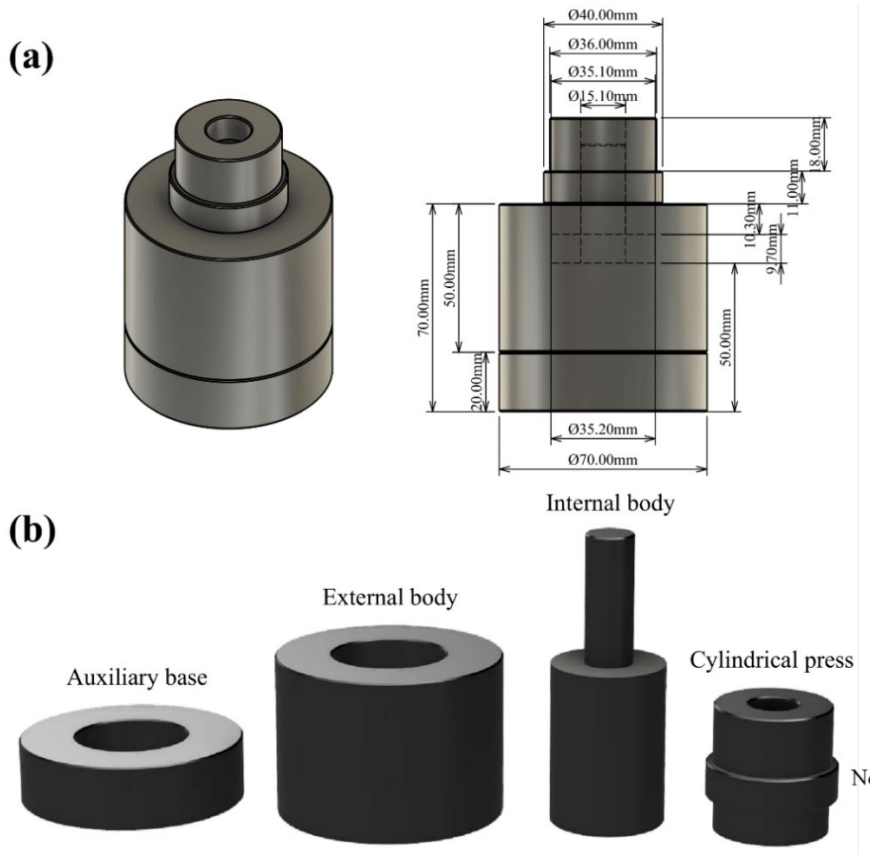

Figure 2-2: *(a) Dimensions of the compaction mould. (b) Different components of the compaction mould.*

Once the auxiliary base and the external body are stacked, the internal body is fitted into the inner bore, leaving the final space where the samples are compacted. Lastly, the cylindrical press, endowed with a notch, is inserted into the rod of the internal body and pressure was applied using a hydraulic press (ENERPAC XLP 25 ton press) until the notch of the cylindrical press touches the upper surface of the external body, obtaining a compacted sample with the dimensions shown in Figure 2-3.

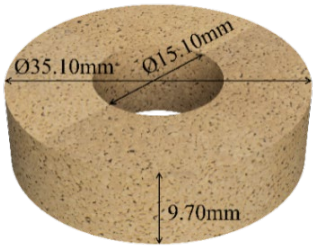

Figure 2-3: *Pre-compacted sample.*

2.3 Experimental configuration

2.3.1 Sample fitting within artificial fractures

A series of artificial fractures or cells (Figure 2-4 (a)) were manufactured to investigate the flocculation phenomenon in different clay-type materials (Table 2-1). The design of the artificial fractures is a modified version of the device developed by Hedström et al. (2016). Each artificial fracture comprises an upper and a lower transparent extruded acrylic plate (Figure 2-4 (b)). The dimensions of each plate are as follows: length - 250.00 mm, breadth - 250.00 mm, and thickness - 20.00 mm.

The lower acrylic plate is fitted with four lateral perforations (Figure 2-4 (b)). Three of these perforations are located on the right-hand side and unite to form an internal vertical channel (internal channel (outlet); Figure 2-4 (b)). The remaining perforation is positioned on the left-hand side (Figure 2-4 (b)) and is connected to a secondary internal channel (internal channel (inlet); Figure 2-4 (b)). The purpose of these perforations is to mimic the natural percolation of groundwater through vertical fractures in an underground repository. Besides, at the centre of the internal surface of the lower acrylic plate, there is a ring-shaped perforation (Figure 2-4 (b)) designed to accommodate the pre-compacted clay samples. This central perforation features dimensions of 5.10 mm depth, with an inner and outer diameter of 15.00 mm and 35.20 mm, respectively.

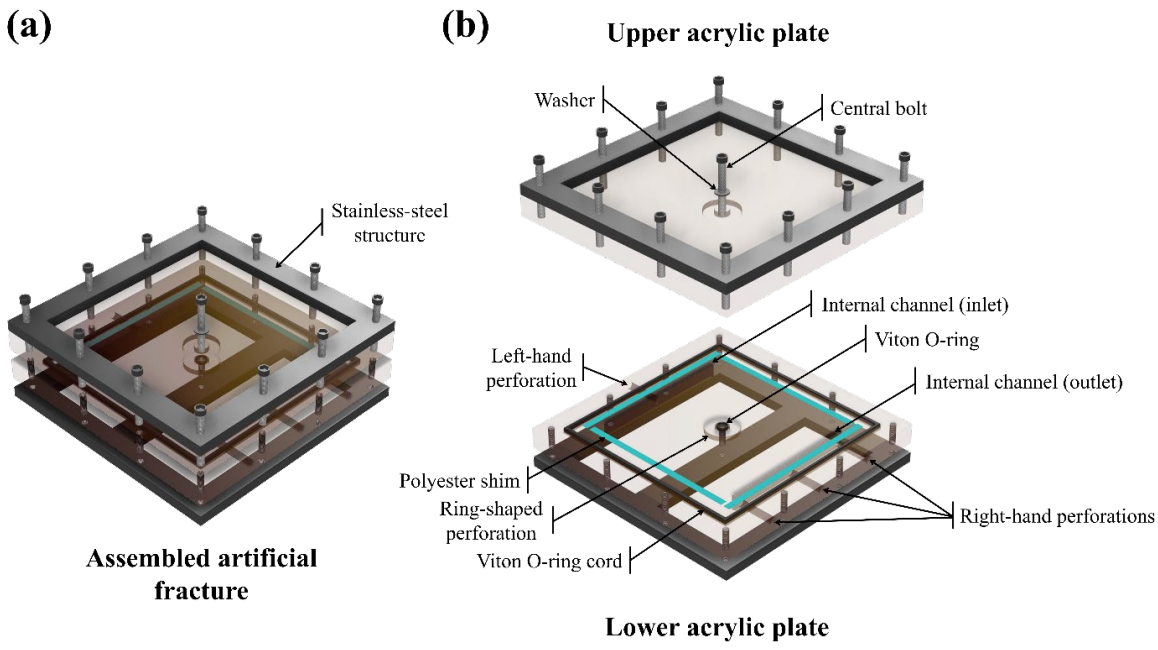

Figure 2-4: *(a) Assembled artificial fracture. (b) Upper and lower acrylic plates.*

The upper acrylic plate consists of a flat external surface, internally housing an identical ring-shaped perforation to the lower plate. In addition, the lower and upper plates are also fitted with 12 threaded holes along their perimeter.

After placing a pre-compacted sample (Figure 2-4) in the lower plate ring-shaped perforation, the upper plate can be attached and secured with a central bolt. Once both plates are joined together, the impermeability at the centre of the assembly is attained using a Viton O-ring. The artificial fractures or cells externally consist of a stainless-steel structure with threaded holes that support the joined upper and lower plates. The assembly is then tightened using 12 bolts at the threaded holes surrounding the perimeter of the stainless-steel structure (Figure 2-4 (a)). The artificial fracture's water-tightness is attained by using a Viton O-ring cord placed along the internal surface of the lower plate. Finally, the fracture aperture is accomplished by surrounding the hydration channels with four polyester blue shims of 0.10 mm thickness, placed along the lower plate's inner surface (Figure 2-4 (b)).

2.3.2 Artificial fracture hydration

Subsequent to mounting an artificial fracture, it was vertically placed on a flat surface. The artificial fracture was then saturated with 1mM NaCl solution. To fill up an artificial fracture with the saturating or water solution, the perforation located at the left-hand side was utilised as an inlet (Figure 2-5 (a)). Besides, the top perforation located at the right-hand side of an artificial fracture was used as an outlet, and remained open until the water solution began to flow out of the artificial fracture through said perforation. Sequentially, the top perforation was closed using a tube plug (Figure 2-5 (a)). The remaining two perforations situated on the right-hand side of an artificial fracture remained closed at all times, utilising tube plugs to prevent any loss of water solution during the saturation process.

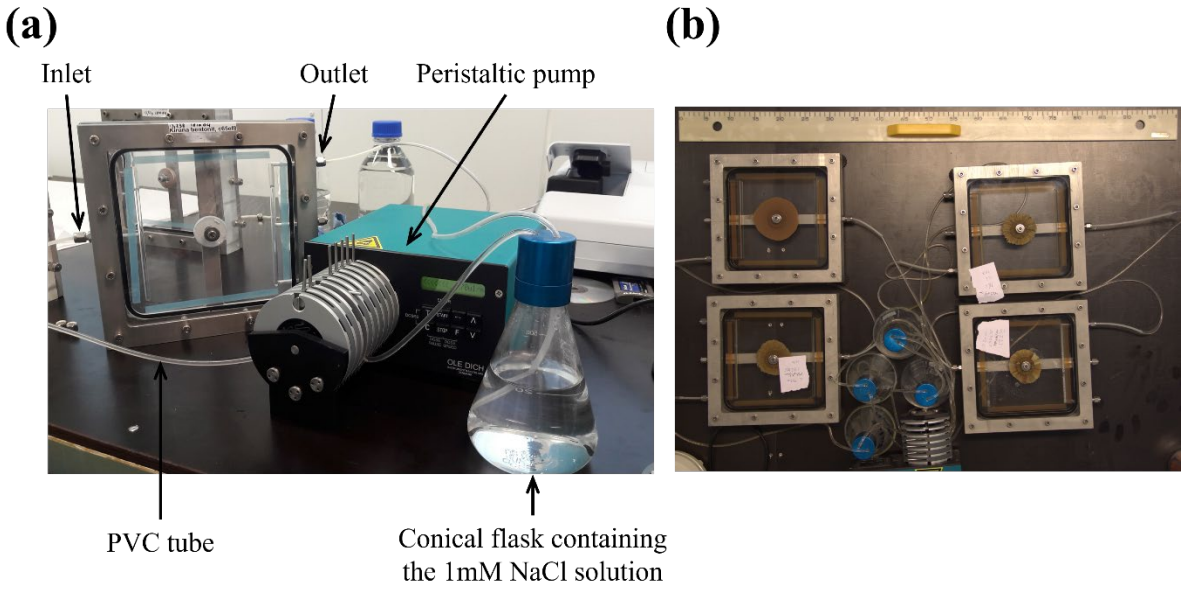

Figure 2-5: *(a) Water solution injection system. (b) Saturation of several artificial fractures (Photo by D. Svensson).*

The water solution injection system was composed of an Ole Dich type 110AC(R)40G300 peristaltic pump (Figure 2-5 (a)), equipped with eight channels, enabling the simultaneous saturation of multiple artificial fractures (Figure 2-5 (b)). A soft PVC tube was connected to the peristaltic pump and then plugged into a conical flask containing the water solution (Figure 2-5 (a)). This connection was made to the inlet and outlet of an artificial fracture. As a result, the water solution was drawn from the conical flask and pumped into an artificial fracture at intervals of 70 µl/min until reaching its complete saturation. A low ionic strength and divalent cation-free water solution based on Alonso et al. (2019) was selected for this experimental programme.

The amount of solution used per experiment was determined by the inner volume of the fracture, which in turn relies on the thickness of the polyester blue shims (0.10 mm) and the amount of force applied at the time of tightening the bolts to secure closure. Overall, the volumes of solutions varied between 65 and 70 ml (Table 2-3). Besides, the different durations of the experiments (days) are also compiled in Table 2-3.

Table 2-3: ***Volumes and experiment durations.***

Clay	Volume (ml)	Experiment duration (days)
Asha 505	65 to 70	32, 34 and 69
Bara-kade	65 to 70	31, 33 (x2) and 63
Moroccan	65 to 70	28, 35 (x2), 41 (x2), 44, 74 and 206
MX80	65 to 70	233
Turkish	65 to 70	28, 33 (x3), 34 (x3), 35 and 74
Sardinian	65 to 70	28, 31 (x2), 32 and 34 (x3)
CaBen	65 to 70	272
Kiruna	65 to 70	259
Westerwald	65 to 70	42, 43 (x2) and 44 (x2)
Sumecton	65 to 70	31, 32 and 44

2.3.3 Artificial fracture dismantling

Once the allotted experimental time had elapsed, the artificial fractures were dismantled. The excavation process consisted of two stages to recover and evaluate: (*i*) the loose clay material (Figure 2-6 (a)); (*ii*) the sedimented clay material (Figure 2-6 (a)); (*iii*) the expanded clay material (Figure 2-6 (a)); and (*iv*) the clay material remaining in the ring-shaped perforation (Figure 2-6 (a)).

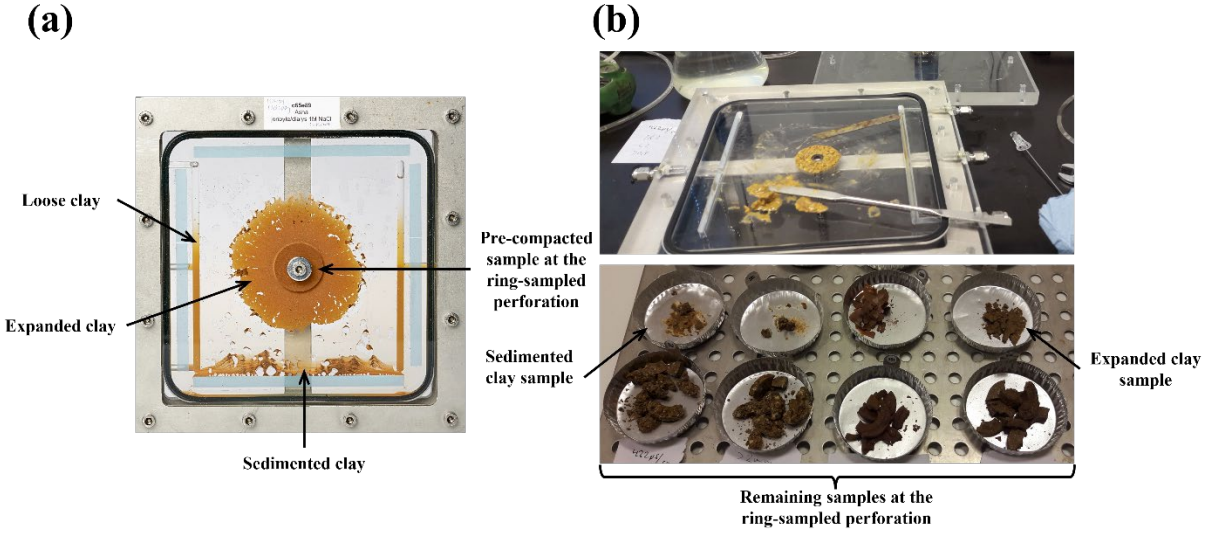

Figure 2-6: *(a) Different samples to be collected. (b)Dismantling process and collected samples (Photo by D. Svensson).*

The first stage was to collect the remaining solution within a vertical fracture. The artificial fracture was then placed horizontally on a flat surface; the bolts were loose, and the fracture opened. The remaining solution at the surface of the fracture and in the two vertical channels is characterised by the presence of clay flocs or loose clay materials. This solution was collected using a pipette and transferred into a known-weight glass container. The sedimented clay material was also collected using a pipette and placed in an aluminium container, previously weighed (Figure 2-6 (b)). Both glass and aluminium containers containing the samples were weighed before and after drying at 105 °C for 24 hours to determine their wet and dry weight.

The second stage consisted of collecting the expanded and remaining clay material at the ring-shaped perforation. To facilitate sample collection, the artificial fractures were oven-dried at 40 °C for 24 hours. Succeeding, a spatula was utilised to scrape out the expanded and remaining clay material at the inner surfaces of an artificial fracture. The collected samples were placed in two known-weight aluminium containers to determine the wet weight (Figure 2-6 (b)). Finally, the collected samples were oven-dried at 105 ºC for 24 hours, and the samples were weighed again to pinpoint their dry weight.

2.4 Experimental campaign overview: 2019-2021

The present section lists the experiments conducted between 2019 and 2021 (Tables 2-4 and 2-5). Although all clay materials examined underwent a homoionisation process aimed at facilitating ion exchange reactions to achieve a higher concentration of Na^+ at the exchange complex, the results presented in section 5, along with the corresponding figures and tables, continue to differentiate between Na- and Ca-dominated bentonites and the synthetic saponite. This distinction is maintained to assess the efficacy of the established homoinisation process across the various clay materials, as well as distinguishing behavioural differences.

Table 2-4: List of sedimentation tests.

Sedimentation test no.	Clay material	Duration (days)	Starting test date	Stopping test date
SediTest-01	Asha 505	69	09/04/2019	17/06/2019
SediTest-03	CaBen FLB	272	25/01/2019	24/10/2019
SediTest-02	Kiruna	259	07/02/2019	24/10/2019
SediTest-04	Moroccan	206	01/04/2019	24/10/2019
SediTest-05	MX80	233	05/03/2019	24/10/2019
SediTest-06	Sardinian	32	07/11/2019	09/12/2019
SediTest-07	Bara-Kade	63	18/11/2019	20/01/2020
SediTest-08	Moroccan	74	07/11/2019	20/01/2020
SediTest-09	Turkish	74	07/11/2019	20/01/2020
SediTest-10	Asha 505	32	20/08/2020	21/09/2020
SediTest-11	Asha 505	34	25/08/2020	28/09/2020
SediTest-12	Bara-Kade	31	27/01/2020	27/02/2020
SediTest-13	Moroccan	44	12/02/2020	27/03/2020
SediTest-14	Moroccan	28	11/05/2020	08/06/2020

Table 2-5: List of sedimentation tests.

Sedimentation test no.	Clay material	Duration (days)	Starting test date	Stopping test date
SediTest-15	Sardinian	31	27/01/2020	27/02/2020
SediTest-16	Sardinian	28	11/05/2020	08/06/2020
SediTest-17	Sardinian	31	21/08/2020	21/09/2020
SediTest-18	Sardinian	31	21/08/2020	21/09/2020
SediTest-19	Sumecton	44	12/02/2020	27/03/2020
SediTest-20	Sumecton	32	07/05/2020	08/06/2020
SediTest-21	Sumecton	31	08/05/2020	08/06/2020
SediTest-22	Turkish	35	04/02/2020	10/03/2020
SediTest-23	Turkish	28	11/05/2020	08/06/2020
SediTest-24	Westerwald	44	06/10/2020	19/11/2020
SediTest-25	Westerwald	44	06/10/2020	19/11/2020
SediTest-26	Westerwald	43	07/10/2020	19/11/2020
SediTest-27	Westerwald	43	07/10/2020	19/11/2020
SediTest-28	Westerwald	42	08/10/2020	19/11/2020
SediTest-29	Bara-Kade	33	24/03/2021	26/04/2021
SediTest-30	Bara-Kade	33	24/03/2021	26/04/2021
SediTest-31	Moroccan	41	19/01/2021	01/03/2021
SediTest-32	Moroccan	41	19/01/2021	01/03/2021
SediTest-33	Moroccan	35	18/05/2021	22/06/2021
SediTest-34	Moroccan	35	18/05/2021	22/06/2021
SediTest-35	Sardinian	34	12/01/2021	15/02/2021
SediTest-36	Sardinian	34	12/01/2021	15/02/2021
SediTest-37	Sardinian	34	12/01/2021	15/02/2021
SediTest-38	Turkish	33	24/03/2021	26/04/2021
SediTest-39	Turkish	33	24/03/2021	26/04/2021
SediTest-40	Turkish	33	24/03/2021	26/04/2021
SediTest-41	Turkish	34	19/05/2021	22/06/2021
SediTest-42	Turkish	34	19/05/2021	22/06/2021
SediTest-43	Turkish	34	19/05/2021	22/06/2021

3 Calculated data

One of the main goals of this experimental programme is to generate empirical data on sedimentation rates from the different clay materials examined. Thus, the following sections briefly depict the calculated data.

3.1 Initial dry density of pre-compacted samples

The **initial dry density of pre-compacted samples** (kg/m^3) at the onset of each experiment was calculated as a quotient between the weight of a pre-compacted sample and the volume of the sample, which corresponds to the inner volume of the compaction mould.

$$\rho_s = m_{dry,\,I} \,/\, V_s \qquad \text{Equation (3-1)}$$

ρ_s = dry density of the pre-compacted sample (g/cm^3)
$m_{dry,\,I}$ = initial dry mass or amount of bentonite to be used (g)
V_s = volume of the sample (cm^3)

3.2 Collected total mass

To estimate the **collected total dry mass** (g) after the termination of an experiment, the collected dry loose clay, dry sedimented material, dry expanded clay and dry clay remaining at the ring-shaped perforation was added up.

$$m_{total} = m_{loose} + m_{sedimented} + m_{expanded} + m_{remaining\ sample} \qquad \text{Equation (3-2)}$$

m_{total} = collected total dry mass (g)
m_{loose} = dry loose clay material (g)
$m_{sedimented}$ = dry sedimented clay material (g)
$m_{expanded}$ = dry expanded clay material (g)
$m_{remaining\ sample}$ = dry clay remaining at the ring-shaped perforation (g)

3.3 Mass of lost clay

The **mass of lost clay** (g) corresponds to the sum of the dry mass of the loose clay material and the dry mass of the sedimented clay material.

$$m_{lost\ clay} = m_{loose} + m_{sedimented} \qquad \text{Equation (3-3)}$$

$m_{lost\ clay}$ = mass of lost clay (g)
m_{loose} = dry loose clay material (g)
$m_{sedimented}$ = dry sedimented clay material (g)

3.4 Initial water content

The **initial water content** (%) was calculated considering the initial mass of the sample and the collected total dry mass. The calculated initial water content may be considered a potential source of error since it was measured only once per dialysed clay material, assuming similarity across all the samples further prepared from the same clay material. Besides, the initial water content can be altered during the sample manufacturing and installation within the artificial fractures.

$$\omega_{calc}\ (\%) = ((m_{dry,\,I} - m_{total}) \,/\, (m_{dry,\,I})) \cdot 100 \qquad \text{Equation (3-4)}$$

ω_{calc} = calculated initial water content (%)
$m_{dry,\,I}$ = mass of clay material (g)
m_{total} = collected total mass (g)

3.5 Mass loss rate and mass loss (wt%)

The **mass loss rate** (g/day) was calculated by dividing the mass of lost clay by the total duration of an experiment.

$$\dot{m} = m_{lost\ clay} / t \qquad \text{Equation (3-5)}$$

$\dot{m}$ = mass loss rate (g/day)
$m_{lost\ clay}$ = mass of lost clay (g)
t = experiment duration (days)

The **mass loss** (wt%) was computed as the quotient of the combined mass of collected dry loose clay and dry sedimented material to the total collected mass, with the quotient then multiplied by 100 to express the result as a percentage.

$$\Delta m\ (wt\%) = ((m_{loose} + m_{sedimented}) / (m_{total})) \cdot 100 \qquad \text{Equation (3-6)}$$

Δm = mass loss (wt%)
m_{total} = collected total dry mass (g)
m_{loose} = dry loose clay material (g)
$m_{sedimented}$ = dry sedimented clay material (g)

3.6 Average expansion of a clay material

The **average expansion of a clay material** (cm) was calculated by dividing the sum of its final expansion in four directions by the number of values in the set (four).

$$\bar{r} = (r_{0^\circ} + r_{90^\circ} + r_{180^\circ} + r_{270^\circ}) / 4 \qquad \text{Equation (3-7)}$$

$\bar{r}$ = average expansion of a clay material
r_0 = radius at 0º (cm)
r_{90} = radius at 90º (cm)
r_{180} = radius at 180º (cm)
r_{270} = radius at 270º (cm)

3.7 Total surface area of the expanded clay material facing the fracture

To calculate the **total surface area of the expanded clay material facing the fracture** (cm^2), it was assumed that it accommodates the shape of a hollow cylinder. Therefore, calculations were made considering: (*i*) the fracture aperture; (*ii*) the inner radius, which is equivalent to the radius of the pre-compacted sample; and (*iii*) the calculated outer radius as the sum of the average expansion of a clay material and the total radius of a pre-compacted sample (Figure 2-3).

$$A_{halo,\ fracture} = 2 \cdot \pi \cdot \delta \cdot (r_1 + r_2) + 2 \cdot \pi \cdot (r_1^2 + r_2^2) \qquad \text{Equation (3-8)}$$

$A_{halo,\ fracture}$ = surface area of the expanded clay material (cm^2)
δ = fracture aperture (0.01 cm)
r_1 = outer radius ($\bar{r}$ + 1.755 cm)
r_2 = inner radius (1.755 cm)

3.8 Area-specific mass loss rate

The **Area-specific mass loss rate** ($cm^2 \cdot g/day$) was calculated as the quotient between the mass loss rate and the surface area of the expanded clay material.

$$J = \dot{m} \cdot \left(1 \,/\, A_{halo,\ fracture}\right) \qquad \text{Equation (3-9)}$$

J = Area-specific mass loss rate ($cm^2 \cdot g/day$)

$\dot{m}$ = mass loss rate (g/day)

$A_{halo,\ fracture}$ = surface area of the expanded clay material facing the fracture (cm^2)

3.9 Volume of the expanded clay material

The **volume of the expanded clay material** (cm^3) or **volume of the halo** was calculated considering: (*i*) the fracture aperture; (*ii*) the inner radius, which is equivalent to the radius of the pre-compacted sample; and (*iii*) the calculated outer radius as the sum of the average expansion of a clay material and the total radius of a pre-compacted sample (Figure 2-3).

$$V_{halo} = \pi \cdot \left(r_1^2 - r_2^2\right) \cdot \delta \qquad \text{Equation (3-10)}$$

V_{halo} = volume of the expanded clay material (cm^3)

r_1 = outer radius ($\bar{r}$ + 1.755 cm)

r_2 = inner radius (1.755 cm)

δ = fracture aperture (0.01 cm)

3.10 Halo's dry density

The **halo's dry density** (g/cm^3) was calculated by factoring in the dry mass and the volume of the expanded clay material.

$$\rho_{halo} = m_{expanded} \,/\, V_{halo} \qquad \text{Equation (3-11)}$$

ρ_{halo} = halo's dry density (g/cm^3)

$m_{expanded}$ = dry expanded clay material (g)

V_{halo} = volume of the expanded clay material (cm^3)

4 Post-mortem analyses

Post-mortem analyses were consistently conducted after each sedimentation test.

4.1 Clay material's electrical conductivity

Smectites are known for their cation exchange capacity and large and chemically active specific surface area (Emmerich 2013). Due to their structure and chemical composition, their electrical conductivity is strongly correlated with their cation exchange capacity (Emmerich 2013). Furthermore, the presence of hydrophilic cations such as Na and Ca, with a high affinity for water, increases smectite saturation and, thus, swelling, facilitating ion movement and increasing their electrical conductivity.

To measure the clay materials' electrical conductivity (EC), 1 g of the remanent sample at the ring-shaped perforation was ground to ensure uniformity. Thereafter, the ground sample was mixed with Milli-Q water in a 1:40 ratio within a beaker. The slurry was stirred continuously for 5-10 mins, and the electrical conductivity measurement was taken within 1 to 5 mins of mixing, ensuring that the settlement of the clay did not affect the results. The electrical conductivity of the slurry was measured using an electrical conductivity meter (HACH HQ40d) fitted with an electrical conductivity probe. The probe was submerged in the slurry, and the electrical conductivity and temperature were read directly from the meter. Once a measurement was done, the probe was thoroughly rinsed with Milli-Q water before using it again.

4.2 X-ray fluorescence spectroscopy (XRF)

Besides the electrical conductivity of the clay materials, their elemental composition was also examined during the sedimentation tests to identify possible chemical changes in the ring-shaped samples. Subsamples from the pre-compacted ring were ground to an approximate size of 53 μm in an agate mortar and compacted into a disc shape.

A Panalytical Epsilon 3-XL spectrometer fitted with a Rh x-ray tube was used to investigate the elemental composition of the different clay materials. During measurements, helium gas was utilised to: (*i*) improve the quality of the collected spectra, especially for light elements, such as magnesium and silicon; and (*ii*) reduce air absorption, measuring, therefore, in as pure of an atmosphere as possible. Measurement set-up was based on the standard provided by the spectrometer manufacturer, known as Omnian (MP 2009).

5 Results

5.1 Calculated data

5.1.1 Initial dry density of pre-compacted samples

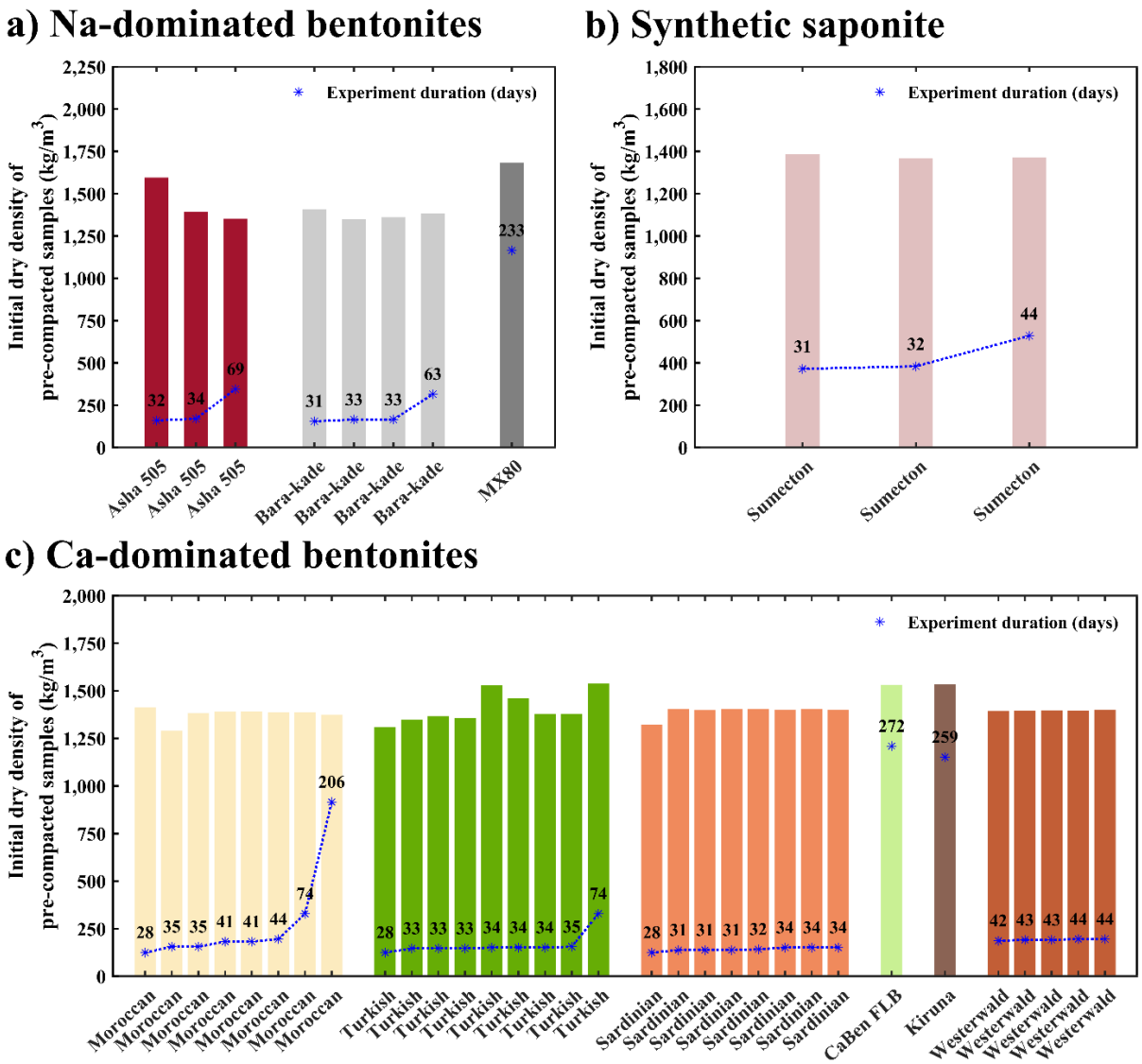

Figure 5-1: *Initial dry density of the pre-compacted samples.*

The initial dry density of the pre-compacted samples was determined as the quotient between the weight of the samples once compacted and the inner volume of the compaction mould (Equation 3-1). Results from the initial dry density are compiled in Figure 5-1 and Tables 5-1 and 5-2.

Overall, by comparing the initial dry density values corresponding to the same clay materials and the values attributed to the different clay materials, variations between and within samples can be observed. The highest values of initial dry density can be assigned to the Asha 505 (32 days) and MX80 (233 days), both of Na-dominated nature. In comparison, the lowest values are those attributed to the Moroccan (35 days) and Turkish (28 days) bentonites, both considered Ca-dominated bentonites. Furthermore, when comparing the initial dry density values from the different Na- (Figure 5-1 (a) and Table 5-1) and Ca dominated bentonites (Table 5-2 and Figure 5 1 (c)), and the synthetic saponite (Figure 5 1 (b) and Table 5-2), it can be noted that the initial dry density values fluctuate between samples from different clay materials.

Table 5-1: Initial dry density of the pre-compacted Na-dominated bentonites and synthetic saponite.

Clay material	Initial dry density of pre-compacted samples (kg/m^3)	Standard deviation (kg/m^3)
Asha 505 (32 days)	1,595	0.106
Asha 505 (34 days)	1,393	0.106
Asha 505 (69 days)	1,352	0.106
Bara-kade (31 days)	1,407	0.027
Bara-kade (33 days)	1,348	0.027
Bara-kade (33 days)	1,361	0.027
Bara-kade (63 days)	1,384	0.027
MX80 (233 days)	1,682	0.000
Sumecton (31 days)	1,386	0.009
Sumecton (32 days)	1,366	0.009
Sumecton (44 days)	1,371	0.009

Clays' initial dry density can fluctuate due to their mineralogical composition and initial water content (Gang 2019). Thus, the initial water content may be one of the determining factors in explaining the substantial variations in values within samples of the same clay material, even though all samples were prepared following the same previously described method (section 2.2). Once the dialysis process was completed, the initial water content was measured only once per dialysed clay material, assuming that said value was the same throughout the dialysate material. Therefore, variations in the initial water content induced by this assumption, as well as during the manufacturing process of the samples, together with their different mineralogical composition, may have prevailed upon changes in the initial dry density values.

Table 5-2: Initial dry density of the pre-compacted Ca-dominated bentonites.

Clay material	Initial dry density of the pre-compacted samples (kg/m^3)	Standard deviation (kg/m^3)
Moroccan (28 days)	1,414	0.026
Moroccan (35 days)	1,290	0.026
Moroccan (35 days)	1,384	0.026
Moroccan (41 days)	1,390	0.026
Moroccan (41 days)	1,392	0.026
Moroccan (44 days)	1,386	0.026
Moroccan (74 days)	1,387	0.026
Moroccan (206 days)	1,374	0.026
Turkish (28 days)	1,308	0.126
Turkish (33 days)	1,349	0.126
Turkish (33 days)	1,367	0.126
Turkish (33 days)	1,356	0.126
Turkish (34 days)	1,528	0.126
Turkish (34 days)	1,460	0.126
Turkish (34 days)	1,377	0.126
Turkish (35 days)	1,377	0.126
Turkish (74 days)	1,539	0.126
Sardinian (28 days)	1,323	0.032
Sardinian (31 days)	1,403	0.032
Sardinian (31 days)	1,398	0.032
Sardinian (31 days)	1,404	0.032
Sardinian (32 days)	1,405	0.032
Sardinian (34 days)	1,402	0.032
Sardinian (34 days)	1,404	0.032
Sardinian (34 days)	1,400	0.032
CaBen FLB (272 days)	1,531	0.000
Kiruna (259 days)	1,533	0.000
Westerwald (42 days)	1,394	0.200
Westerwald (43 days)	1,394	0.200
Westerwald (43 days)	1,397	0.200
Westerwald (44 days)	1,395	0.200
Westerwald (44 days)	1,400	0.200

5.1.2 Mass loss rate and mass loss (wt%)

The mass loss rate was calculated by dividing the sum of the loose and sedimented clay material dry masses by the duration of each experiment (Equation 3-5). The mass of lost rate refers to the amount of bentonite lost per experiment day. Nevertheless, the mass loss rate should not be considered an exact mass loss per day but rather an approximate value due to the rapid sedimentation observed during the first days of an experiment for most of the samples. Results on the calculated mass loss rate are gathered and Tables 5-3 and 5-4.

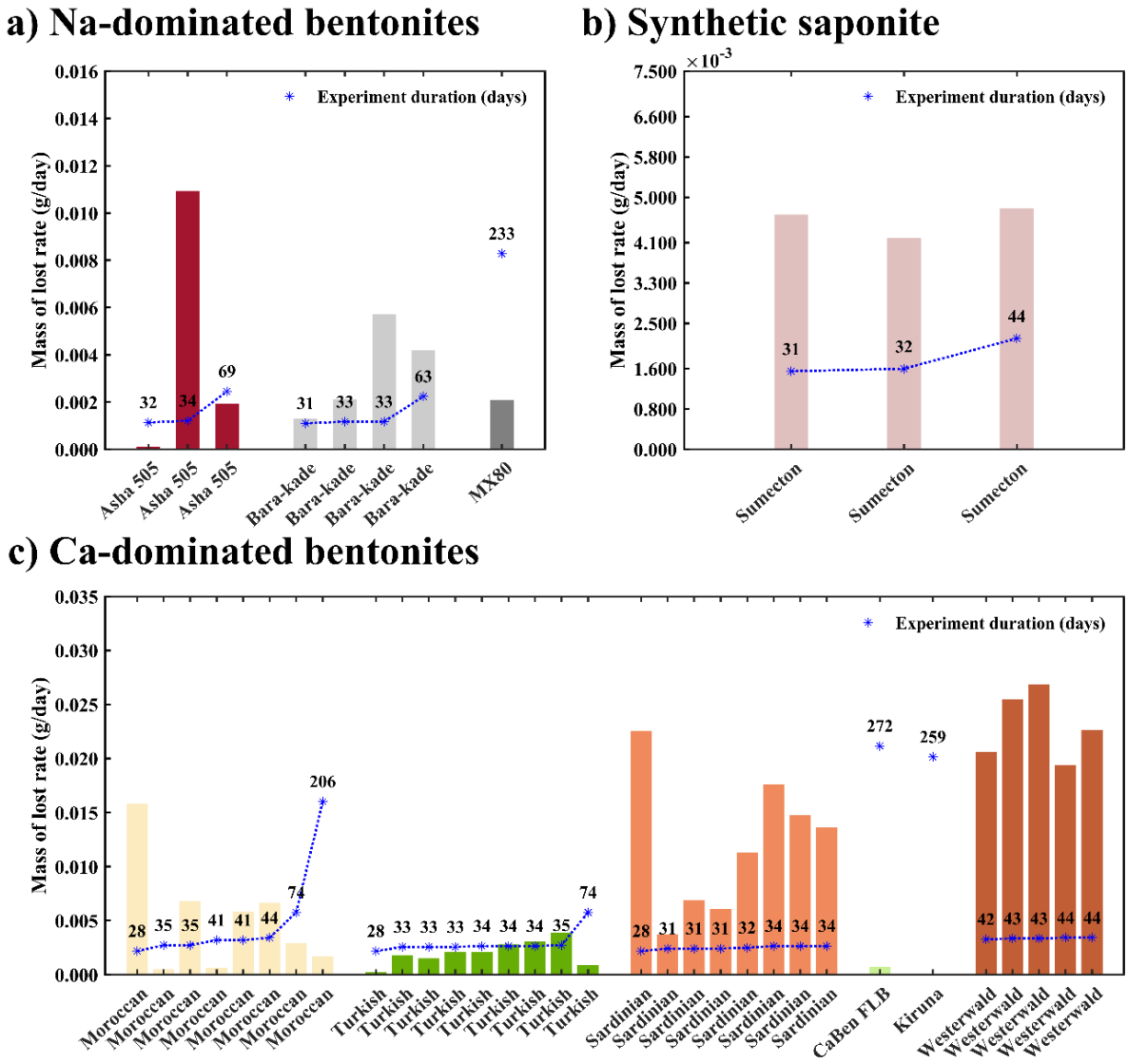

***Figure 5-2**: Results of the calculated mass loss (g/day).*

In the main, Westerwald is the bentonite with the most apical rate of mass lost, while the lowest mass losses per day are reflected by the Kiruna and CaBen FLB bentonites (Table 5-4).

Besides, the most significant mass loss rate occurs between days three to five of an experiment until 25-35 days for all clays. At large, as the experiments' duration increases, the mass loss rate appears to decrease. This effect is observable in those samples where the duration of the sedimentation tests was longest, such as Asha 505 (69 days), Bara-kade (63 days), Moroccan (206 days), Turkish (74 days), CaBen FLB (272 days) and Kiruna (259 days). Such an effect might be explained by the fact that after 30-35 days of experiment duration, the evaluated clays, regardless of their sodic or calcium nature, appear to reach an 'equilibrium' with the surrounding solution, stabilising the rate of mass lost. Additionally, Sumecton (Figure 5 2 (b)) shows a consistent mass loss rate across the three samples, irrespective of the duration of the experiment.

Table 5-3: Mass loss rate of the Na-dominated bentonites and synthetic saponite.

Clay material	Mass loss rate (g/day)	Standard deviation (g/day)	Mass loss (wt%)	Standard deviation (wt%)
Asha 505 (32 days)	0.0001	0.0780	0.034	1.196
Asha 505 (34 days)	0.0109	0.0780	3.222	1.196
Asha 505 (69 days)	0.0019	0.0780	1.207	1.196
Bara-kade (31 days)	0.0013	0.0023	0.363	0.774
Bara-kade (33 days)	0.0021	0.0023	0.609	0.774
Bara-kade (33 days)	0.0057	0.0023	1.634	0.774
Bara-kade (63 days)	0.0042	0.0023	2.252	0.774
MX80 (233 days)	0.0021	0.0000	4.037	0.000
Sumecton (31 days)	0.0047	0.0009	1.270	0.297
Sumecton (32 days)	0.0042	0.0009	1.190	0.297
Sumecton (44 days)	0.0048	0.0009	1.854	0.297

The mass loss (wt%) was calculated by dividing the combined mass of dry loose and sedimented clay material by the total collected mass, multiplied by 100 (Equation 3-5). The mass loss (wt%) represents the percentage of bentonite lost relative to the initial mass. Figure 5-2 and Tables 5-3 and 5-4 present a comprehensive analysis of the mass loss (wt%) observed in various bentonite samples. The mass loss (wt%) is a critical parameter indicating the percentage of bentonite lost relative to the initial mass. Notably, the data reveal significant variations in mass loss (wt%) across different bentonite types and experimental durations.

Westerwald emerges as the bentonite exhibiting the highest mass loss (wt%), indicating substantial degradation over the experimental period. Conversely, Kiruna and CaBen FLB bentonites demonstrate notably lower mass losses (wt%), suggesting comparatively lesser degradation. Furthermore, Sumecton exhibits a consistent mass loss rate across all three samples, regardless of the experiment duration, suggesting a stable degradation behaviour.

Table 5-4: Mass loss rate of the Ca-dominated bentonites.

Clay material	Mass loss rate (g/day)	Standard deviation (g/day)	Mass loss (wt%)	Standard deviation (g/day)
Moroccan (28 days)	0.0158	0.083	3.893	1.073
Moroccan (35 days)	0.0005	0.083	0.165	1.073
Moroccan (35 days)	0.0068	0.083	2.052	1.073
Moroccan (41 days)	0.0006	0.083	0.229	1.073
Moroccan (41 days)	0.0058	0.083	2.052	1.073
Moroccan (44 days)	0.0066	0.083	2.500	1.073
Moroccan (74 days)	0.0029	0.083	1.890	1.073
Moroccan (206 days)	0.0017	0.083	3.072	1.073
Turkish (28 days)	0.0002	0.030	0.059	0.256
Turkish (33 days)	0.0018	0.030	0.522	0.256
Turkish (33 days)	0.0015	0.030	0.425	0.256
Turkish (33 days)	0.0021	0.030	0.611	0.256
Turkish (34 days)	0.0021	0.030	0.616	0.256
Turkish (34 days)	0.0028	0.030	0.818	0.256
Turkish (34 days)	0.0031	0.030	0.902	0.256
Turkish (35 days)	0.0039	0.030	1.175	0.256
Turkish (74 days)	0.0009	0.030	0.560	0.256
Sardinian (28 days)	0.0225	0.0121	5.553	1.756
Sardinian (31 days)	0.0037	0.0121	0.986	1.756
Sardinian (31 days)	0.0069	0.0121	1.817	1.756
Sardinian (31 days)	0.0061	0.0121	1.598	1.756
Sardinian (32 days)	0.0113	0.0121	3.017	1.756
Sardinian (34 days)	0.0176	0.0121	4.949	1.756
Sardinian (34 days)	0.0148	0.0121	4.181	1.756
Sardinian (34 days)	0.0136	0.0121	3.862	1.756
CaBen FLB (272 days)	0.0007	0.0000	1.656	0.000
Kiruna (259 days)	0.00004	0.00000	0.083	0.000
Westerwald (42 days)	0.0206	0.0108	7.096	1.034
Westerwald (43 days)	0.0255	0.0108	8.767	1.034
Westerwald (43 days)	0.0269	0.0108	9.262	1.034
Westerwald (44 days)	0.0194	0.0108	6.922	1.034
Westerwald (44 days)	0.0227	0.0108	7.964	1.034

5.1.3 Average expansion of a clay material

The average expansion of the different clay materials was calculated considering their final expansion in four directions divided by the number of values in the set, which correspond to the final extension of the expansion measured from the edge of the ring-shaped sample to the final rim of the expanded clay (Equation 3-6). The measurements were taken at the termination of each experiment using a ruler at the upper exterior surface of an artificial fracture, considering the following directions: 0º, 90º, 180º and 270º by taking photos (Appendix I includes the photos taken during the sedimentation test). It is essential to acknowledge that the expansion of the clay materials was calculated considering the central tendency of a set of numbers, and so, it must be seen as an approximate expansion value rather than an accurate one.

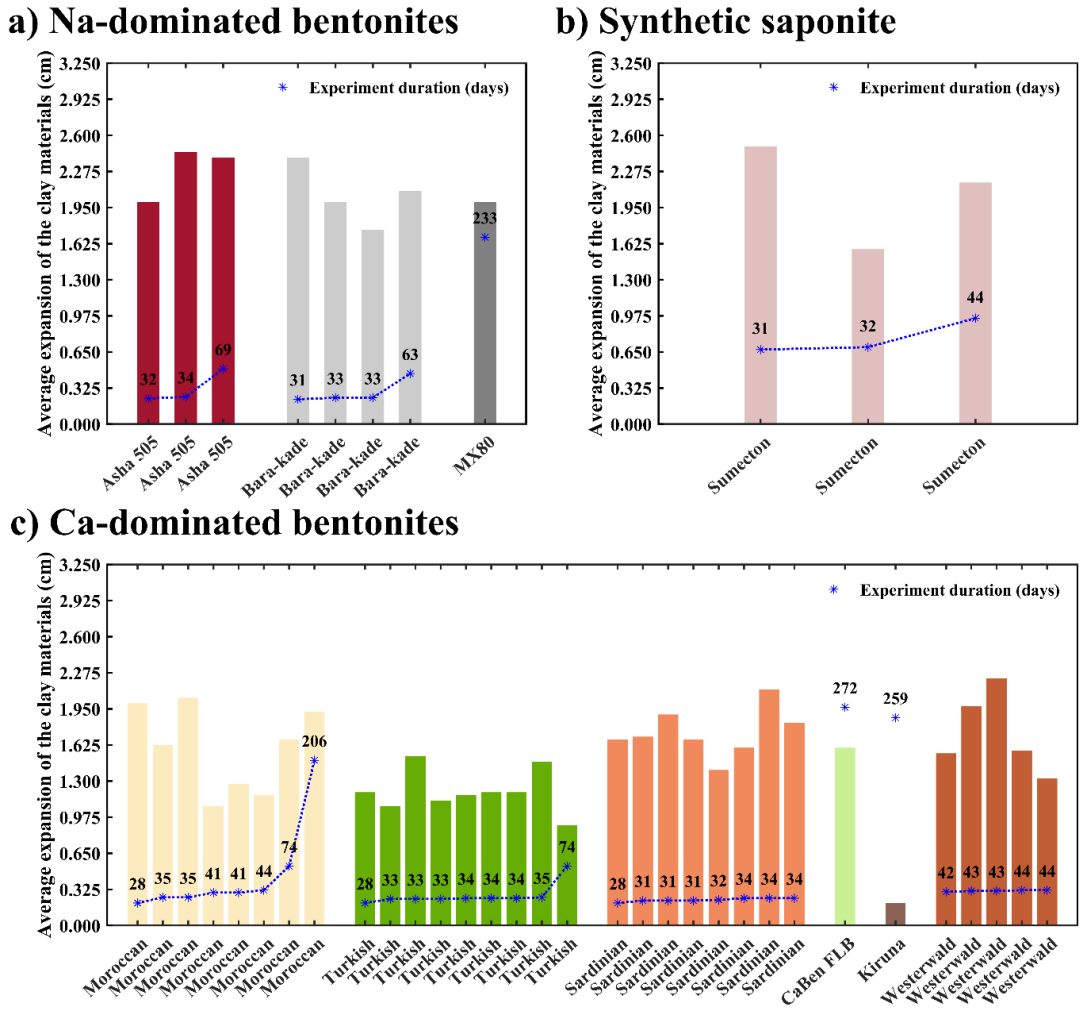

Figure 5-3: Result of the calculated average expansion.

Table 5-5: Average expansion of the Na-dominated bentonites and synthetic saponite.

Clay material	Average expansion (cm)	Standard deviation (cm)
Asha 505 (32 days)	2.000	0.202
Asha 505 (34 days)	2.450	0.202
Asha 505 (69 days)	2.400	0.202
Bara-kade (31 days)	2.400	0.233
Bara-kade (33 days)	2.000	0.233
Bara-kade (33 days)	1.750	0.233
Bara-kade (63 days)	2.100	0.233
MX80 (233 days)	2.000	0.000
Sumecton (31 days)	2.500	0.384
Sumecton (32 days)	1.575	0.384
Sumecton (44 days)	2.175	0.384

Table 5-6: Average expansion of the Ca-dominated bentonites.

Clay material	Average expansion (cm)	Standard deviation (cm)
Moroccan (28 days)	2.000	0.369
Moroccan (35 days)	1.625	0.369
Moroccan (35 days)	2.050	0.369
Moroccan (41 days)	1.075	0.369
Moroccan (41 days)	1.275	0.369
Moroccan (44 days)	1.175	0.369
Moroccan (74 days)	1.675	0.369
Moroccan (206 days)	1.925	0.369
Turkish (28 days)	1.200	0.197
Turkish (33 days)	1.075	0.197
Turkish (33 days)	1.525	0.197
Turkish (33 days)	1.125	0.197
Turkish (34 days)	1.175	0.197
Turkish (34 days)	1.200	0.197
Turkish (34 days)	1.200	0.197
Turkish (35 days)	1.475	0.197
Turkish (74 days)	0.900	0.197
Sardinian (28 days)	1.675	0.233
Sardinian (31 days)	1.700	0.233
Sardinian (31 days)	1.900	0.233
Sardinian (31 days)	1.675	0.233
Sardinian (32 days)	1.400	0.233
Sardinian (34 days)	1.600	0.233
Sardinian (34 days)	2.125	0.233
Sardinian (34 days)	1.825	0.233
CaBen FLB (272 days)	1.600	0.000
Kiruna (259 days)	0.200	0.000
Westerwald (42 days)	1.550	0.324
Westerwald (43 days)	1.975	0.324
Westerwald (43 days)	2.225	0.324
Westerwald (44 days)	1.575	0.324
Westerwald (44 days)	1.325	0.324

After 259 and 74 days of experiment duration, Kiruna and Turkish bentonites showed minor expansion, as illustrated in Figure 5-3 (c) and Table 5-6. As previously stated, Kiruna bentonite is characterised as being ~100 % Ca-dominated bentonite. Although Kiruna bentonite was subjected to a homoionisation process, the difficulties encountered in altering the occupancy of Ca^{2+} by Na^{+} at the interlayer space might be explained by the influence exerted by some of its accessory minerals. The lesser expansion of the Turkish bentonite (74 days) oscillates on the ranges seen in the other Turkish samples.

Figures 5-3 (a) and (b) and Table 5-5 depict the expansion values corresponding to the Na-dominated bentonites and synthetic saponite. The highest expansion corresponds to Asha 505 (34 days and 69 days), Bara-kade (31 days) and Sumecton (31 days). The predominant expansion of Asha 505 and Bara-kade can be easily explained due to the higher concentration of Na^+ in the interlayer space compared to the Ca-dominated bentonites. In the case of Sumecton, given that it is a chemically synthesised clay material, its high expansion can be justified since Sumecton was subjected to a thermal treatment to improve its swelling capability, among other properties (KI 1943).

5.1.4 Total surface area of the expanded clay material facing the fracture

The total surface area of the expanded clay material facing the fracture refers to the calculated total area that the surface of the expanded clay occupies within the 0.01 cm of fracture aperture (Equation 3-7).

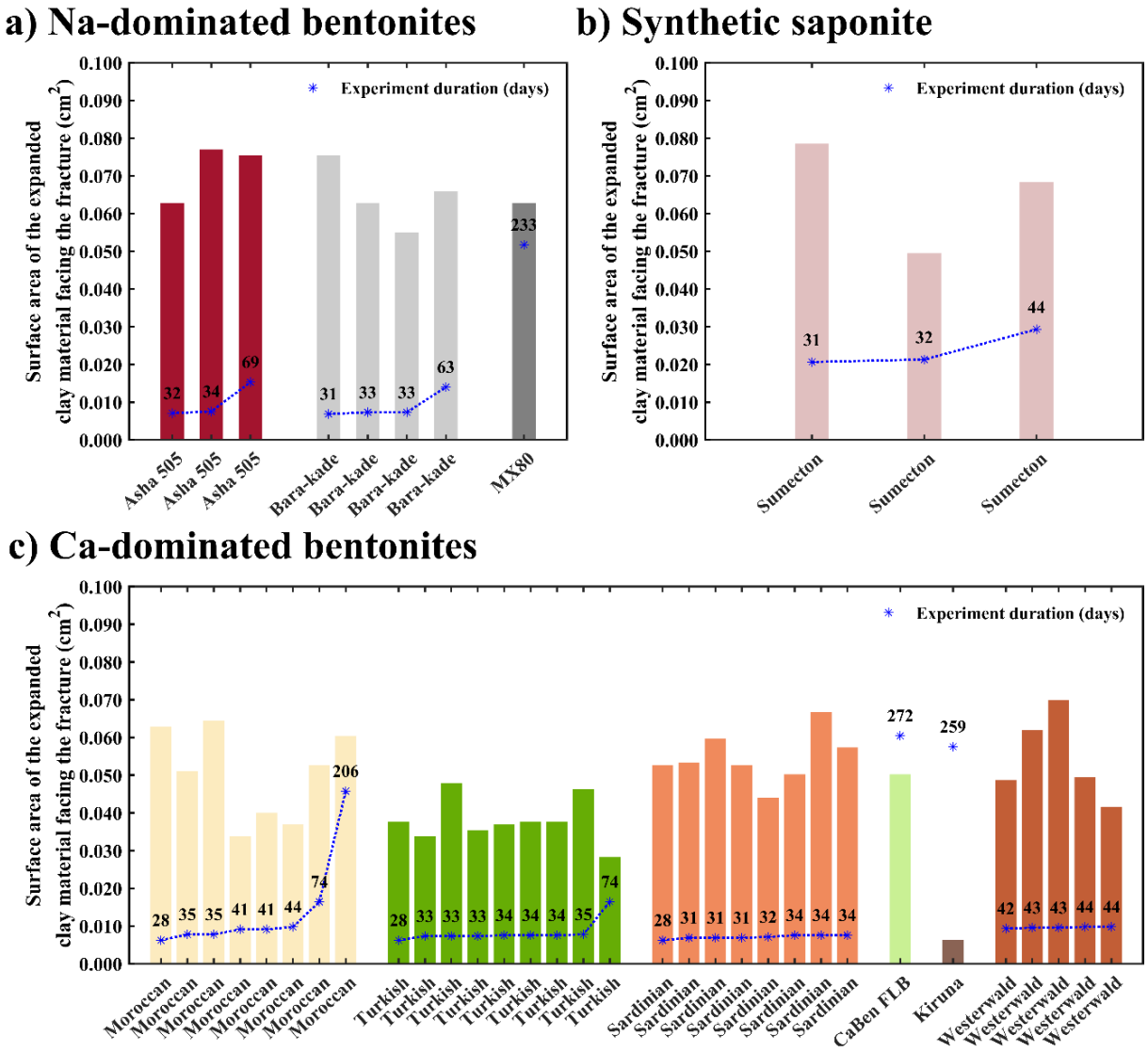

Figure 5-4: *Results of the total surface area of the expanded clays facing the fracture.*

Table 5-7: Total surface area of the expanded clay of the Na-dominated bentonites and synthetic saponite facing the fracture.

Clay material	Surface area of expanded clay material facing the fracture (cm^2)	Standard deviation (cm^2)
Asha 505 (32 days)	0.063	0.019
Asha 505 (34 days)	0.077	0.019
Asha 505 (69 days)	0.075	0.019
Bara-kade (31 days)	0.075	0.008
Bara-kade (33 days)	0.063	0.008
Bara-kade (33 days)	0.055	0.008
Bara-kade (63 days)	0.066	0.008
MX80 (233 days)	0.063	0.000
Sumecton (31 days)	0.079	0.037
Sumecton (32 days)	0.049	0.037
Sumecton (44 days)	0.068	0.037

Since the determination of the total surface area is based on the 'shape' of the surface from which the calculation is intended to be made. For the studied clay materials, it was surmised that the halo shape was equal to that of a hollow cylinder, whose inner diameter corresponds to the total diameter of the pre-compacted sample (Figure 2-3). The outer diameter is equal to the sum of the inner diameter and the average expansion of the clay material, and the height is equivalent to the fracture aperture. Figures 5-4 (a) and (b) and Table 5-7 exhibit the results corresponding to the total surface area of the expanded clay from the Na-dominated bentonites and the synthetic saponite. Widely, the calculated values ranged between 0.049 and 0.079 cm^2, with the lowest total surface area attributed to Sumecton after 32 days of experiment and the highest to Asha 505 and Sumecton after 34 and 31 days of experiment, respectively.

Figure 5-4 (b) and Table 5-8 display the results of the total surface area of the expanded clay from the Ca-dominated bentonites. Kiruna bentonite's lowest total surface area (0.006 cm^2) could be explained by its mineral composition, which appears to influence its expansion. The highest total surface area is attributable to Westerwald bentonite (0.070 cm^2). Besides, within the Ca-dominated bentonites, the calculated total surface area of the expanded Turkish clay appears to fluctuate less than the calculated for the Moroccan, Sardinian and Westerwald bentonites.

Table 5-8: Total surface area of the expanded clay of the Ca-dominated bentonites facing the fracture.

Clay material	Surface area of expanded clay material facing the fracture (cm^2)	Standard deviation (cm^2)
Moroccan (28 days)	0.063	0.031
Moroccan (35 days)	0.051	0.031
Moroccan (35 days)	0.064	0.031
Moroccan (41 days)	0.034	0.031
Moroccan (41 days)	0.040	0.031
Moroccan (44 days)	0.037	0.031
Moroccan (74 days)	0.053	0.031
Moroccan (206 days)	0.060	0.031
Turkish (28 days)	0.038	0.024
Turkish (33 days)	0.034	0.024
Turkish (33 days)	0.048	0.024
Turkish (33 days)	0.035	0.024
Turkish (34 days)	0.037	0.024
Turkish (34 days)	0.038	0.024
Turkish (34 days)	0.038	0.024
Turkish (35 days)	0.046	0.024
Turkish (74 days)	0.028	0.024
Sardinian (28 days)	0.053	0.064
Sardinian (31 days)	0.053	0.064
Sardinian (31 days)	0.060	0.064
Sardinian (31 days)	0.053	0.064
Sardinian (32 days)	0.044	0.064
Sardinian (34 days)	0.050	0.064
Sardinian (34 days)	0.067	0.064
Sardinian (34 days)	0.057	0.064
CaBen FLB (272 days)	0.050	0.000
Kiruna (259 days)	0.006	0.000
Westerwald (42 days)	0.049	0.102
Westerwald (43 days)	0.062	0.102
Westerwald (43 days)	0.070	0.102
Westerwald (44 days)	0.049	0.102
Westerwald (44 days)	0.042	0.102

5.1.5 Area-specific mass loss rate

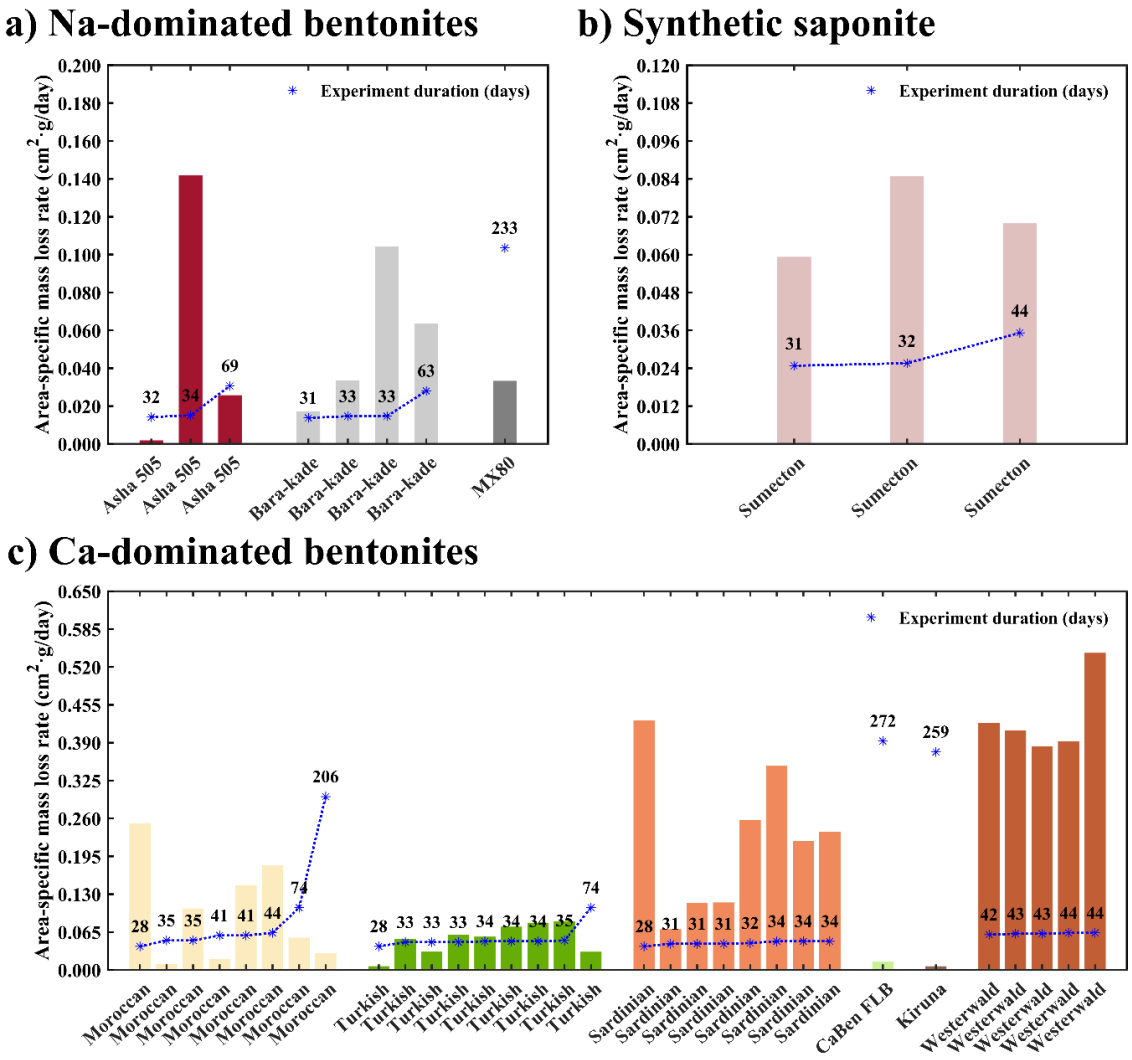

Figure 5-5: Results of the area-specific mass loss rate.

Table 5-9: Area-specific mass loss rate of the Na-dominated bentonites and synthetic saponite.

Clay material	Area-specific mass loss rate (g/day·cm^2)	Standard deviation (g/day·cm^2)
Asha 505 (32 days)	0.002	0.059
Asha 505 (34 days)	0.142	0.059
Asha 505 (69 days)	0.026	0.059
Bara-kade (31 days)	0.017	0.039
Bara-kade (33 days)	0.034	0.039
Bara-kade (33 days)	0.104	0.039
Bara-kade (63 days)	0.064	0.039
MX80 (233 days)	0.033	0.000
Sumecton (31 days)	0.059	0.026
Sumecton (32 days)	0.085	0.026
Sumecton (44 days)	0.070	0.026

The mass loss rate and the total surface area of the expanded clay material were utilised to calculate the area-specific mass loss rate (Equation 3-8). The area-specific mass loss rate could be considered an indicator of the mass loss per day and cm^2 of expanded clay material. Nonetheless, the area-specific mass loss rate should not be viewed as a precise value but as a proximate value of mass loss per day and cm^2 of expanded clay material since the most significant mass loss seems to occur at the early stages of an experiment. Figure 5-5 and Tables 5-9 and 5-10 gather the calculated area-specific mass loss rate results.

Figure 5-5 (c) and Table 5-10 depict the results of the area-specific mass loss rate of the Ca-dominated bentonites. On the whole, the Westerwald bentonite samples exhibit greater values of area-specific mass loss rate than the rest of the Ca-dominated bentonites examined. The most considerable variation within samples of the same clay material is notably apparent in the case of the Moroccan and Sardinian bentonites, irrespective of the experiment duration.

Figures 5-5 (a) and (b) and Table 5-9 display the results relative to the Na-dominated bentonites' and synthetic saponite area-specific mass loss rate. The largest and lowest values can be assigned to the Asha 505 bentonite. Bara-kade and Sumecton show a more reasonable increase in area-specific mass loss rate, which peaks at 30-35 days before decreasing with the experiment's duration. As previously speculated, the observed decrease may be driven by the equilibrium reached with the water solution stabilising the mass loss rate (section 5.1.2).

By comparing the synthetic saponite, Na- and Ca-dominated bentonites results, it was concluded that the maximal area-specific mass loss rate corresponds to the Ca-dominated bentonites. Additionally, during the experiments involving the Westerwald and Sardinian bentonites, a high sedimentation rate was observed at the top of the lower polyester blue shim, along with an increase in loose clay material surrounding the halo or expanded clay, leading to a higher mass loss rate, thus, increasing the area-specific mass loss rate.

Table 5-10: Area-specific mass loss rate of the Ca-dominated bentonites.

Clay material	Area-specific mass loss rate (g/day·cm^2)	Standard deviation (g/day·cm^2)
Moroccan (28 days)	0.251	0.084
Moroccan (35 days)	0.010	0.084
Moroccan (35 days)	0.106	0.084
Moroccan (41 days)	0.019	0.084
Moroccan (41 days)	0.145	0.084
Moroccan (44 days)	0.179	0.084
Moroccan (74 days)	0.055	0.084
Moroccan (206 days)	0.028	0.084
Turkish (28 days)	0.006	0.026
Turkish (33 days)	0.053	0.026
Turkish (33 days)	0.031	0.026
Turkish (33 days)	0.060	0.026
Turkish (34 days)	0.057	0.026
Turkish (34 days)	0.074	0.026
Turkish (34 days)	0.081	0.026
Turkish (35 days)	0.084	0.026
Turkish (74 days)	0.031	0.026
Sardinian (28 days)	0.428	0.109
Sardinian (31 days)	0.070	0.109
Sardinian (31 days)	0.116	0.109
Sardinian (31 days)	0.116	0.109
Sardinian (32 days)	0.257	0.109
Sardinian (34 days)	0.350	0.109
Sardinian (34 days)	0.221	0.109
Sardinian (34 days)	0.237	0.109
CaBen FLB (272 days)	0.014	0.000
Kiruna (259 days)	0.006	0.000
Westerwald (42 days)	0.423	0.059
Westerwald (43 days)	0.411	0.059
Westerwald (43 days)	0.384	0.059
Westerwald (44 days)	0.392	0.059
Westerwald (44 days)	0.544	0.059

5.1.6 Volume of the expanded clay material

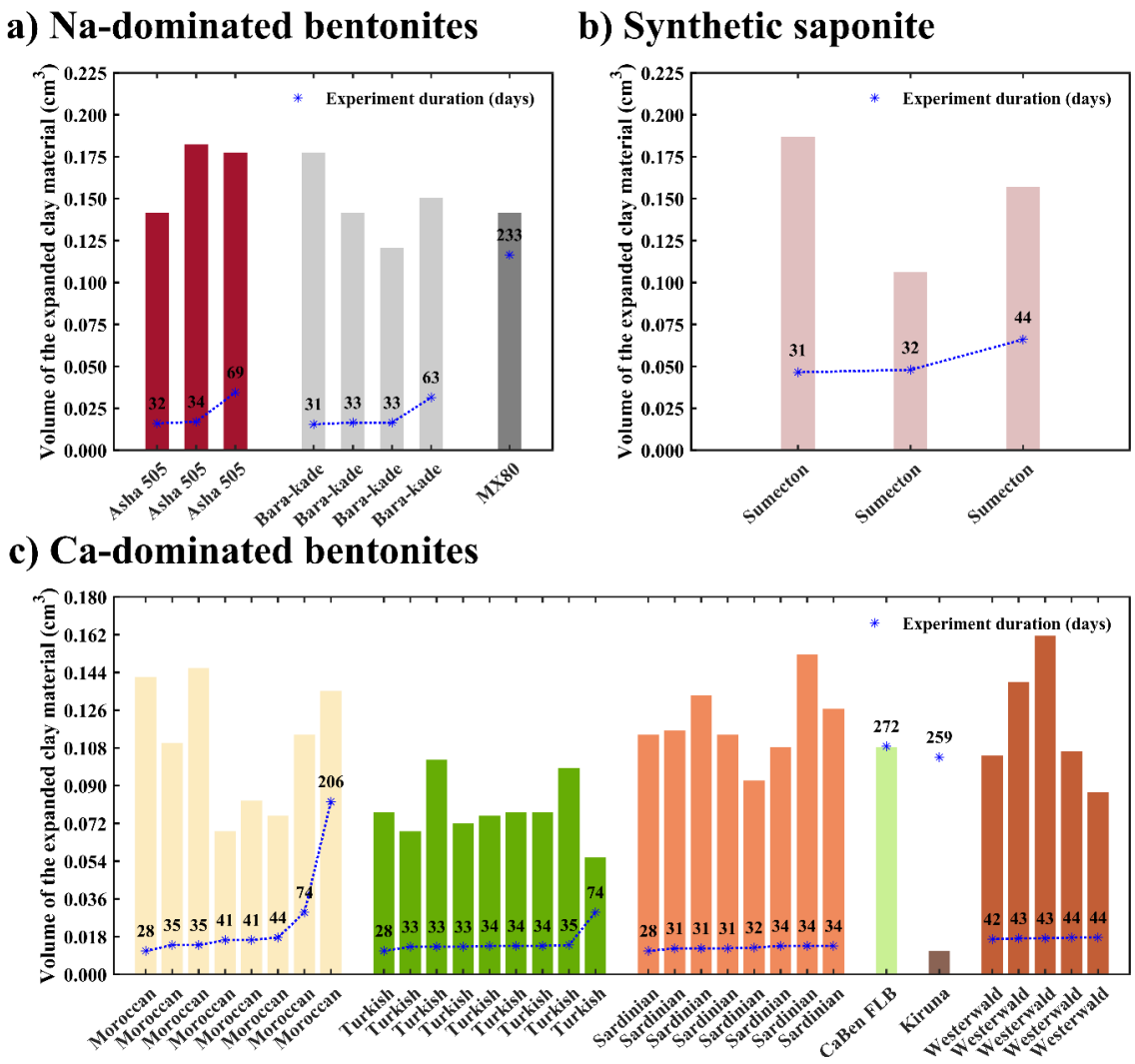

Figure 5-6: Results of the calculated volume of the expanded clay material.

Table 5-11: Volume of the expanded clay of Na-dominated bentonites and the synthetic saponite.

Clay material	Volume of the expanded clay material (cm^3)	Standard deviation (cm^3)
Asha 505 (32 days)	0.142	0.095
Asha 505 (34 days)	0.182	0.095
Asha 505 (69 days)	0.178	0.095
Bara-kade (31 days)	0.178	0.062
Bara-kade (33 days)	0.142	0.062
Bara-kade (33 days)	0.121	0.062
Bara-kade (63 days)	0.150	0.062
MX80 (233 days)	0.142	0.000
Sumecton (31 days)	0.187	0.073
Sumecton (32 days)	0.106	0.073
Sumecton (44 days)	0.157	0.073

The volume of the expanded clay material or volume of the halo was calculated taking into consideration: (*i*) the facture aperture; (*ii*) the average expansion of a clay material; and (*iii*) the dimensions of a ring-shaped sample (Equation 3-9). Furthermore, the clay nature and the amount of solution incorporated also determine the volume of the expanded clay material. Figure 5-6 and Tables 5-11 and 5-12 display the results of the calculated volume of the expanded clay material. Widely, the most substantial volume of expansion matches with the Na-dominated bentonites and the synthetic saponite, whereas the least significant expansion was assigned to the Ca-dominated bentonites.

Table 5-12: Volume of the expanded clay of Ca-dominated bentonites.

Clay material	Volume of the expanded clay material (cm^3)	Standard deviation (cm^3)
Moroccan (28 days)	0.142	0.028
Moroccan (35 days)	0.110	0.028
Moroccan (35 days)	0.146	0.028
Moroccan (41 days)	0.068	0.028
Moroccan (41 days)	0.083	0.028
Moroccan (44 days)	0.076	0.028
Moroccan (74 days)	0.114	0.028
Moroccan (206 days)	0.135	0.028
Turkish (28 days)	0.077	0.018
Turkish (33 days)	0.068	0.018
Turkish (33 days)	0.102	0.018
Turkish (33 days)	0.072	0.018
Turkish (34 days)	0.076	0.018
Turkish (34 days)	0.077	0.018
Turkish (34 days)	0.077	0.018
Turkish (35 days)	0.098	0.018
Turkish (74 days)	0.056	0.018
Sardinian (28 days)	0.114	0.016
Sardinian (31 days)	0.116	0.016
Sardinian (31 days)	0.133	0.016
Sardinian (31 days)	0.114	0.016
Sardinian (32 days)	0.093	0.016
Sardinian (34 days)	0.108	0.016
Sardinian (34 days)	0.153	0.016
Sardinian (34 days)	0.127	0.016
CaBen FLB (272 days)	0.108	0.000
Kiruna (259 days)	0.011	0.000
Westerwald (42 days)	0.104	0.022
Westerwald (43 days)	0.140	0.022
Westerwald (43 days)	0.162	0.022
Westerwald (44 days)	0.106	0.022
Westerwald (44 days)	0.087	0.022

Figures 5-6 (a) and (b) and Table 5-11 depict the results of the expansion volume of the Na-dominated bentonites and synthetic saponite. The data from Asha 505, Bara-kade, and Sumecton indicate that the expansion of the materials investigated is not affected by the duration of the experiment. The Asha 505, Bara-kade, and Sumecton samples showed significant expansion after 34, 31, and 69 days of experimentation.

Figure 5-6 (b) and Table 5-12 unveil the results of the Ca-dominated bentonites. The most sizeable expansion can be attributed to the Sardinian, Westerwald and Moroccan bentonites after 35, 34 and 43 days of experiment duration. Simultaneously, the lowest expansion values are those displayed by the Turkish and Kiruna samples. As indicated for the Na-dominated bentonites, the volume of expansion can be considered independent of the experiment durations.

5.1.7 Halo's dry density

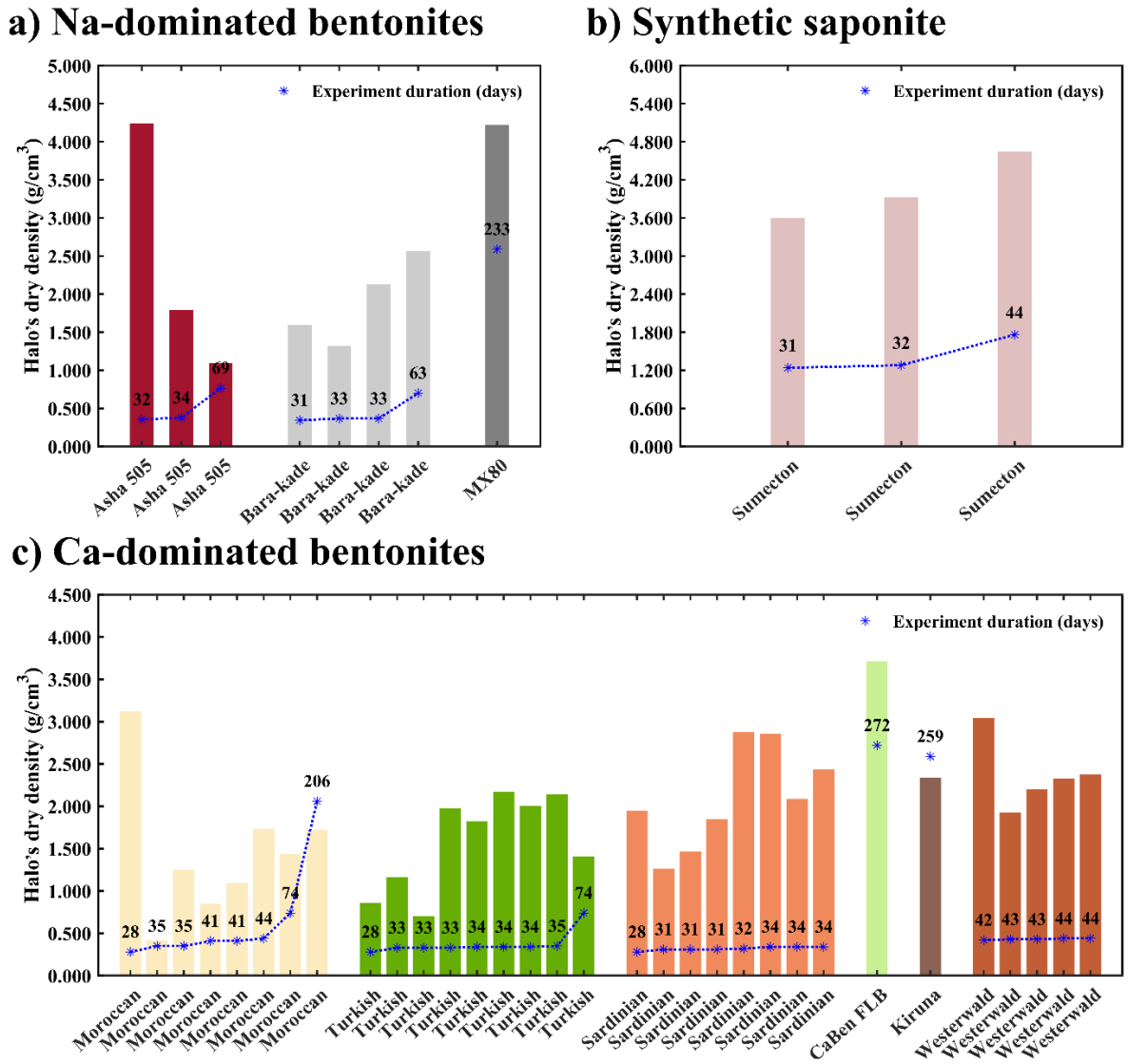

Figure 5-7: *Results of the calculated halo's dry density.*

The halo's dry density was calculated by factoring in the dry mass and the calculated volume of the expanded clay material (Equation 3-10). Thus, the dry density of the halo or expanded clay material is directly related to the amount of expanded material recovered after the excavation and inversely proportional to the expansion volume. As a result, the anticipated dry density of the halo is determined by the amount of dried expanded material collected and the calculated expansion volume.

Figures 5-7 and Tables 5-13 and 5-14 show the results of the halo's dry density of the different clay materials investigated.

Table 5-13: Halo's dry density of Na-dominated bentonites and the synthetic saponite.

Clay material	Halo's dry density (g/cm^3)	Standard deviation (g/cm^3)
Asha 505 (32 days)	4.240	1.300
Asha 505 (34 days)	1.792	1.300
Asha 505 (69 days)	1.095	1.300
Bara-kade (31 days)	1.594	0.588
Bara-kade (33 days)	1.318	0.588
Bara-kade (33 days)	2.125	0.588
Bara-kade (63 days)	2.563	0.588
MX80 (233 days)	4.223	0.000
Sumecton (31 days)	3.603	0.435
Sumecton (32 days)	3.921	0.435
Sumecton (44 days)	4.641	0.435

From Figure 5-7 (a) and Table 5-13, it can be stated that Asha 505 (32 days) and MX80 (233 days) feature the highest values on halo's dry density among the Na-dominated bentonites. Figure 5-7 (b) and Table 5-13 also display the calculated halo's dry density values of Sumecton. The synthetic saponite exhibited high dry density values, which remained consistent among the samples tested.

Figure 5-7 (c) and Table 5-14 disclose the halo's dry density results of the Ca-dominated bentonites. The most relevant values are those of the Moroccan (28 days), CaBen FLB (272 days) and Kiruna (259 days) bentonites.

Overall, the substantial variation in the halo's dry density depicted by the different clay materials examined may be a consequence of a higher mass, even in small amounts of clay, the influence of water retention and the mineral phases present within the clayey matrix of the different clay materials examined.

Table 5-14: Halo's dry density the expanded clay of Ca-dominated bentonites.

Clay material	Halo's dry density (g/cm^3)	Standard deviation (g/cm^3)
Moroccan (28 days)	3.125	0.787
Moroccan (35 days)	0.415	0.787
Moroccan (35 days)	1.253	0.787
Moroccan (41 days)	0.852	0.787
Moroccan (41 days)	1.096	0.787
Moroccan (44 days)	1.735	0.787
Moroccan (74 days)	1.436	0.787
Moroccan (206 days)	1.721	0.787
Turkish (28 days)	0.857	0.545
Turkish (33 days)	1.162	0.545
Turkish (33 days)	0.704	0.545
Turkish (33 days)	1.977	0.545
Turkish (34 days)	1.823	0.545
Turkish (34 days)	2.172	0.545
Turkish (34 days)	2.006	0.545
Turkish (35 days)	2.142	0.545
Turkish (74 days)	1.406	0.545
Sardinian (28 days)	1.950	0.509
Sardinian (31 days)	1.265	0.509
Sardinian (31 days)	1.468	0.509
Sardinian (31 days)	1.845	0.509
Sardinian (32 days)	2.876	0.509
Sardinian (34 days)	2.860	0.509
Sardinian (34 days)	2.088	0.509
Sardinian (34 days)	2.437	0.509
CaBen FLB (272 days)	3.078	0.000
Kiruna (259 days)	3.515	0.000
Westerwald (42 days)	2.559	0.445
Westerwald (43 days)	1.454	0.445
Westerwald (43 days)	1.577	0.445
Westerwald (44 days)	1.941	0.445
Westerwald (44 days)	2.131	0.445

5.1.8 Initial water content

The initial water content was calculated based on the sample's initial mass after compaction and the collected total dry mass (Equation 3-4).

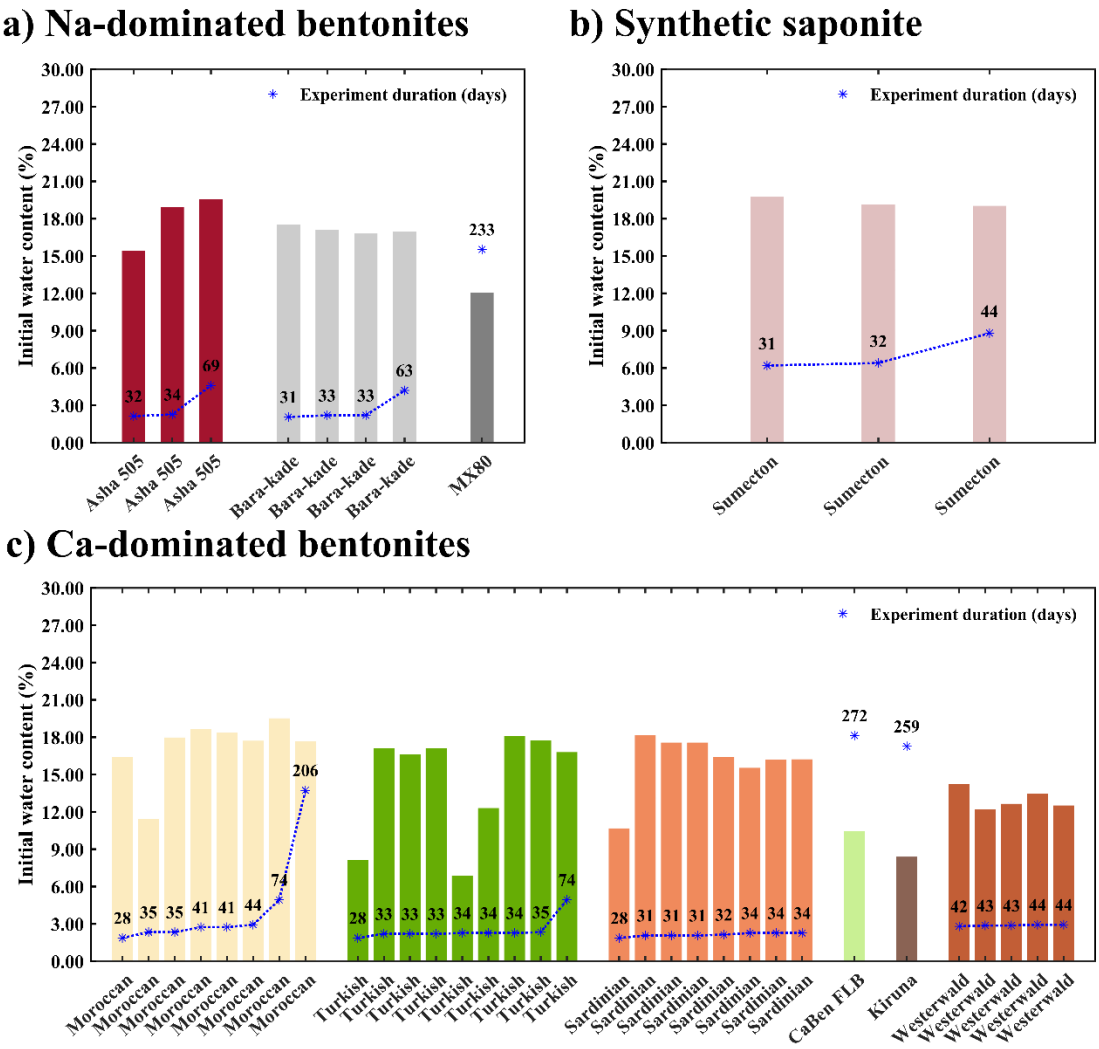

Figure 5-8: Initial water content of the clay materials investigated.

Table 5-15: Initial water content of Na-dominated bentonites and the synthetic saponite.

Clay material	Initial water content (%)	Standard deviation (%)
Asha 505 (32 days)	15.445	1.840
Asha 505 (34 days)	18.917	1.840
Asha 505 (69 days)	19.558	1.840
Bara-kade (31 days)	17.512	0.264
Bara-kade (33 days)	17.088	0.264
Bara-kade (33 days)	16.797	0.264
Bara-kade (63 days)	16.968	0.264
MX80 (233 days)	12.046	0.000
Sumecton (31 days)	19.747	0.317
Sumecton (32 days)	19.131	0.317
Sumecton (44 days)	19.030	0.317

Figure 5-8 and Tables 5-15 and 5-16 gather the information on the initial water content for the Na-dominated bentonites, synthetic saponite and Ca-dominated bentonites.

Table 5-16: ***Initial water content of Ca-dominated bentonites.***

Clay material	Initial water content (%)	Standard deviation (%)
Moroccan (28 days)	16.412	3.298
Moroccan (35 days)	11.412	3.298
Moroccan (35 days)	17.977	3.298
Moroccan (41 days)	18.630	3.298
Moroccan (41 days)	18.377	3.298
Moroccan (44 days)	17.710	3.298
Moroccan (74 days)	19.518	3.298
Moroccan (206 days)	17.650	3.298
Turkish (28 days)	8.144	4.343
Turkish (33 days)	17.113	4.343
Turkish (33 days)	16.613	4.343
Turkish (33 days)	17.129	4.343
Turkish (34 days)	6.847	4.343
Turkish (34 days)	12.305	4.343
Turkish (34 days)	18.102	4.343
Turkish (35 days)	17.742	4.343
Turkish (74 days)	16.797	4.343
Sardinian (28 days)	10.684	2.856
Sardinian (31 days)	18.154	2.856
Sardinian (31 days)	17.564	2.856
Sardinian (31 days)	17.566	2.856
Sardinian (32 days)	16.398	2.856
Sardinian (34 days)	15.534	2.856
Sardinian (34 days)	16.191	2.856
Sardinian (34 days)	16.225	2.856
CaBen FLB (272 days)	10.436	0.000
Kiruna (259 days)	8.391	0.000
Westerwald (42 days)	14.243	0.824
Westerwald (43 days)	12.189	0.824
Westerwald (43 days)	12.646	0.824
Westerwald (44 days)	13.459	0.824
Westerwald (44 days)	12.513	0.824

From Figure 5-8 (a) and (b) and Table 5-15, it can be noted that the Sumecton samples and Asha 505 (69 days) display water content values close to the established threshold of 20 %, whilst the rest of the samples exhibit distant values from that percentage. From Figure 5-9 (c) and Table 5-16, it can be stated that the Moroccan (74 days) and Sardinian (31 days) bentonites are the only Ca-dominated samples displaying initial water values close to 20 %.

On the whole, the large variations encountered with regard to the initial water content within samples of the same clay material and between samples from different clay materials can be due to the initial water content being only measured once per dialysed clay material, assuming, therefore, to be the same between samples of the same clay material before being adjusted to 20 %.

5.1.9 Summary of the calculated data

Table 5-17 presents a comprehensive summary of the characteristics of Na-dominated bentonites, including their expansion, mass loss, mass loss rate, initial dry density, and surface area facing fracture. The data averaged from three to four experiments per clay material reveal notable variations among the samples.

Among the Na-dominated bentonites, Asha 505 demonstrates an average expansion of 2.283 cm with a corresponding mass loss rate of 0.037 g/day and a mass loss (wt%) of 2.042 %. In comparison, MX80 shows a lower expansion of 2.000 cm but a higher mass loss (wt%) of 4.223 %. These results highlight the diverse behaviours of Na-dominated bentonites under similar experimental conditions.

Table 5-17: Summary of the calculated data for the Na-dominated bentonites, including standard deviations. n = number of experiments carried out. The values provided per clay material correspond to the average values of the calculated data.

Clay material	n	Average Expansion (cm)	Mass Loss Rate (g/day)	Mass Loss (wt%)	Initial Dry Density (g/cm^3)	Surface Area Facing Fracture (cm^2)
Asha 505	3	2.283 ± 0.266	0.037 ± 0.060	2.042 ± 1.366	0.072 ± 0.009	1.600 ± 1.200
Bara-kade	4	1.988 ± 0.299	0.032 ± 0.035	1.687 ± 0.349	0.066 ± 0.008	0.994 ± 0.866
MX80	1	2.000 ± 0.000	0.002 ± 0.000	4.223 ± 0.000	0.063 ± 0.000	0.104 ± 0.000
Sumecton	3	2.083 ± 0.510	0.055 ± 0.033	3.721 ± 0.172	0.065 ± 0.015	1.583 ± 0.949

Table 5-18 provides additional insights into the characteristics of Na-dominated bentonites, including area-specific mass loss rate, volume of expanded clay material, halo's dry density, and initial water content. Based on three to four experiments per clay material, the data elucidate the variability in these parameters across different Na-dominated bentonite samples.

Table 5-18: Summary of the calculated data for the Na-dominated bentonites, including standard deviations. n = number of experiments carried out. The values provided per clay material correspond to the average values of the calculated data.

Clay material	n	Area-Specific Mass Loss Rate (g/day·cm^2)	Volume of Expanded Clay Material (cm^3)	Halo's Dry Density (g/cm^3)	Initial Water Content (%)
Asha 505	3	0.050 ± 0.081	0.167 ± 0.060	2.041 ± 1.240	17.640 ± 1.296
Bara-kade	4	0.055 ± 0.041	0.148 ± 0.029	1.883 ± 0.624	17.132 ± 0.429
MX80	1	0.033 ± 0.000	0.142 ± 0.000	4.223 ± 0.000	12.046 ± 0.000
Sumecton	3	0.071 ± 0.018	0.167 ± 0.040	3.721 ± 0.172	19.170 ± 0.429

For instance, Asha 505 exhibits an area-specific mass loss rate of 0.050 g/day·cm^2 and a volume of expanded clay material of 0.167 cm^3, while Sumecton demonstrates a higher area-specific mass loss rate of 0.071 g/day·cm^2 with a comparable volume of expanded clay material.

Table 5-19: Summary of the calculated data for the Ca-dominated bentonites, including standard deviations. n = number of experiments carried out. The values provided per clay material correspond to the average values of the calculated data.

Clay material	n	Average Expansion (cm)	Mass Loss Rate (g/day)	Mass Loss (wt%)	Initial Dry Density (g/cm^3)	Surface Area Facing Fracture (cm^2)
Moroccan	8	1.581 ± 0.451	0.091 ± 0.084	2.929 ± 1.720	1.439 ± 0.600	0.056 ± 0.018
Turkish	9	1.529 ± 0.402	0.049 ± 0.048	1.458 ± 0.796	1.393 ± 0.614	0.076 ± 0.017
Sardinian	8	1.945 ± 0.342	0.238 ± 0.142	3.118 ± 2.118	1.977 ± 0.474	0.092 ± 0.023
CaBen FLB	1	1.600 ± 0.000	0.0007 ± 0.0000	1.656 ± 0.000	1.531 ± 0.000	0.050 ± 0.000
Kiruna	1	0.200 ± 0.000	0.00004 ± 0.0000	0.083 ± 0.000	1.533 ± 0.000	0.006 ± 0.000
Westerwald	5	1.693 ± 0.342	0.318 ± 0.232	4.605 ± 3.380	1.999 ± 0.299	0.110 ± 0.016

Table 5-19 offers an overview of the characteristics of Ca-dominated bentonites, including their expansion, mass loss, mass loss rate, initial dry density, and surface area facing fracture. Derived from one to nine experiments per clay material, the data provide insights into the behaviour of Ca-dominated bentonites under varying experimental conditions.

Moroccan bentonite exhibits a higher average expansion and mass loss (wt%) compared to Turkish and Sardinian bentonites, indicating differences in their sedimentation behaviour.

Table 5-20: Summary of the calculated data for the Ca-dominated bentonites, including standard deviations. n = number of experiments carried out. The values provided per clay material correspond to the average values of the calculated data.

Clay material	n	Area-Specific Mass Loss Rate ($g/day \cdot cm^2$)	Volume of Expanded Clay Material (cm^3)	Halo's Dry Density (g/cm^3)	Initial Water Content (%)
Moroccan	8	0.121 ± 0.105	0.109 ± 0.032	1.682 ± 0.754	15.766 ± 3.017
Turkish	9	0.063 ± 0.066	0.077 ± 0.031	1.634 ± 0.743	14.172 ± 5.430
Sardinian	8	0.208 ± 0.104	0.127 ± 0.032	1.977 ± 0.474	15.570 ± 3.531
CaBen FLB	1	0.014 ± 0.000	0.108 ± 0.000	3.078 ± 0.000	10.436 ± 0.000
Kiruna	1	0.060 ± 0.000	0.011 ± 0.000	3.515 ± 0.000	8.391 ± 0.000
Westerwald	5	0.340 ± 0.286	0.123 ± 0.029	1.814 ± 0.744	12.221 ± 1.522

Finally, Table 5-20 presents additional insights into the characteristics of Ca-dominated bentonites, including area-specific mass loss rate, volume of expanded clay material, halo's dry density, and initial water content. Based on one to nine experiments per clay material, the data reveal variations in these parameters across different Ca-dominated bentonite samples.

For instance, Moroccan bentonite exhibits an area-specific mass loss rate of 0.121 $g/day \cdot cm^2$ and a volume of expanded clay material of 0.109 cm^3, while CaBen FLB demonstrates a lower area-specific mass loss rate of 0.014 $g/day \cdot cm^2$ with a comparable volume of expanded clay material.

5.2 Post-mortem analyses

5.2.1 Clay material's electrical conductivity

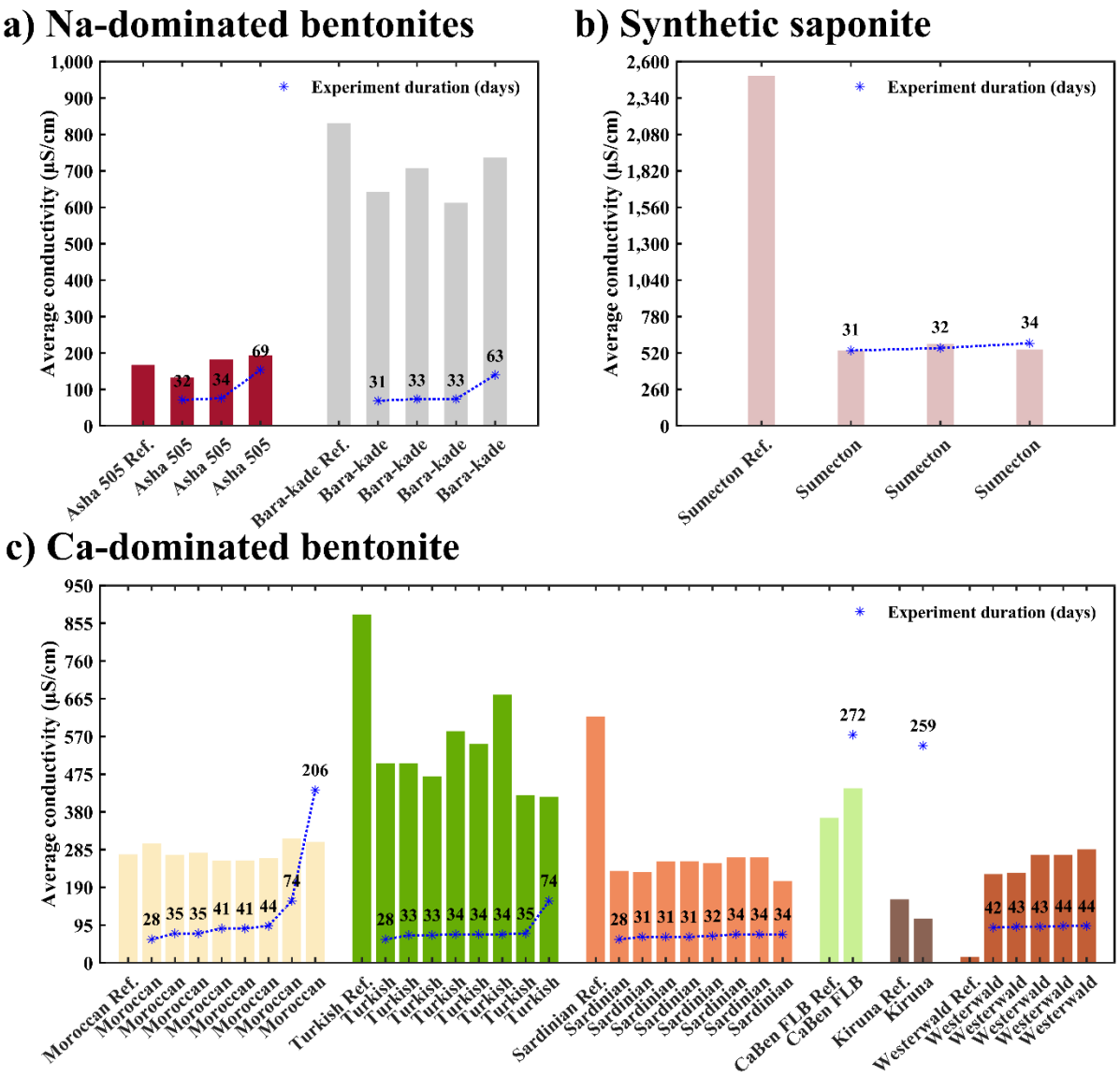

Figure 5-9: *Electrical conductivity of the clay materials investigated.*

The EC of the clay materials was measured following the method described in section 4.1. The EC was quantified twice per sample, and the average conductivity is presented in Figure 5-9 and Tables 5-17 and 5-18, together with the average values of their reference counterparts.

Figures 5-9 (a) and (b) and Table 5-17 collect the EC data of the Na-dominated bentonites and synthetic saponite. The Asha 505 samples showed conductivity values close to those exhibited by the reference material, while the Bara-kade samples displayed lower conductivity values than those of the pristine sample. In addition, the synthetic saponite exhibited very low EC values in comparison with the benchmark specimen.

Table 5-21: Average conductivity values of Na-dominated bentonites and the synthetic saponite.

Clay material	Average temperature (°C)	Average conductivity (µS/cm)
Asha 505 Ref.	24.1	167.5
Asha 505 (32 days)	23.9	132.1
Asha 505 (34 days)	22.8	182.6
Asha 505 (69 days)	23.8	194.0
Bara-kade Ref.	20.9	830.0
Bara-kade (31 days)	23.9	642.5
Bara-kade (33 days)	23.6	707.5
Bara-kade (33 days)	22.8	612.0
Bara-kade (63 days)	22.6	736.0
Sumecton Ref.	21.6	2500.0
Sumecton (31 days)	20.8	539.0
Sumecton (32 days)	21.0	586.0
Sumecton (44 days)	22.1	546.0

From the Ca-dominated bentonites (Figure 5-9 (c) and Table 5-18), it can be observed that the Turkish, Sardinian and Kiruna samples experience a decrease in EC in comparison with the reference samples. Nonetheless, CaBen FLB and Westerwald show an increase in EC, while the conductivity values of the Moroccan bentonite remain close to the reference material.

Table 5-22: Average conductivity values of Ca-dominated bentonites.

Clay material	Average temperature (°C)	Average conductivity (µS/cm)
Moroccan Ref.	25.2	273.0
Moroccan (28 days)	20.5	300.5
Moroccan (35 days)	19.8	271.8
Moroccan (35 days)	19.9	277.1
Moroccan (41 days)	19.6	256.9
Moroccan (41 days)	19.8	258.0
Moroccan (44 days)	19.3	263.5
Moroccan (74 days)	21.0	312.5
Moroccan (206 days)	20.5	304.0
Turkish Ref.	24.6	877.0
Turkish (28 days)	21.5	502.5
Turkish (33 days)	24.3	503.0
Turkish (33 days)	24.8	469.5
Turkish (34 days)	27.0	583.5
Turkish (34 days)	25.4	551.0
Turkish (34 days)	21.1	675.5
Turkish (35 days)	20.8	421.5
Turkish (74 days)	23.2	418.0
Sardinian Ref.	22.0	620.5
Sardinian (28 days)	23.3	231.5
Sardinian (31 days)	24.0	228.5
Sardinian (31 days)	23.7	255.5
Sardinian (31 days)	22.7	256.0
Sardinian (32 days)	25.5	250.5
Sardinian (34 days)	25.6	266.0
Sardinian (34 days)	25.4	265.0
Sardinian (34 days)	23.3	205.3
CaBen FLB Ref.	21.3	365.5
CaBen FLB (272 days)	24.4	439.5
Kiruna Ref.	21.5	159.8
Kiruna (259 days)	24.0	111.4
Westerwald Ref.	20.4	15.5
Westerwald (42 days)	20.3	223.5
Westerwald (43 days)	20.2	227.0
Westerwald (43 days)	20.2	272.0
Westerwald (44 days)	20.3	272.0
Westerwald (44 days)	25.2	285.5

5.2.2 X-ray fluorescence spectroscopy (XRF)

Chemical composition data for the Na- and Ca-dominated bentonites and the synthetic saponite is listed in Tables 5-19 and 5-20. XRF analyses were conducted on pre-compacted discs from the remaining clay material at the ring-shaped perforation, and two measurements were taken per each sample. The data gathered in Tables 5-19 and 5-20 is the calculated average of those two measurements, and is presented as a percentage of each element.

Table 5-23: Average elemental composition of the Na-dominated bentonites and synthetic saponite expressed as %.

Clay material	Na_2O	MgO	Al_2O_3	SiO_2	SO_3	Cl	K_2O	CaO	MnO	Fe_2O_3
Asha 505 Ref.	1.594	1.986	22.479	48.651	0.605	0.633	0.141	1.214	0.119	20.156
Asha 505 (32 days)	1.556	1.751	21.984	49.662	0.212	0.034	0.122	0.727	0.135	21.313
Asha 505 (34 days)	1.551	1.753	22.039	49.943	0.216	0.016	0.125	0.723	0.130	20.964
Asha 505 (69 days)	1.595	1.759	22.303	50.437	0.198	0.012	0.123	0.717	0.120	20.385
Bara-kade Ref.	1.628	2.609	21.425	65.324	0.719	0.004	0.632	1.907	0.036	5.513
Bara-kade (31 days)	1.786	2.429	21.648	66.676	0.227	0.001	0.613	0.987	0.045	5.390
Bara-kade (33 days)	1.792	2.442	21.702	66.347	0.232	0.013	0.571	1.169	0.047	5.487
Bara-kade (33 days)	1.782	2.430	21.623	66.429	0.229	0.012	0.556	1.240	0.047	5.457
Bara-kade (63 days)	1.736	2.450	21.643	66.627	0.184	0.002	0.568	1.119	0.046	5.427
Sumecton Ref.	3.211	31.387	5.708	58.015	1.610	0.000	0.012	0.018	0.001	0.018
Sumecton (31 days)	1.968	32.357	5.903	59.717	0.000	0.004	0.004	0.009	0.001	0.019
Sumecton (32 days)	1.969	32.302	5.906	59.763	0.000	0.002	0.006	0.010	0.001	0.021
Sumecton (44 days)	1.944	32.261	5.886	59.847	0.000	0.003	0.005	0.011	0.000	0.022

Table 5-19 displays the elemental composition of the Na-dominated bentonites and the synthetic saponite. In general, the Asha 505 and Bara-kade bentonite samples exhibit a decrease in Mg, Ca, and K, as well as in SO_3 concentration. All Asha 505 samples and the Bara-kade samples run, for 31- and 69-days, experienced a decrease in Cl percentage. However, contrary to what was observed in the Bara-kade samples (31 and 69 days), both Bara kade samples subjected to sedimentation tests for 33 days showed an increase in Cl concentration. Additionally, all Na-dominated samples subjected to sedimentation tests presented a slight increase in Mn concentration. Moreover, the Na percentage in the case of the Asha 505 samples remains close to the values shown by the reference material, whilst the Bara-kade samples depict an increase in Na concentration. Table 5-19 also gathers the elemental composition of the synthetic saponite (Sumecton) and its reference sample. The Sumecton samples show an increase in Mg and a decrease in Na, Ca and K concentration in comparison with their reference counterpart. Besides, all synthetic saponite samples display a subtle increase in Cl percentage and the SO_3 concentration reduces to zero.

Table 5-24: Average elemental composition of the Ca-dominated bentonites expressed as %.

Clay material	Na_2O	MgO	Al_2O_3	SiO_2	SO_3	Cl	K_2O	CaO	MnO	Fe_2O_3
Moroccan Ref.	1.328	2.235	28.823	61.685	0.109	0.134	0.839	1.565	0.029	2.953
Moroccan (28 days)	2.668	1.505	28.710	61.435	0.000	0.002	1.364	1.004	0.011	2.920
Moroccan (35 days)	2.705	1.484	28.990	61.433	0.011	0.012	1.049	0.961	0.011	2.976
Moroccan (35 days)	2.801	1.369	28.403	61.261	0.014	0.007	1.747	1.269	0.010	2.743
Moroccan (41 days)	2.766	1.431	28.713	61.345	0.009	0.014	1.292	1.149	0.011	2.904
Moroccan (41 days)	2.850	1.345	28.235	61.193	0.004	0.008	1.856	1.338	0.013	2.774
Moroccan (44 days)	2.705	1.491	28.711	61.385	0.000	0.005	1.353	1.051	0.011	2.912
Moroccan (74 days)	2.691	1.548	28.672	61.448	0.003	0.003	1.366	1.069	0.009	2.824
Moroccan (206 days)	2.658	1.483	28.769	61.448	0.009	0.020	1.287	1.041	0.011	2.893
Turkish Ref.	2.052	2.087	19.322	65.666	0.046	0.003	1.417	3.769	0.118	5.042
Turkish (28 days)	1.145	2.127	19.678	66.267	0.000	0.002	1.249	3.695	0.135	5.207
Turkish (33 days)	1.164	2.059	19.426	66.156	0.016	0.010	1.297	3.973	0.136	5.257
Turkish (33 days)	1.153	2.099	19.708	66.035	0.011	0.017	1.279	3.866	0.135	5.199
Turkish (34 days)	1.174	2.078	19.607	66.119	0.015	0.009	1.287	3.904	0.134	5.179
Turkish (34 days)	1.164	2.072	19.535	66.107	0.015	0.013	1.291	3.939	0.135	5.223
Turkish (34 days)	1.171	2.092	19.503	66.155	0.001	0.006	1.313	3.873	0.134	5.242
Turkish (35 days)	1.151	2.100	19.586	66.172	0.004	0.012	1.255	3.806	0.133	5.285
Turkish (74 days)	1.121	2.153	19.601	66.256	0.002	0.002	1.262	3.705	0.133	5.262
Sardinian Ref.	1.108	5.661	18.766	62.535	0.042	0.088	1.360	1.976	0.090	7.611
Sardinian (28 days)	1.891	4.593	19.124	61.925	0.030	0.036	1.699	1.421	0.097	8.279
Sardinian (31 days)	1.867	4.656	19.149	62.219	0.024	0.020	1.613	1.384	0.096	8.098
Sardinian (31 days)	1.898	4.544	19.272	61.906	0.028	0.026	1.662	1.380	0.098	8.314
Sardinian (31 days)	1.908	4.533	19.441	61.982	0.021	0.024	1.640	1.330	0.096	8.172

Table 5-24: Average elemental composition of the Ca-dominated bentonites expressed as %.

Clay material	Na_2O	MgO	Al_2O_3	SiO_2	SO_3	Cl	K_2O	CaO	MnO	Fe_2O_3
Sardinian (32 days)	1.901	4.437	19.850	62.121	0.012	0.011	1.552	1.303	0.102	7.874
Sardinian (34 days)	1.908	4.604	19.104	61.980	0.032	0.027	1.772	1.353	0.099	8.233
Sardinian (34 days)	1.875	4.619	18.978	61.661	0.032	0.018	1.680	1.860	0.095	8.296
Sardinian (34 days)	1.914	4.682	19.101	62.000	0.028	0.025	1.751	1.344	0.110	8.146
CaBen FLB Ref.	0.480	3.583	17.086	64.049	0.066	0.002	1.993	4.541	0.045	6.879
CaBen FLB (272 days)	0.717	3.289	16.688	64.700	0.034	0.007	1.844	4.142	0.101	7.020
Kiruna Ref.	0.000	3.434	21.850	56.697	0.097	0.003	0.770	14.212	0.310	2.429
Kiruna (259 days)	0.000	3.536	22.465	58.227	0.058	0.006	0.748	11.285	0.335	3.091
Westerwald Ref.	0.000	3.101	15.765	59.190	0.003	0.003	0.994	3.059	0.218	13.940
Westerwald (42 days)	2.481	3.053	16.464	56.276	0.001	0.022	0.911	0.667	0.241	16.061
Westerwald (43 days)	2.497	2.897	15.943	57.651	0.000	0.040	0.881	0.550	0.231	15.637
Westerwald (43 days)	2.481	2.900	16.074	57.725	0.000	0.031	0.877	0.552	0.233	15.447
Westerwald (44 days)	2.481	2.903	16.002	57.853	0.001	0.031	0.873	0.546	0.236	15.439
Westerwald (44 days)	2.492	2.906	15.994	57.816	0.000	0.035	0.887	0.553	0.237	15.412

Table 5-20 compiles the information on the chemical composition of the Ca-dominated bentonites. Changes in the elemental composition of the different Ca-dominated bentonites are following described in comparison with the reference samples:

- The Moroccan bentonite samples display an enlargement in Na and K and a diminishment in Mg and Ca concentrations. Additionally, the Cl, SO_3 and Mn percentages decrease in comparison to the values shown by the reference sample.
- The Turkish bentonite samples run for different periods exhibited an apparent decrease in Na and K percentages. In contrast, the Mg and Ca concentrations remained close to the values displayed by the reference material. The Cl concentration increases for those samples that run for 33 (x2), 34 (x3), and 35 days, while those samples that run for 28- and 74-days showed values close to the reference sample. Besides, the SO_3 concentration decreases for all analysed samples.
- The Sardinian bentonite samples run independently of the experiment duration depict a concentration increase in Na and K and a decrease in Mg and Ca. The SO_3 and Cl concentrations were depleted for all samples.
- The CaBen FLB bentonite samples showed a decrease in Mg, Ca, K, SO_3, and Cl concentrations and an increase in Na and Mn.

- The Kiruna bentonite samples reflect similar values in the majority of its chemical components. Notably, the Na concentration remains zero. Furthermore, there is an increase in Fe Concentration.
- The Westerwald samples show a decrease in Mg, Ca, and K concentrations while showing an apparent increase in Na. Moreover, the Cl and Fe concentrations increase.

6 Conclusions and further work

6.1 Calculated data and post-mortem analyses main conclusions

The following sections summarise the main conclusions achieved through the calculated and post-mortem analyses. As a general conclusion, the variations observed in the different clay materials can be considered independent of the experiment's duration.

6.1.1 Initial water content and initial dry density

The initial water content was estimated per dialysed clay material rather than per sample subdued to a sedimentation test. This may be considered a potential source of error since the initial water content may vary across the same dialysed clay material. For all performed tests, the initial dry density was 1.45 g/cm^3 and water saturation was adjusted to 20 %, considering the measured initial water content irrespective of its variance across the same dialysed clay material. Furthermore, the dry density decreases as the water content increases; therefore, since the initial water content was not measured per sample, those samples with a greater mass due to a higher initial water content show lower initial densities, inducing variations on initial densities between samples of the same clay material.

6.1.2 Mass loss rate

The rate at which mass was lost was determined by taking into account the entire duration of the experiment. Significant sedimentation seems to occur rapidly over the first two to three weeks of a test for all clay samples examined. Therefore, the calculated mass loss rate may be an overestimation of the mass loss, considering that the major sedimentation happens rather quickly. After 25-35 days of experiment, all clay samples evaluated appear to reach an 'equilibrium' with the surrounding water solution, slowing or even stopping the mass loss rate. This effect is especially notable in those samples where the duration of the experiment is longer.

Moreover, based on the results presented in this report, the clays exhibit the following relative order of average sedimentation mass loss rate (wt%) from highest to lowest: Westerwald (4.605 wt% ± 3.380), MX80 (4.223 wt% ± 0.000), Sumecton (3.721 wt% ± 0.172), Sardinian (3.118 wt% ± 2.118), Moroccan (2.929 wt% ± 1.720), Asha 505 (2.042 wt% ± 1.366), Bara-kade (1.687 wt% ± 0.349), CaBEN FLB (1.656 wt% ± 0.000), Turkish (1.458 wt% ± 0.796), and Kiruna (0.083 wt% ± 0.000).

Due to the ongoing development of the methodology, these values should be interpreted with caution as they are currently indicative.

6.1.3 Total surface area of the expanded clay material facing the fracture

The total surface area of the expanded clay material facing the fracture was calculated considering: (*i*) the fracture aperture; (*ii*) the radius of the pre-compacted sample; (*iii*) the outer radius of the expanded material as the difference between the average expansion of the clay material examined and the radius of the pre-compacted sample (Equation 3-7). The average expansion of a clay material was calculated considering its average expansion in four directions. Therefore, the calculated outer diameter may have been overestimated or underestimated, given that the expansion is by no means uniform in the four directions considered. Besides, the greater the calculated average expansion, the larger the total surface area of the expanded clay is. Overall, the largest surface was shown by the Asha 505 and Sumecton samples after 34 and 31 days of experiment duration.

6.1.4 Area-specific mass loss rate

The area-specific mass loss rate was assessed considering the mass loss rate and total surface of the expanded clay material facing the fracture. As previously stated, the mass loss rate was estimated, considering that the mass loss was uniform throughout the experiment duration. Besides, the total surface of the expanded clay materials was calculated assuming a homogeneous expansion through average; however, for most clay materials, the expansion was non-uniform along the four directions considered. Thus, the calculated values of area-specific mass loss rate can be considered as approximate values rather than an exact one.

Overall, the Sardinian and Westewald bentonites, both considered Ca-dominated bentonites, showed a higher area-specific mass loss rate in comparison with the Na-dominated bentonites and synthetic saponites.

6.1.5 Volume of the expanded clay material or volume of the halo

The volume of the expanded clay material or volume of the halo was determined considering: (*i*) the fracture aperture; (*ii*) the radius of the pre-compacted samples; and (*iii*) the calculated outer radius (Equation 3-9). Furthermore, the volume of the expanded clay material is also determined by the thickness of the polyester blue shims and the force applied while tightening the central bolt and the bolts located along the perimeter of the artificial fractures.

Broadly, the most significant expansion occurred with Na-dominated bentonites and synthetic saponite (Asha 505, Bara-kade, and Sumecton bentonites). In contrast, the least significant expansion was observed with Ca-dominated bentonites (Turkish and Kiruna bentonites).

6.1.6 Halo's dry density

The halo's dry density was calculated considering the dry mass and volume of the expanded clay material. The dry density of the halo can vary significantly depending on the type of clay material evaluated. This variation is likely due to a higher mass of clay, even in small quantities, as well as the water retention and mineral phases present in the clay matrix of different materials. By and large, the Asha 505 and MX80 bentonites showed the highest values on the halo's dry density among the Na-dominated bentonites, while the most significant values on the halo's dry density are those exhibited by the Moroccan, CaBen FLB and Kiruna bentonites.

6.1.7 X-ray fluorescence (XRF)

XRF data was collected from subsamples of the remanent sample at the ring-shaped perforation and reference materials that were not subjected to dialysis. Detailed analysis of XRF-based elemental composition showed that for the Na-dominated bentonites, there was a decrease in Mg, Ca, K, Cl and SO_3 and an increase in Na concentrations, while the synthetic saponite exhibited an increase in Mg, Cl and SO_3, and a decrease in Na, Ca and K percentages. However, the data collected on the Ca-dominated bentonites showed significant differences between the different bentonites analysed. At large, the Na concentration increases for all the samples as a result of the homogenisation process, with the exception of the Kiruna sample, while the SO_3 percentages decrease for the Moroccan, Turkish, Sardinian and CaBen FLB bentonite samples. In the case of Cl concentration, it decreases for the Moroccan, Sardinian and CaBen FLB bentonites whilst increasing for the Westerwald and Turkish bentonites.

6.1.8 Clay material's electrical conductivity

As a general rule, there are several factors that can exert variations over the EC in clays, such as; moisture retention, the presence of dissolved salts, temperature changes, and the ion concentration and size, occupying the interlayer space. While measuring the EC, there were changes in temperature that may influence the decrease or increase in EC. Ultimately, the high Na concentration in the case of the Westerwald samples may explain the large increase in EC since the hydrophilicity of Na is larger than Ca. Nonetheless, the Bara-kade, Sumecton, Turkish, Sardinian and Westerwald samples reflected an apparent decrease in their electrical conductivity despite the fact that there was an increase in Na percentage with respect to Ca. Therefore, and despite the reverse dialysis, the influence of dissolved salts cannot be ruled out in the EC decrease observed in the case of the Bara-kade, Sumecton, Turkish, Sardinian and Westerwald bentonites.

6.2 Further work

As a continuation of this experimental programme, several challenges could be addressed and are following described:

1. To have better control over the initial testing conditions, it is proposed to measure the initial water content three times per sample to be run, applying the average of those three values as representative of the initial water content before adjusting the water saturation to 20 %.
2. Improve the dialysis method for Kiruna bentonite to promote the exchange at the exchange complex.
3. Developing a methodology to accurately measure the expansion of the clay materials, facilitating a veracious determination of the total surface area of the expanded clay facing the fracture, the area-specific mass loss rate, the volume of the expanded clay material, and the halo's dry density.
4. Finally, during the sedimentation tests, leakage and bubble formation within the artificial fractures were detected. The formed bubbles intercepted with the homogenous development of the halo from the investigated different clay materials. Thus, it is proposed to engineer new fractures that will diminish bubble formation and avoid leakage. Furthermore, the artificial fractures for this experimental programme were designed for flow and horizontal experiments and, therefore, a new experimental design is required to study the effect of buffer erosion in vertical fractures.

7 References

SKB's (Svensk Kärnbränslehantering AB) publications can be found at www.skb.com/publications.

Alonso U, Missana T, Gutiérrez M G, Morejón J, Mingarro M, Fernández A M, 2019. CIEMAT studies within the POSKBAR Project. Bentonite expansion, sedimentation and erosion in artificial fractures. SKB TR-19-08, Svensk Kärnbränslehantering AB.

Bentonite Performance Minerals LLC, 1928. Bara-Kade granular. Available at: https://www.bentonite.com/en/products/bara-kade-granular [3 December 2023].

Emmerich K, 2013. Chapter 2.13 - Full Characterization of Smectites. Developments in Clay Science 5, 381–404.

Fontaine F, Christidis G E, Yans J, Hollanders S, Hoffman A, Fagel N, 2020.

Characterization and origin of two Fe-rich bentonites from Westerwald (Germany). Applied Clay Science 187, 105444.

Gang Z, Yunliang L, Jin L, Zutang W, Ke W, Jiyong J, Shunshun T, Bingwen Q, Yurong Z, Xiangrong Z, 2019. Dynamic behavior of clay with different water content under planar shock conditions. International Journal of Impact Engineering 129, 57–65.

Hedström M, Ekvy Hansen E, Nilsson U, 2016. Montmorillonite phase behaviour. Relevance for buffer erosion in dilute groundwater. SKB TR-15-07, Svensk Kärnbränslehantering AB.

IGD-TP, 2019. KiNa: Kiruna Natural Analogue. Available at: https://igdtp.eu/activity/kina-kiruna-natural-analogue/ [3 December 2023].

KI, 1943. Kunimine Industries. Available at: https://www.kunimine.co.jp/ [3 December 2023].

Lundgren C, Johannesson L-E, 2020. Optimering av buffertpellets för KBS-3. Laboratorieförsök på fyra olika pellets. SKB R-19-25, Svensk Kärnbränslehantering AB.

MP, 2009. Malvern Panalytical. Available at: https://www.malvernpanalytical.com [3 December 2023].

SKB, 2022. Post-closure safety for the final repository for spent nuclear fuel at Forsmark. Main report, PSAR version. SKB TR-21-01, Svensk Kärnbränslehantering AB.

Svensson D, Dueck A, Nilsson U, Olsson S, Sandén T, Lydmark S, Jägerwall S, Pedersen K, Hansen S, 2011. Alternative buffer material. Status of the ongoing laboratory investigation of reference materials and test package 1. SKB TR-11-06, Svensk Kärnbränslehantering AB.

Svensson D, Eriksson P, Johannesson L-E, Lundgren C, Bladström T, 2019. Development and testing of methods suitable for quality control of bentonite as KBS-3 buffer and backfill. SKB TR-19-25, Svensk Kärnbränslehantering AB.

8 Appendix 1 – Sedimentation test photos of the different clay materials investigated

The photos shown in the present appendix were taken by Daniel Svensson and Hanna Kronberg (SKB).

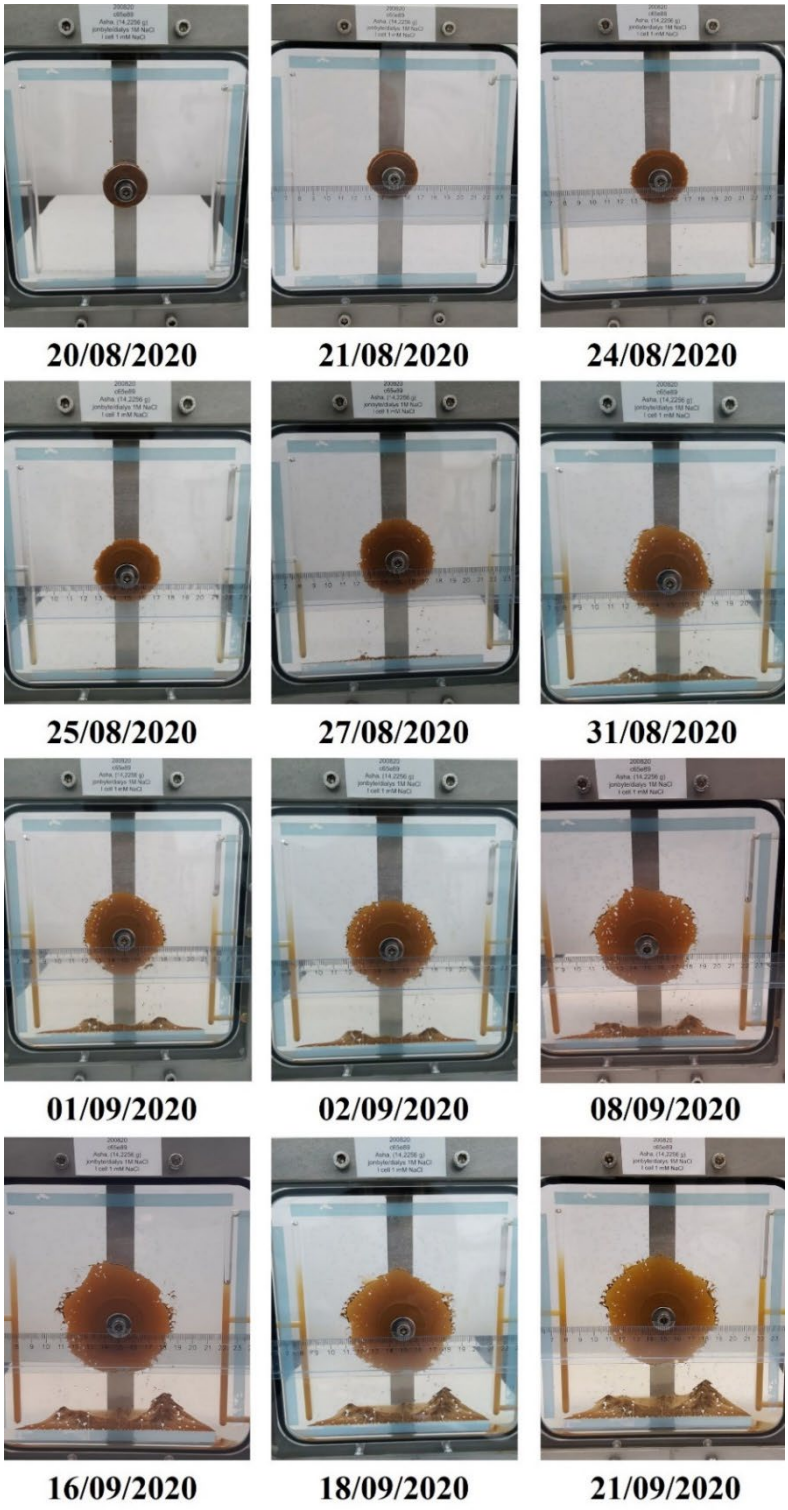

Figure A1- 1: *Asha 505 (32 days).*

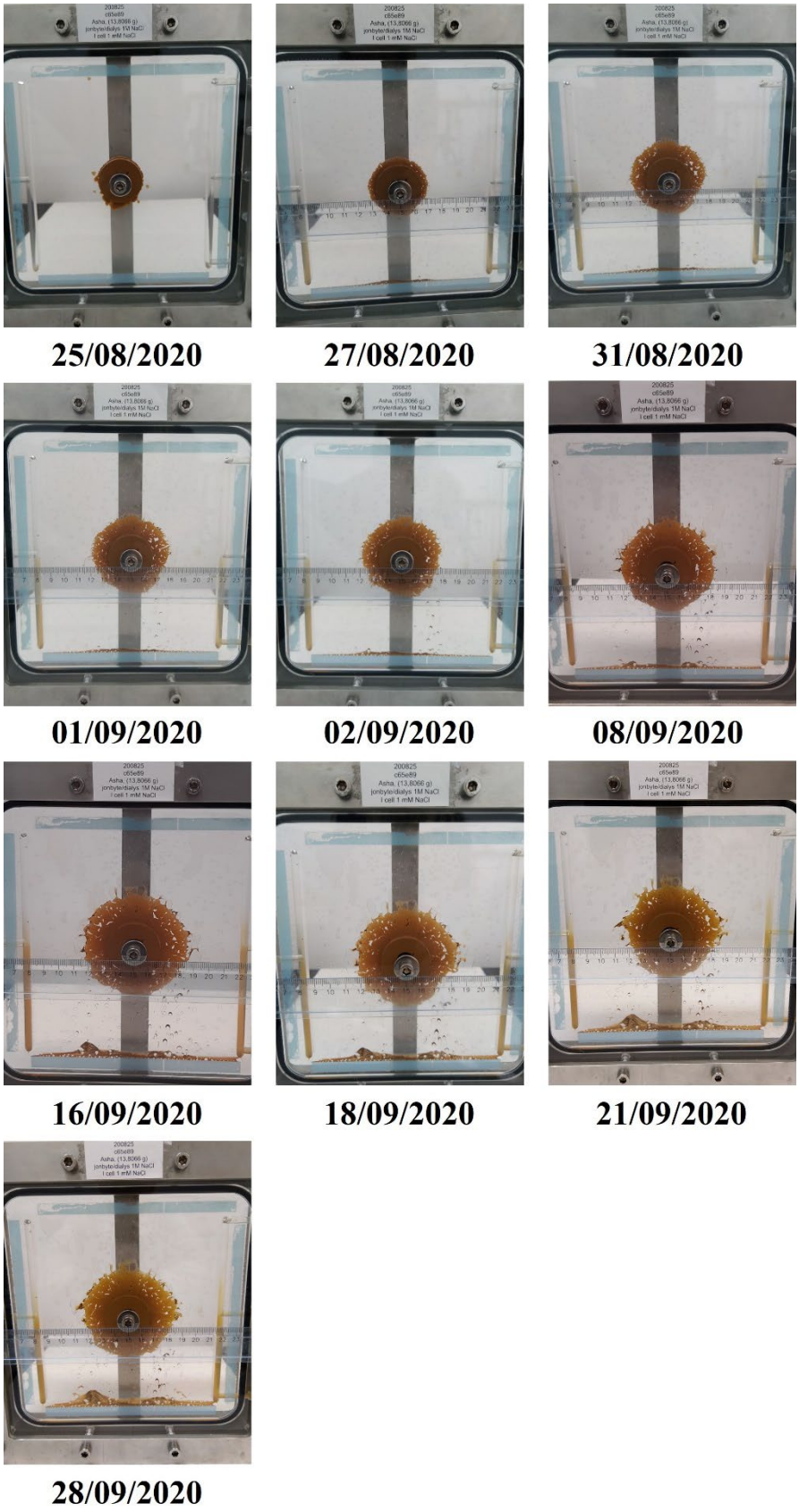

Figure A1- 2: *Asha 505 (34 days).*

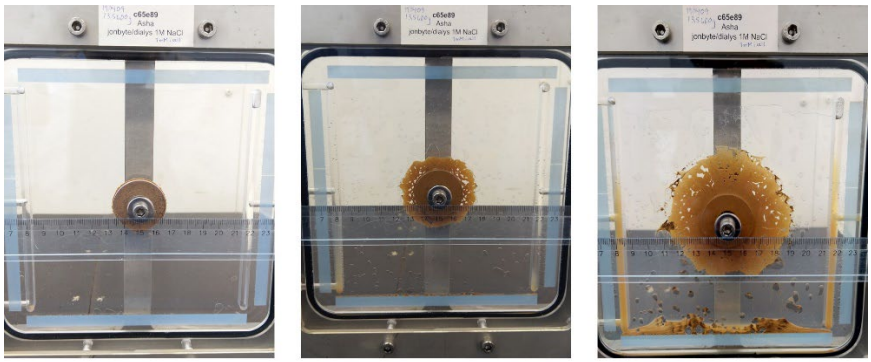

25/08/2020 27/08/2020 31/08/2020

Figure A1- 3: *Asha 505 (69 days).*

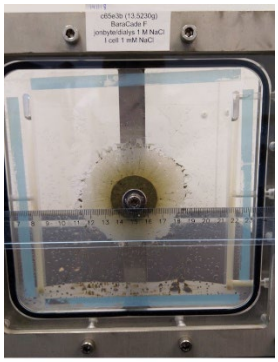

19/12/2019

Figure A1- 4: *Bara-kade (31 days). Only one photo was taken at the termination of the experiment.*

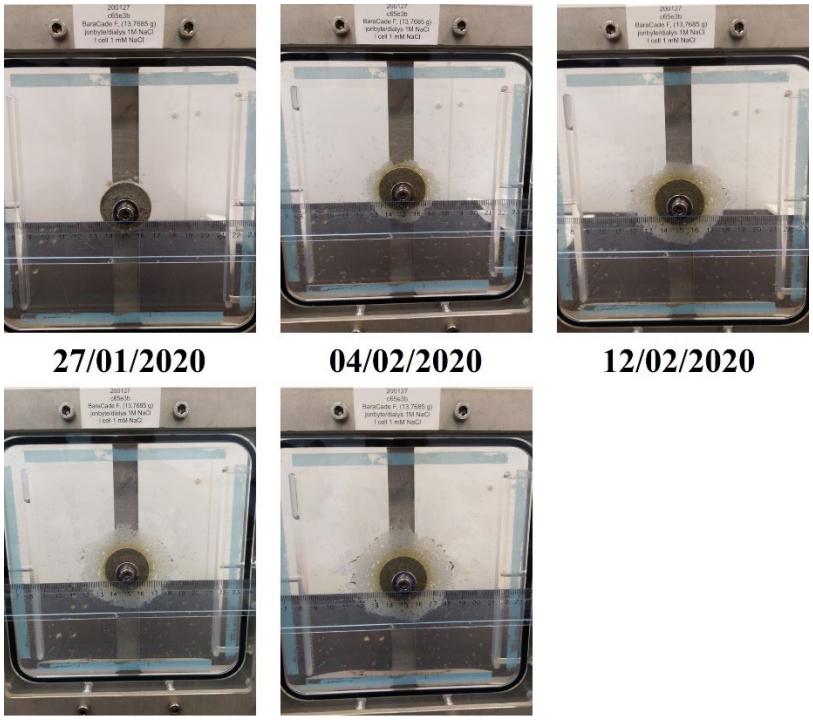

27/01/2020 04/02/2020 12/02/2020

17/02/2020 29/02/2020

Figure A1- 5: *Bara-kade (33 days).*

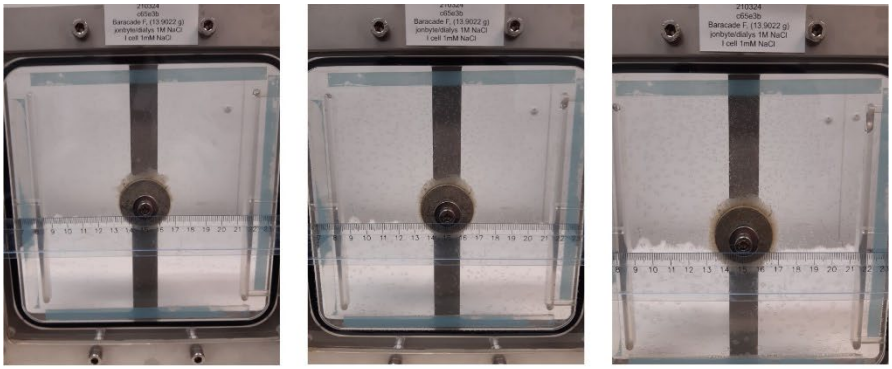

24/03/2021 26/03/2021 29/03/2021

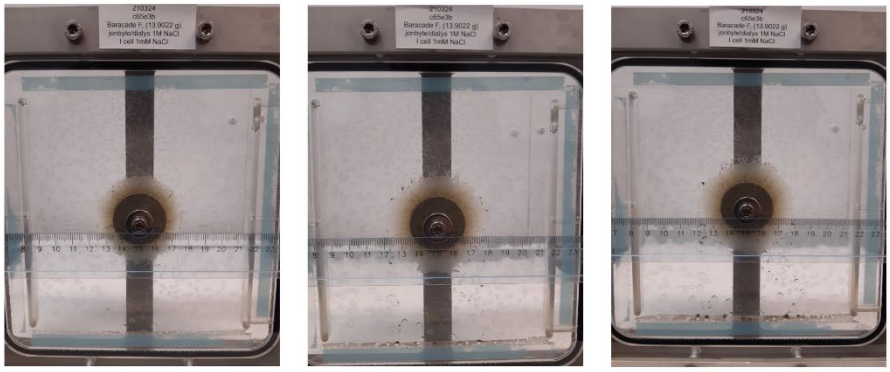

01/04/2021 07/04/2021 12/04/2021

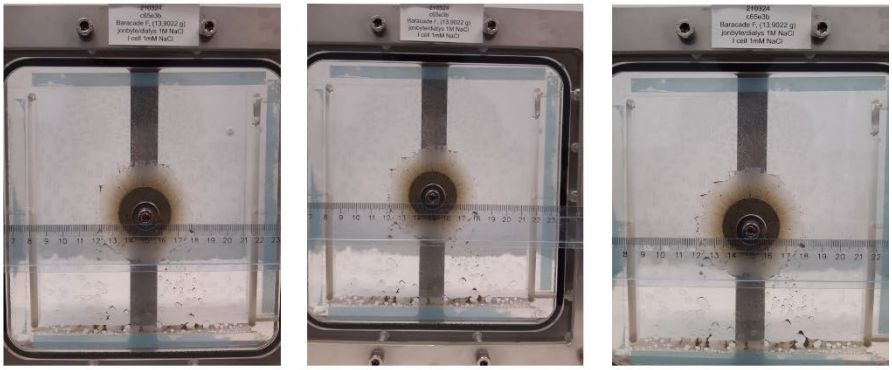

15/04/2021 19/04/2021 23/04/2021

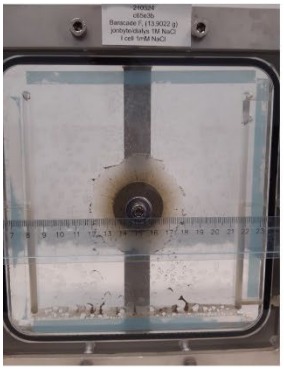

26/04/2021

Figure A1- 6: *Bara-kade (33 days).*

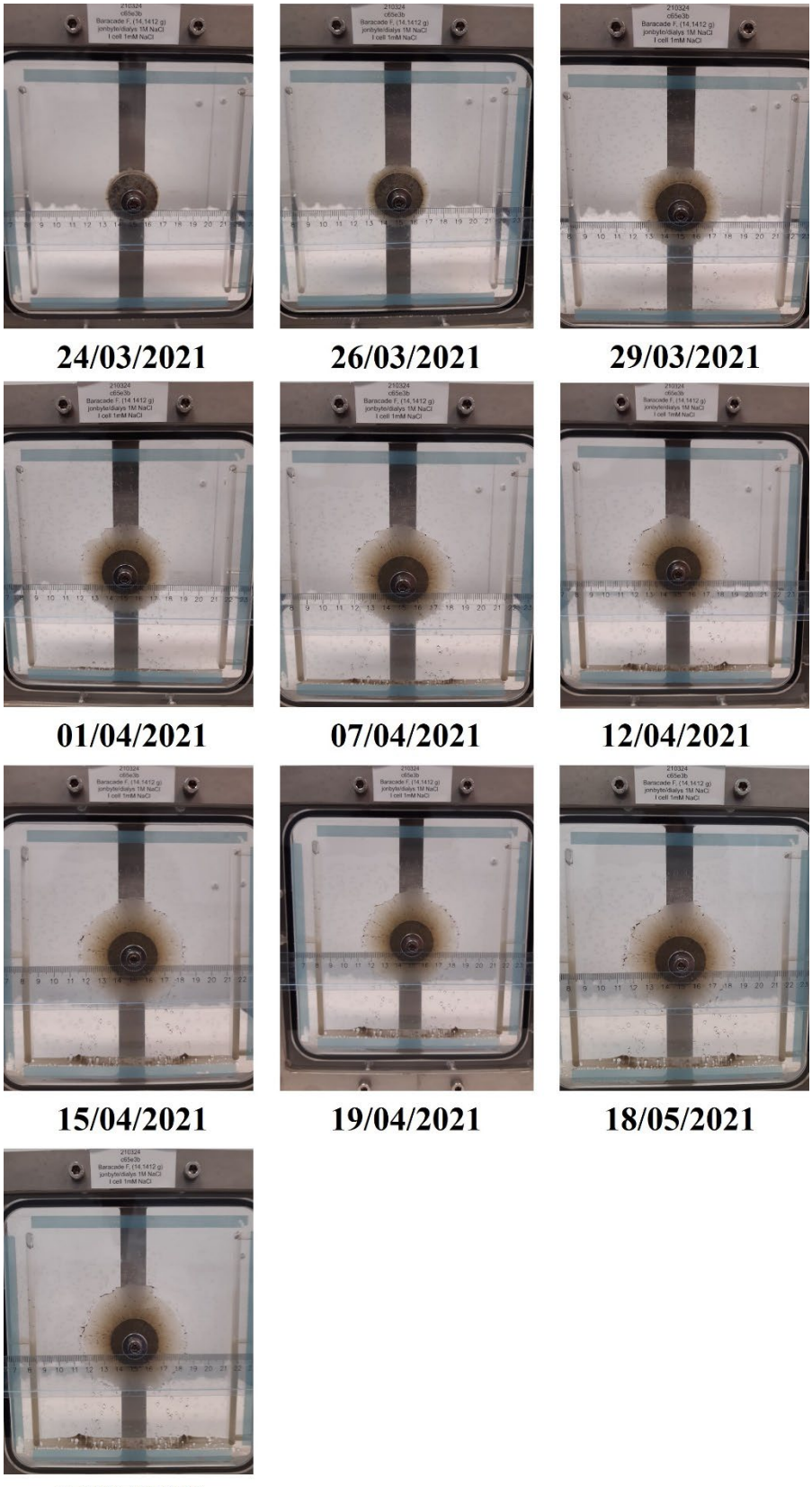

Figure A1- 7: *Bara-kade (63 days).*

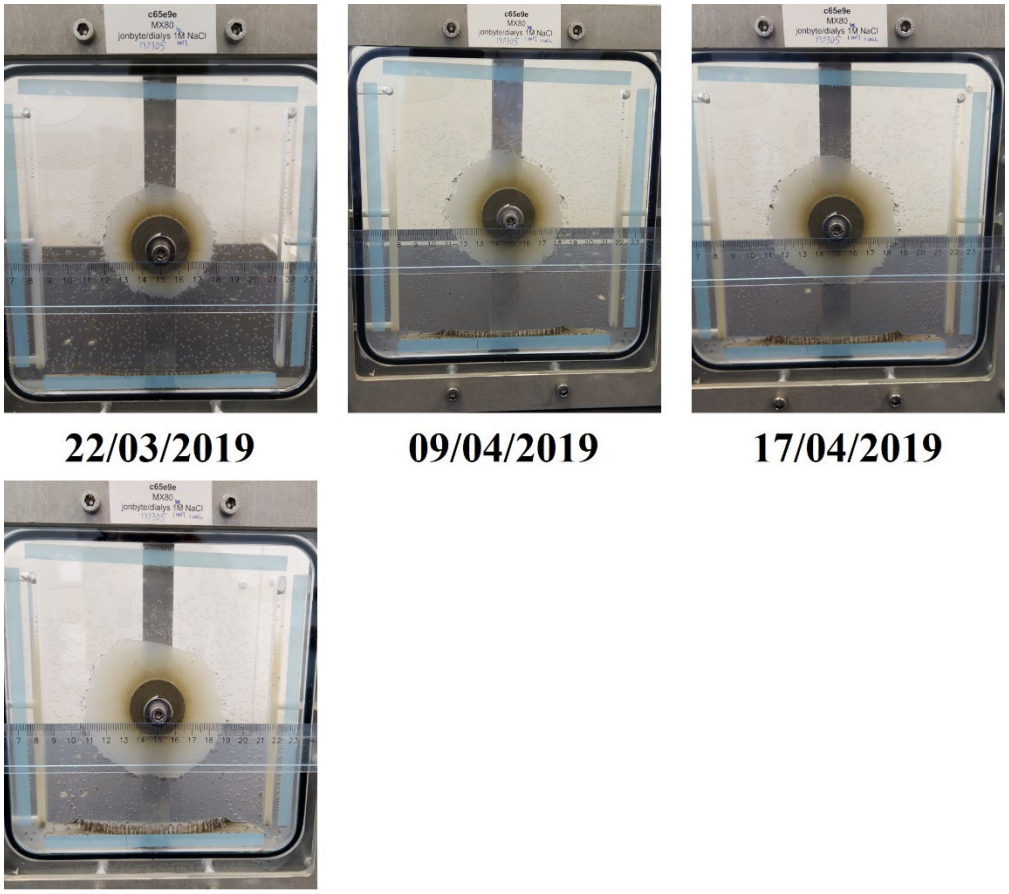

Figure A1- 8: *MX80 (233 days).*

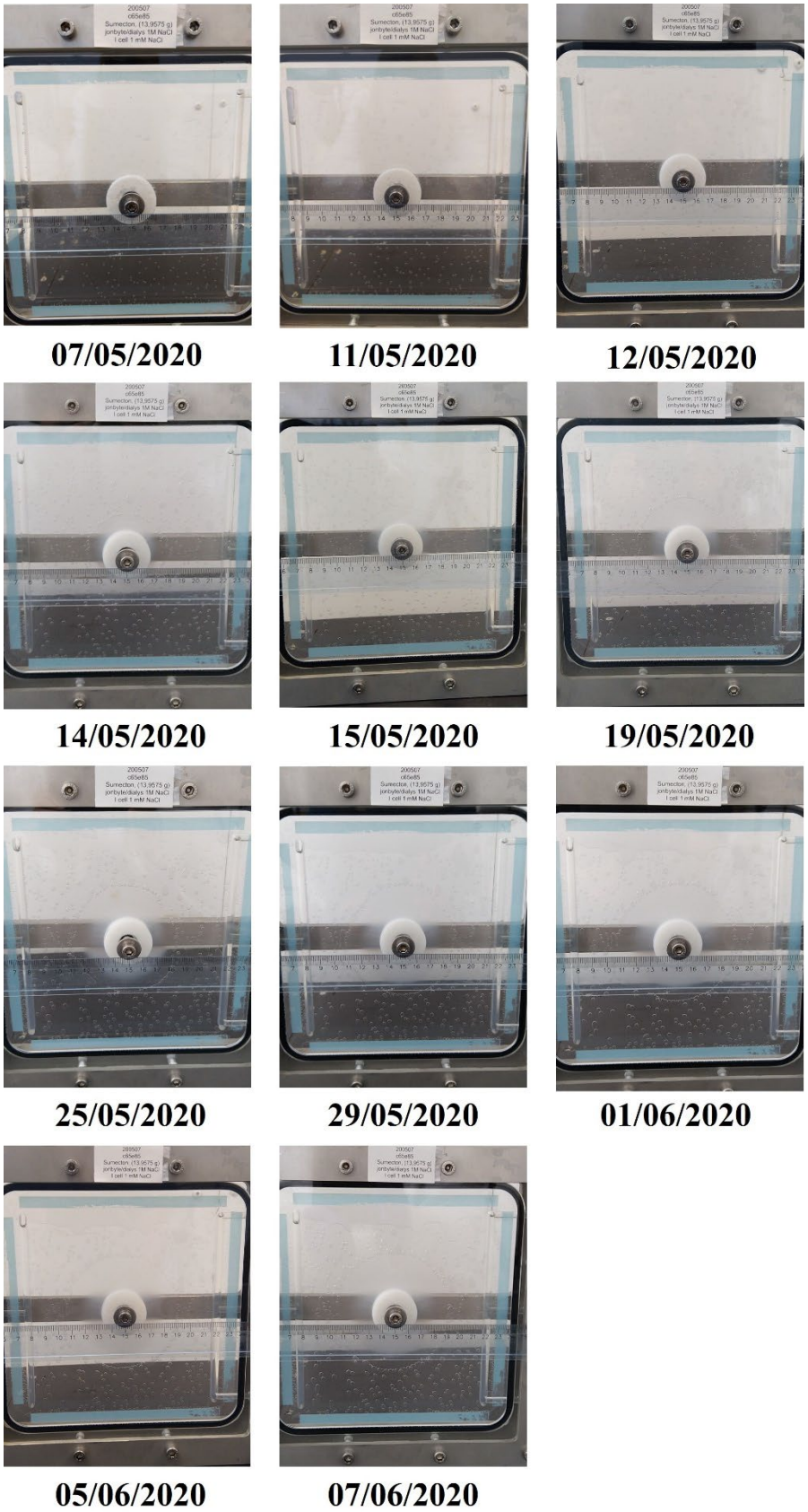

Figure A1- 9: *Sumecton (31 days).*

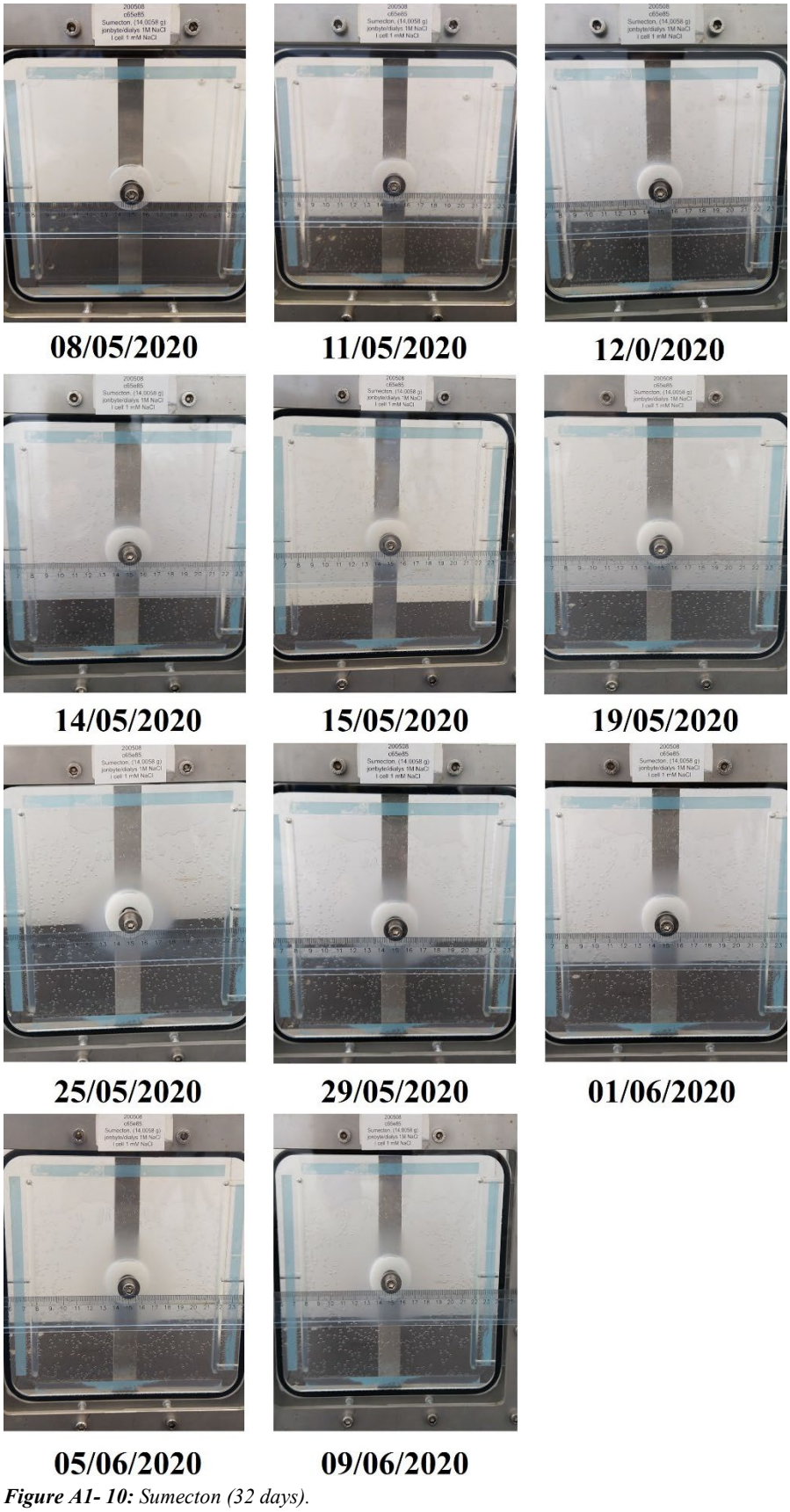

Figure A1- 10: *Sumecton (32 days).*

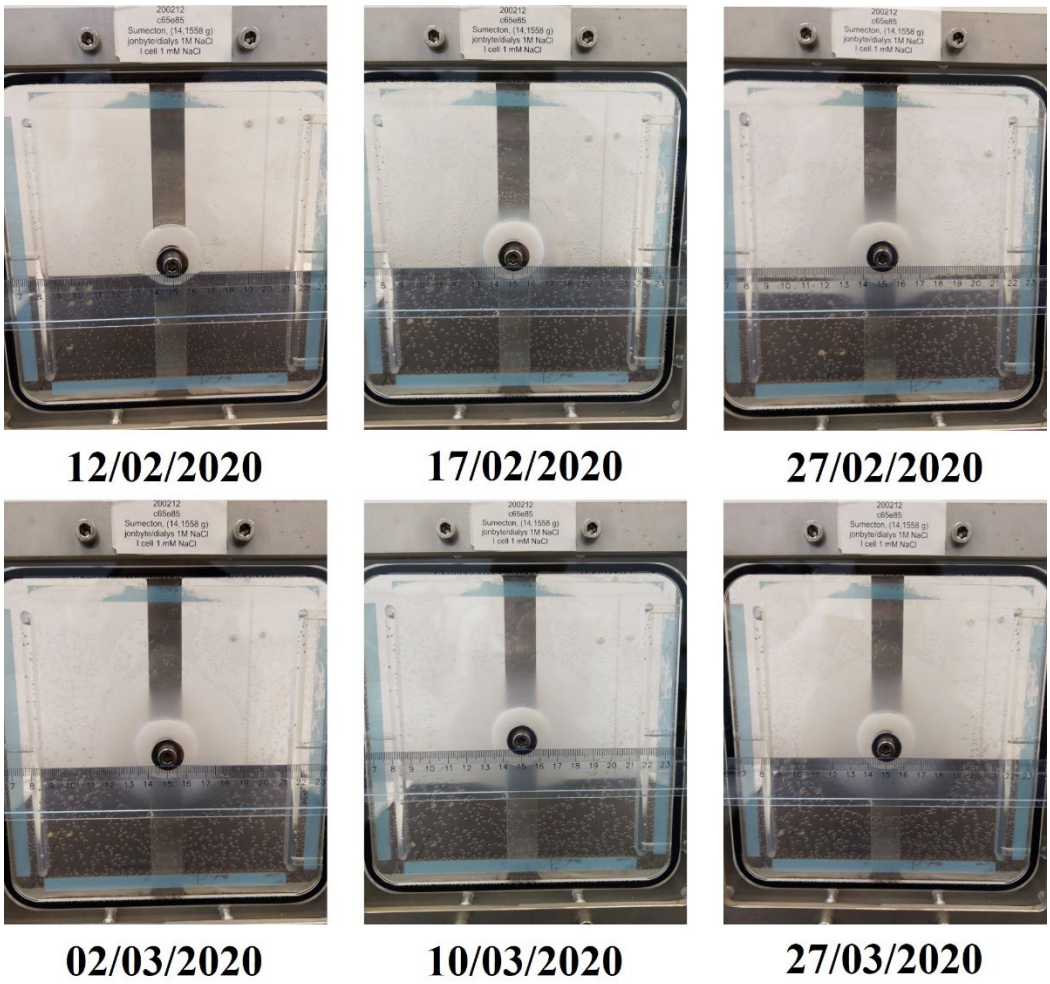

Figure A1- 11: *Sumecton (44 days).*

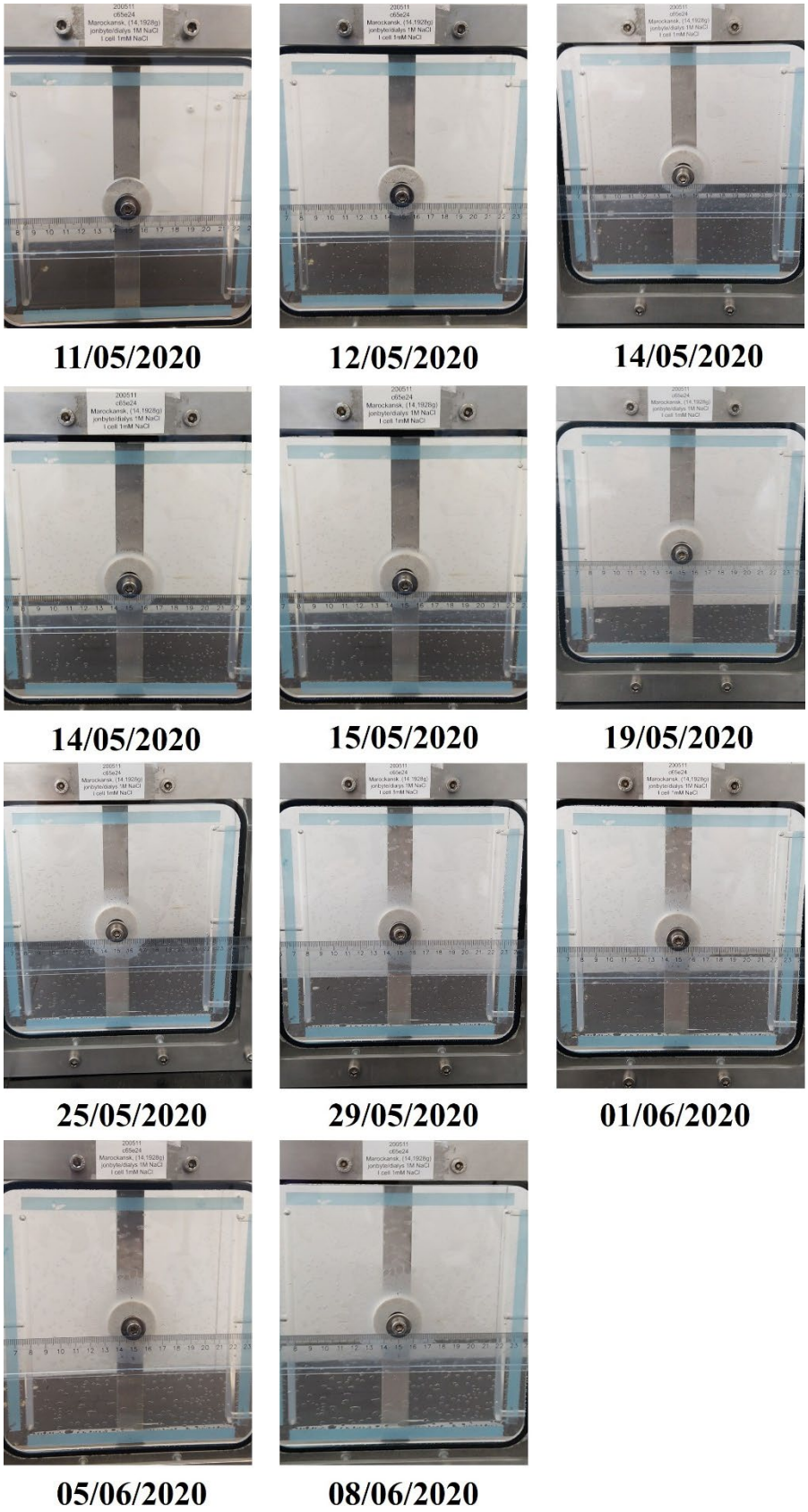

Figure A1- 12: *Moroccan (28 days).*

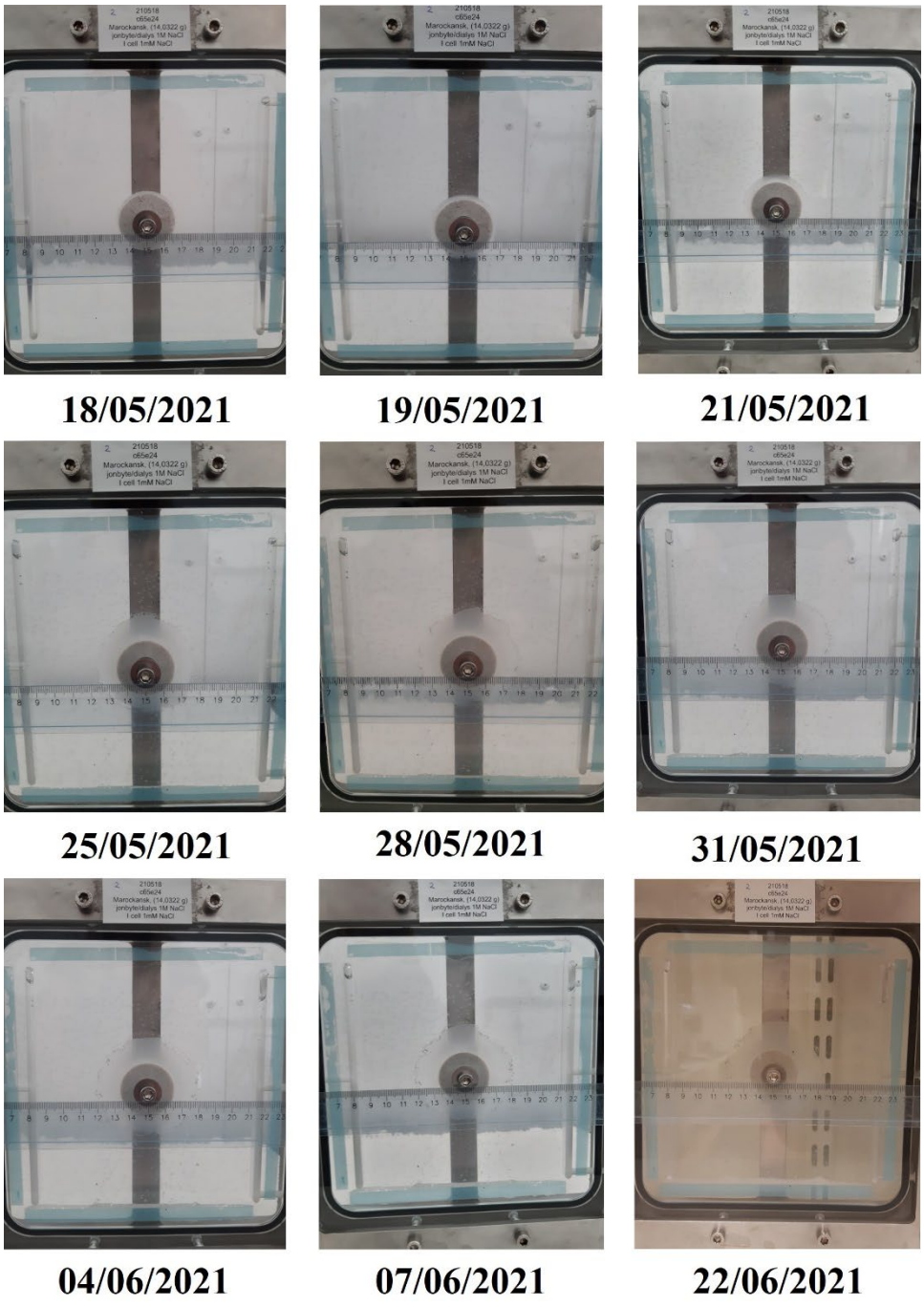

Figure A1- 13: *Moroccan (35 days).*

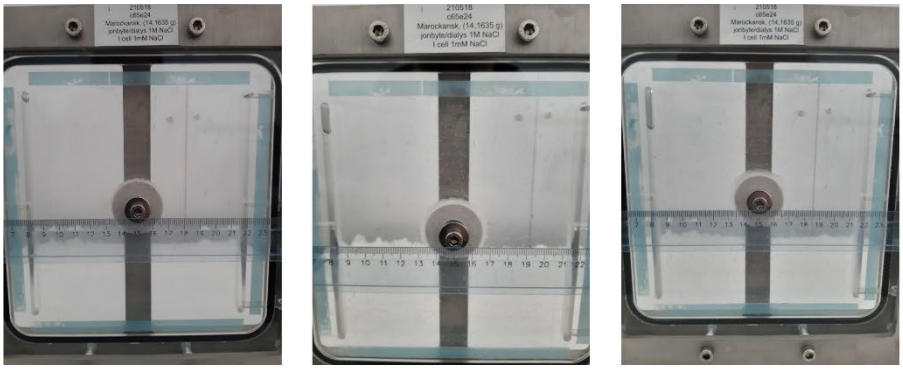

21/05/2021 23/05/2021 25/05/2021

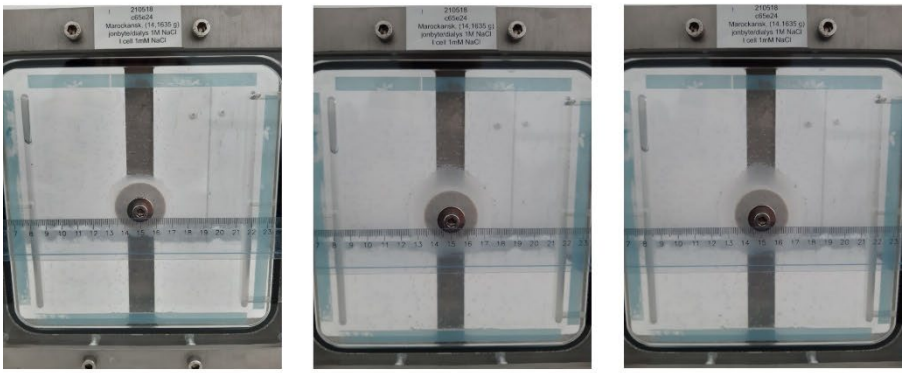

27/05/2021 29/05/2021 30/05/2021

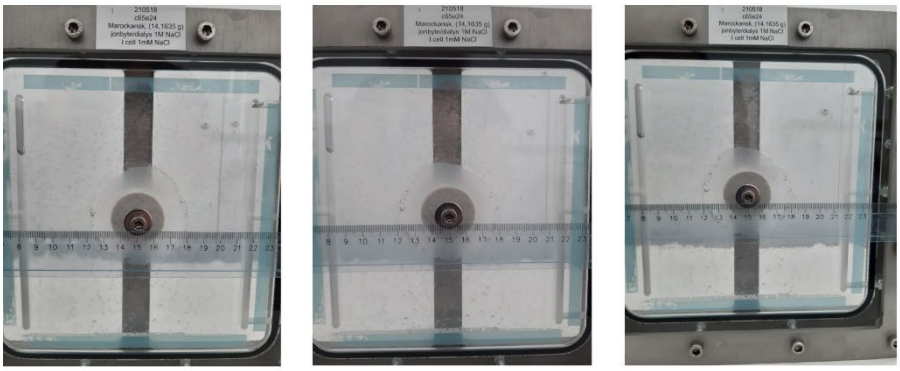

31/05/2021 04/06/2021 07/06/2021

25/06/2021

Figure A1- 14: *Moroccan (35 days).*

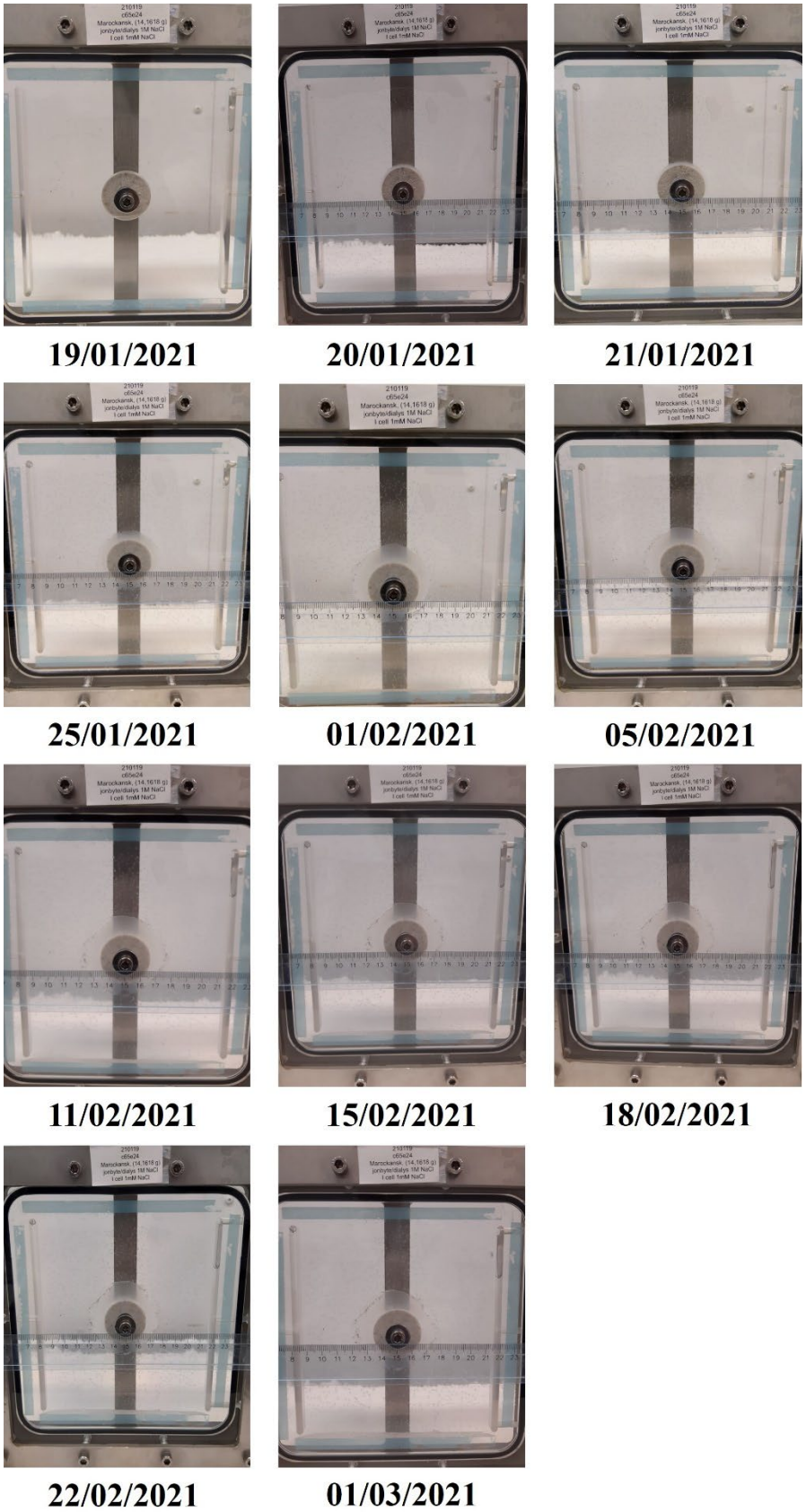

Figure A1- 15: *Moroccan (41 days).*

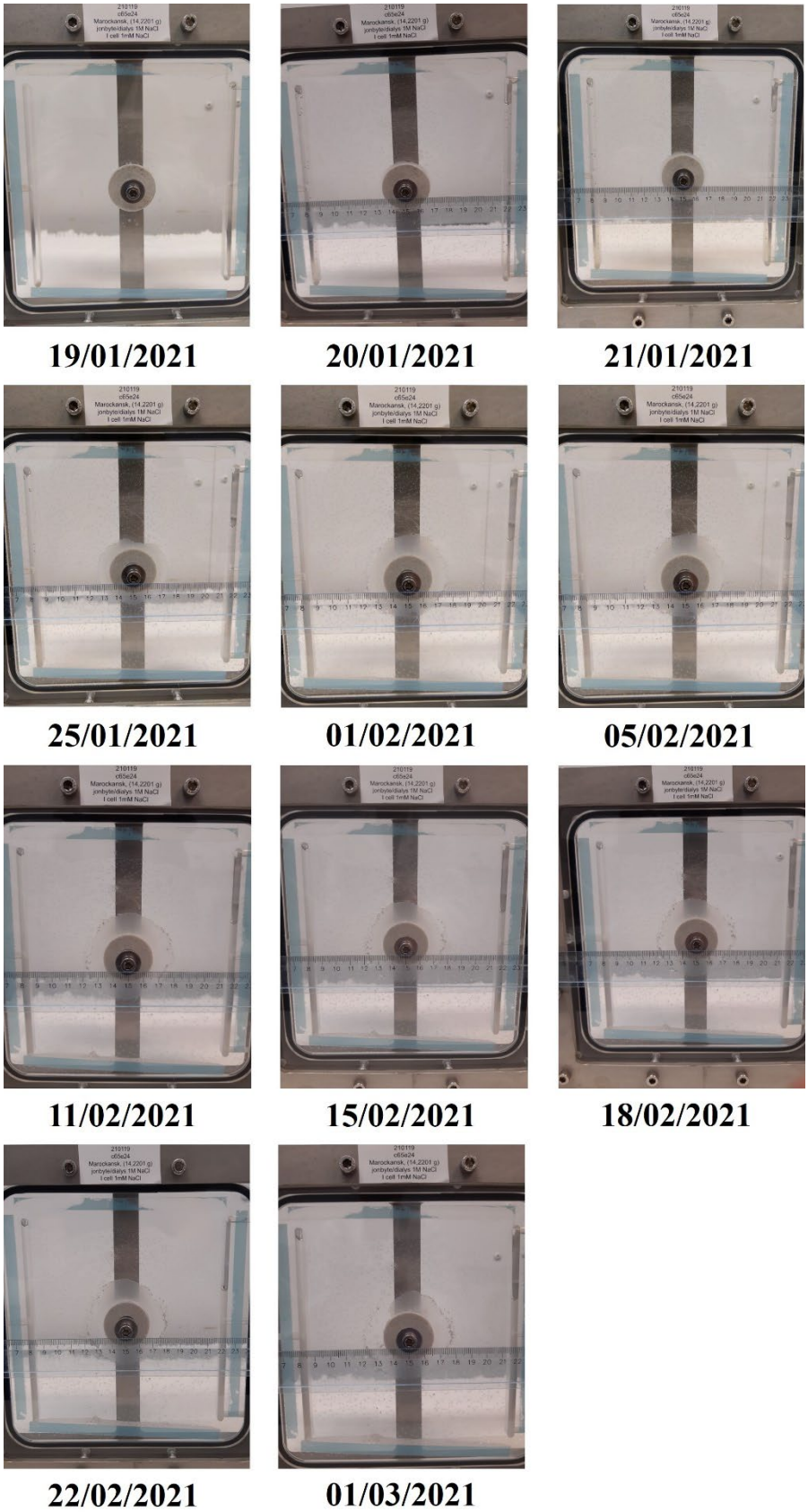

Figure A1- 16: *Moroccan (41 days).*

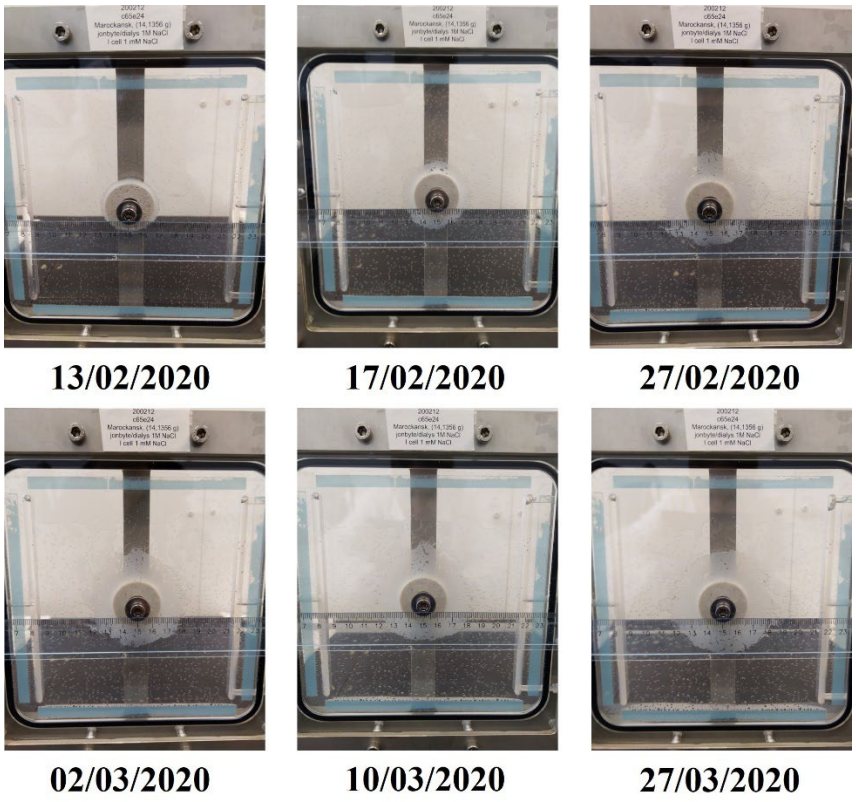

Figure A1- 17: *Moroccan (44 days).*

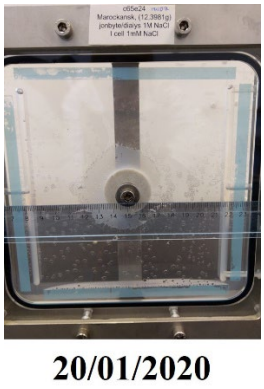

Figure A1- 18: *Moroccan (74 days). Only one photo was taken at the termination of the experiment.*

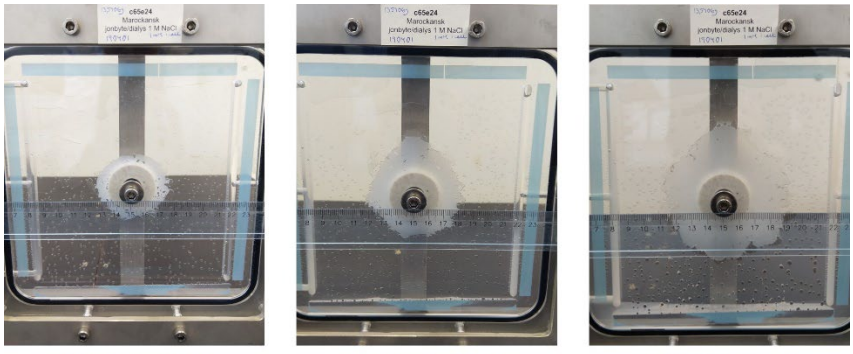

Figure A1- 19: *Moroccan (74 days).*

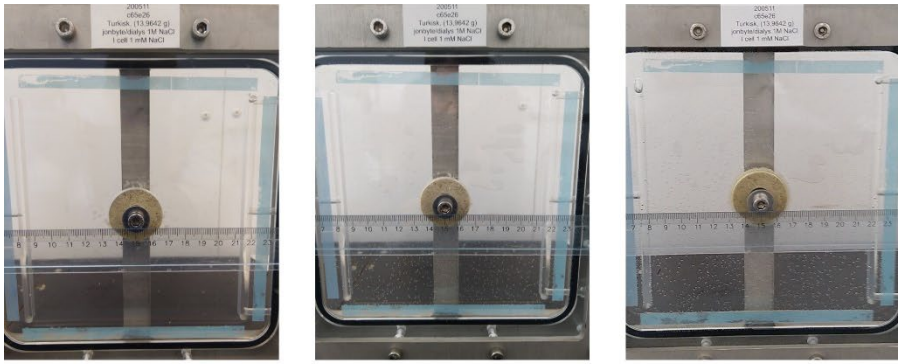

11/05/2020 12/05/2020 14/05/2020

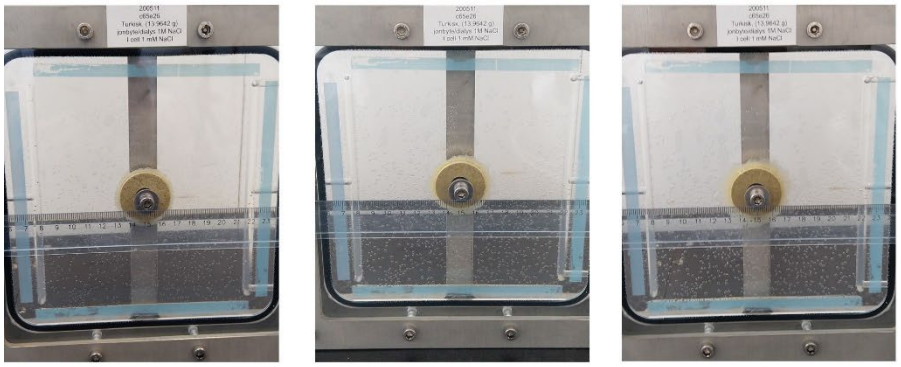

15/05/2020 19/05/2020 25/05/2020

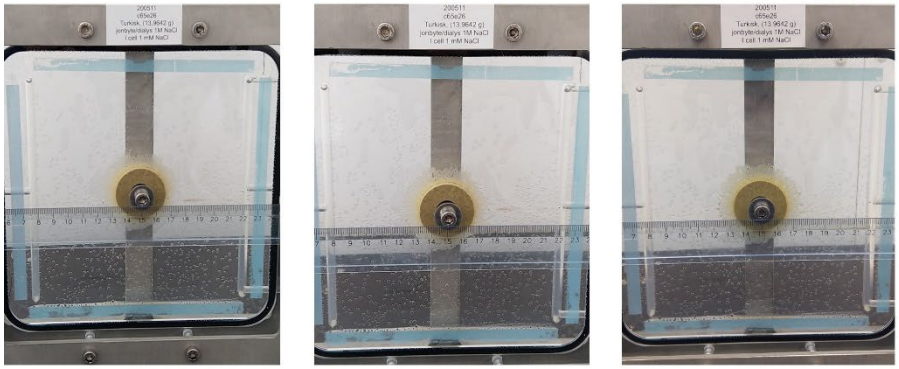

29/05/2020 01/06/2020 05/06/2020

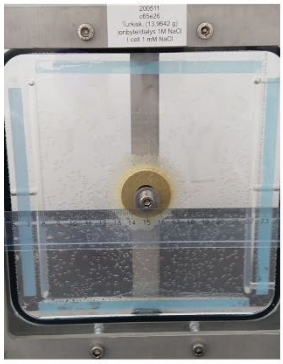

08/06/2020

Figure A1- 20: *Turkish (28 days).*

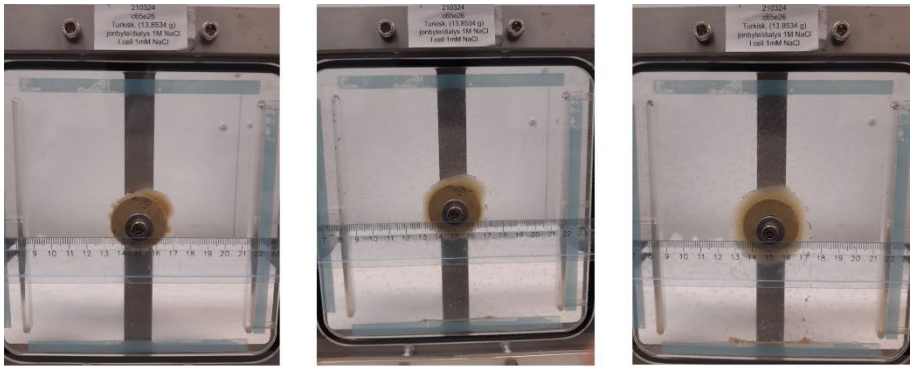

24/03/2021 26/03/2021 29/03/2021

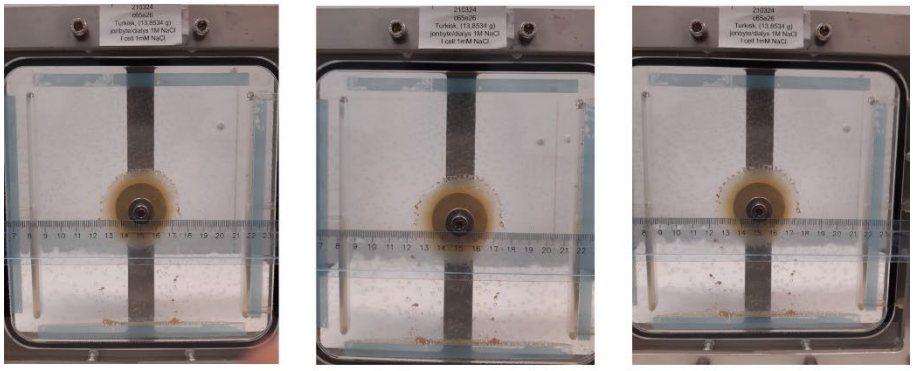

01/04/2021 07/04/2021 12/04/2021

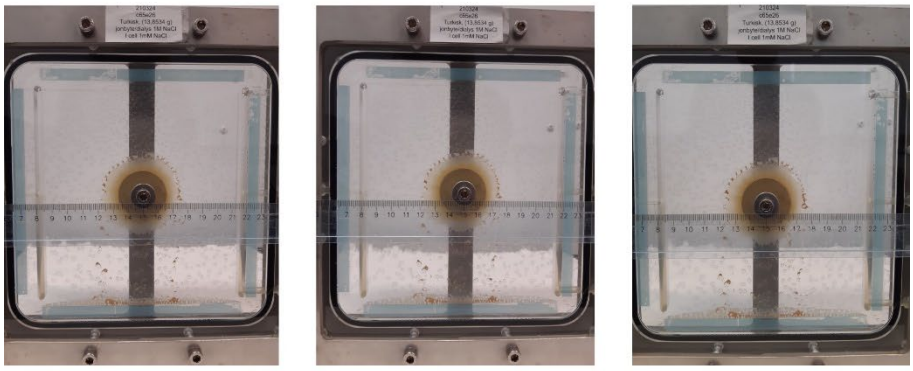

15/04/2021 19/04/2021 23/04/2021

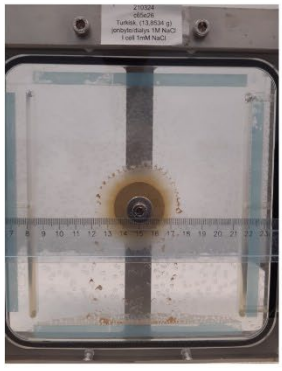

26/04/2021

Figure A1- 21: *Turkish (33 days).*

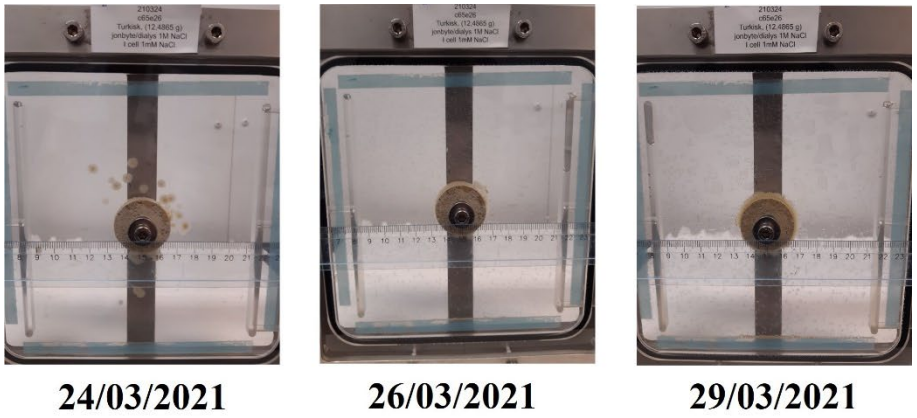

Figure A1- 22: *Turkish (33 days).*

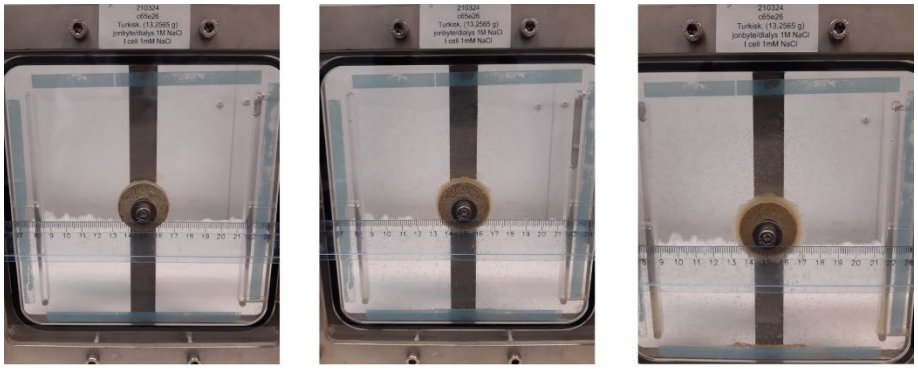

24/03/2021 26/03/2021 29/03/2021

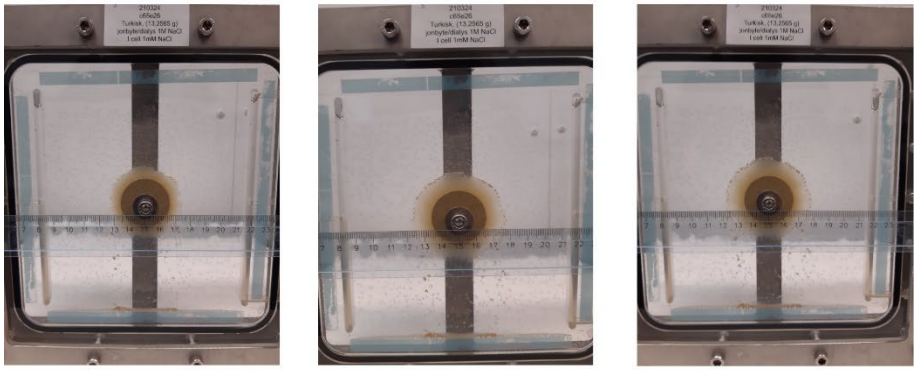

01/04/2021 07/04/2021 12/04/2021

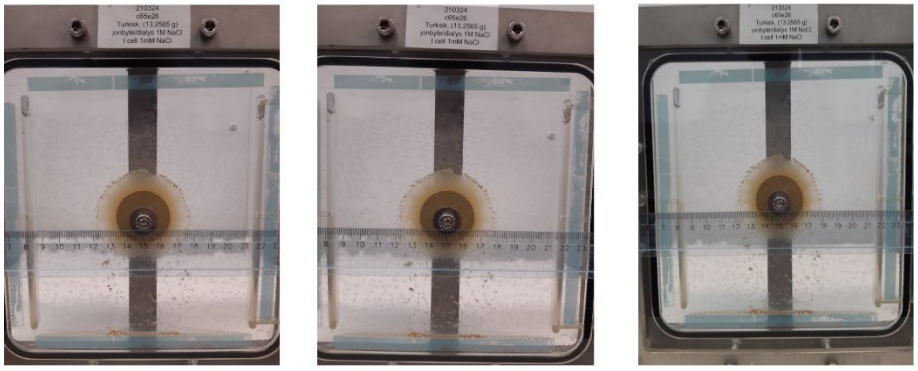

15/04/2021 19/04/2021 23/04/2021

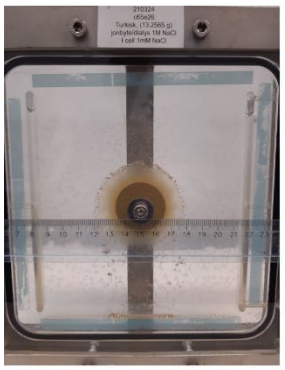

26/04/2021

Figure A1- 23: *Turkish (33 days).*

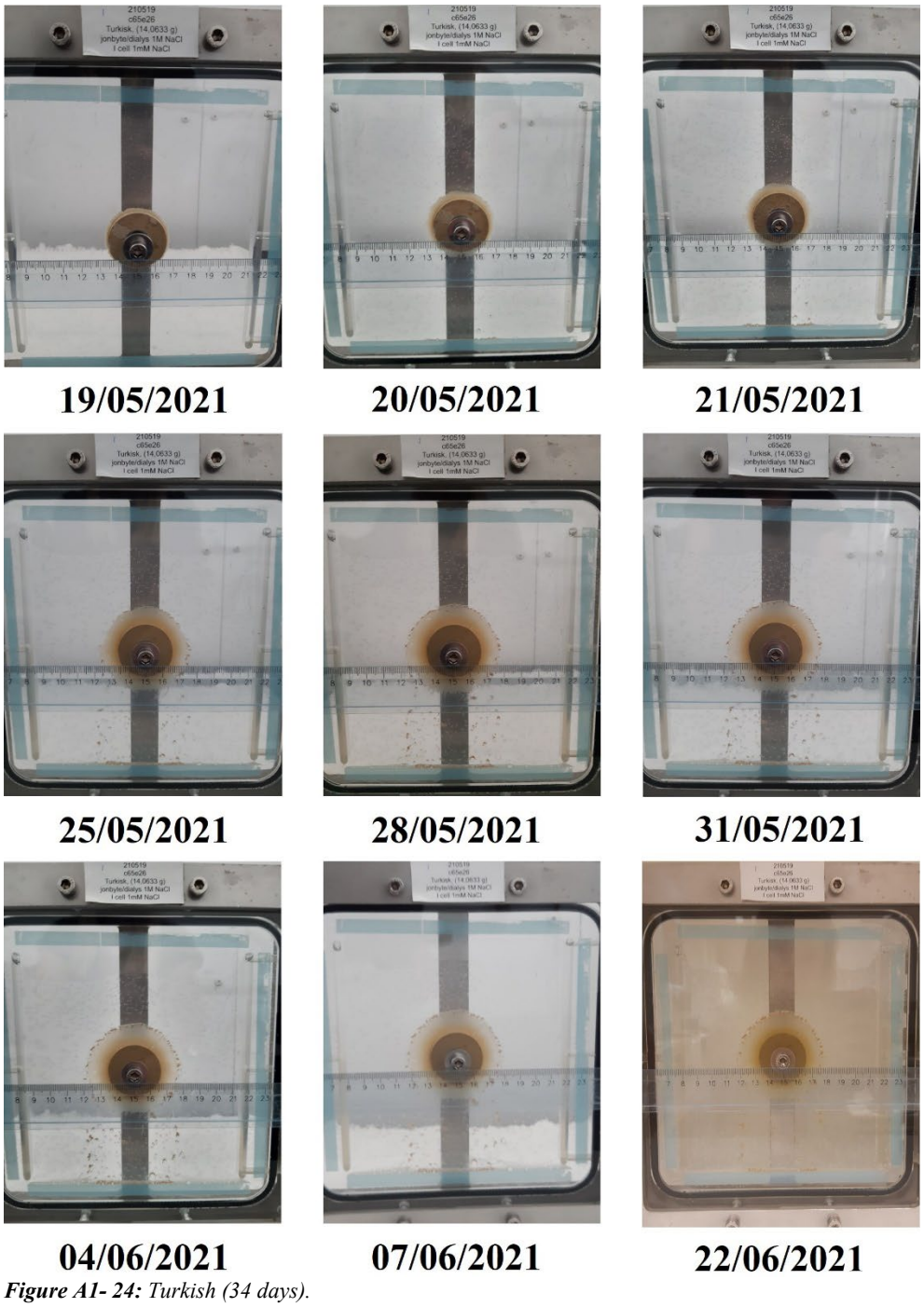

Figure A1- 24: *Turkish (34 days).*

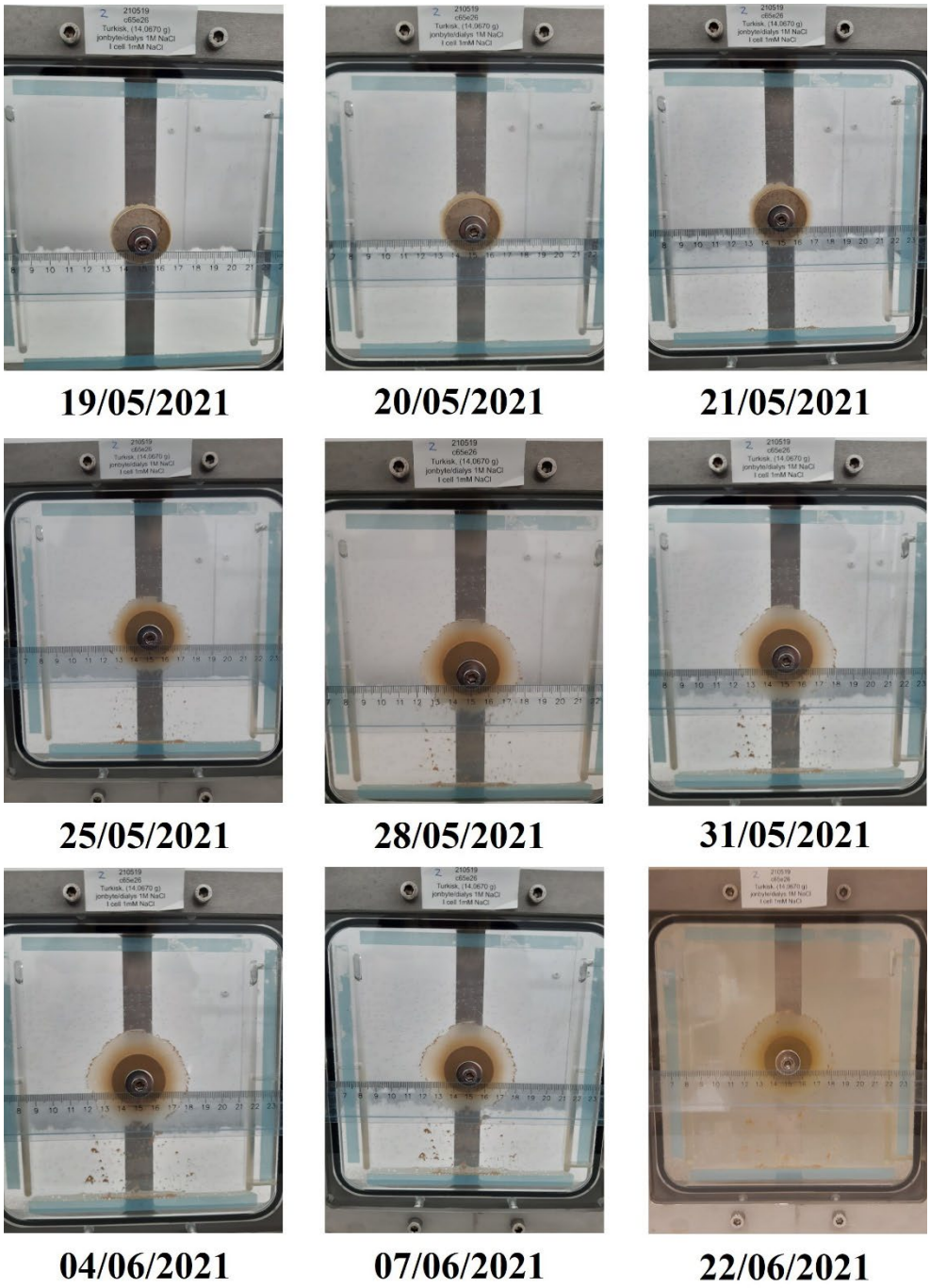

Figure A1- 25: *Turkish (34 days).*

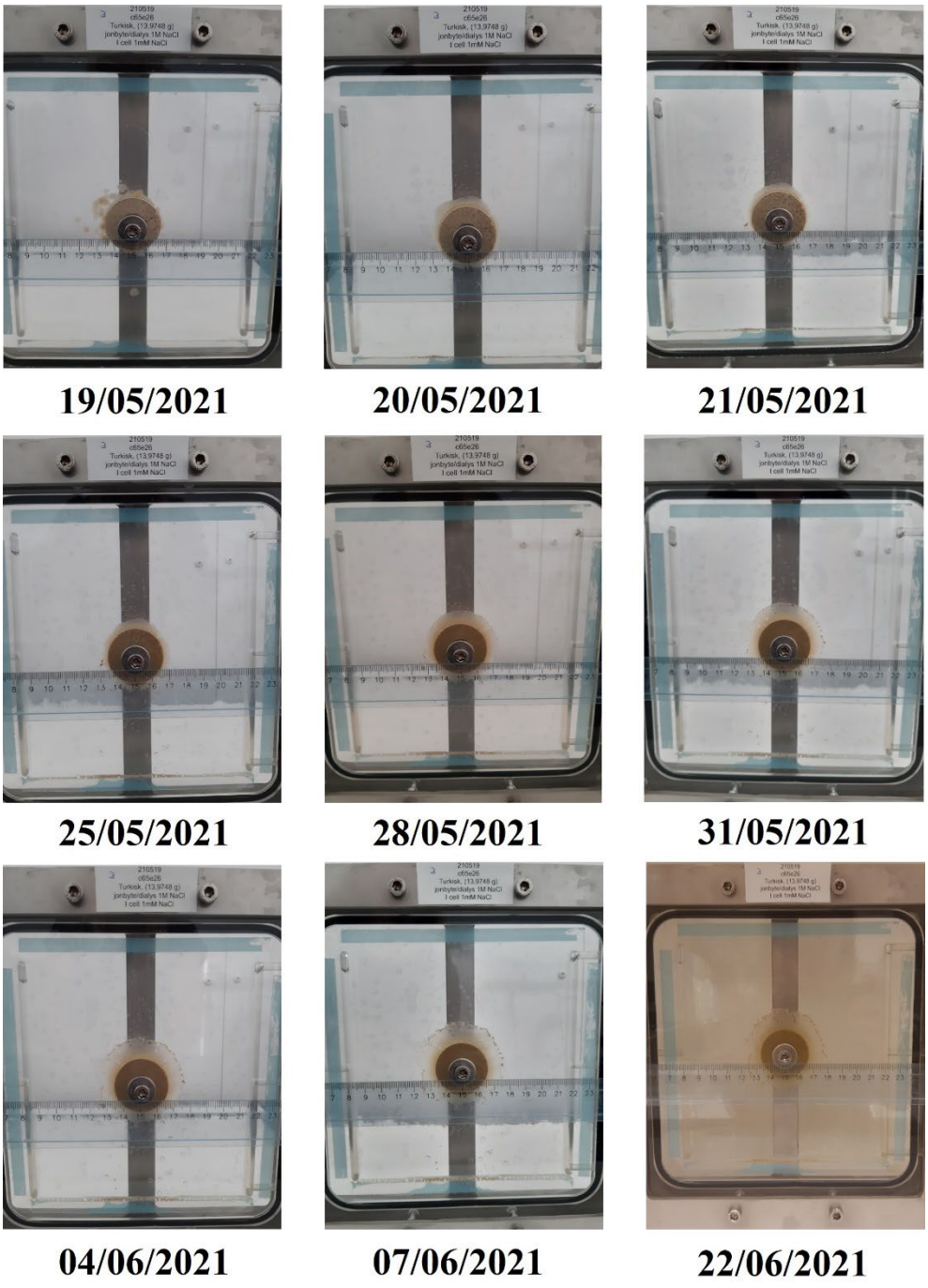

Figure A1- 26: *Turkish (34 days).*

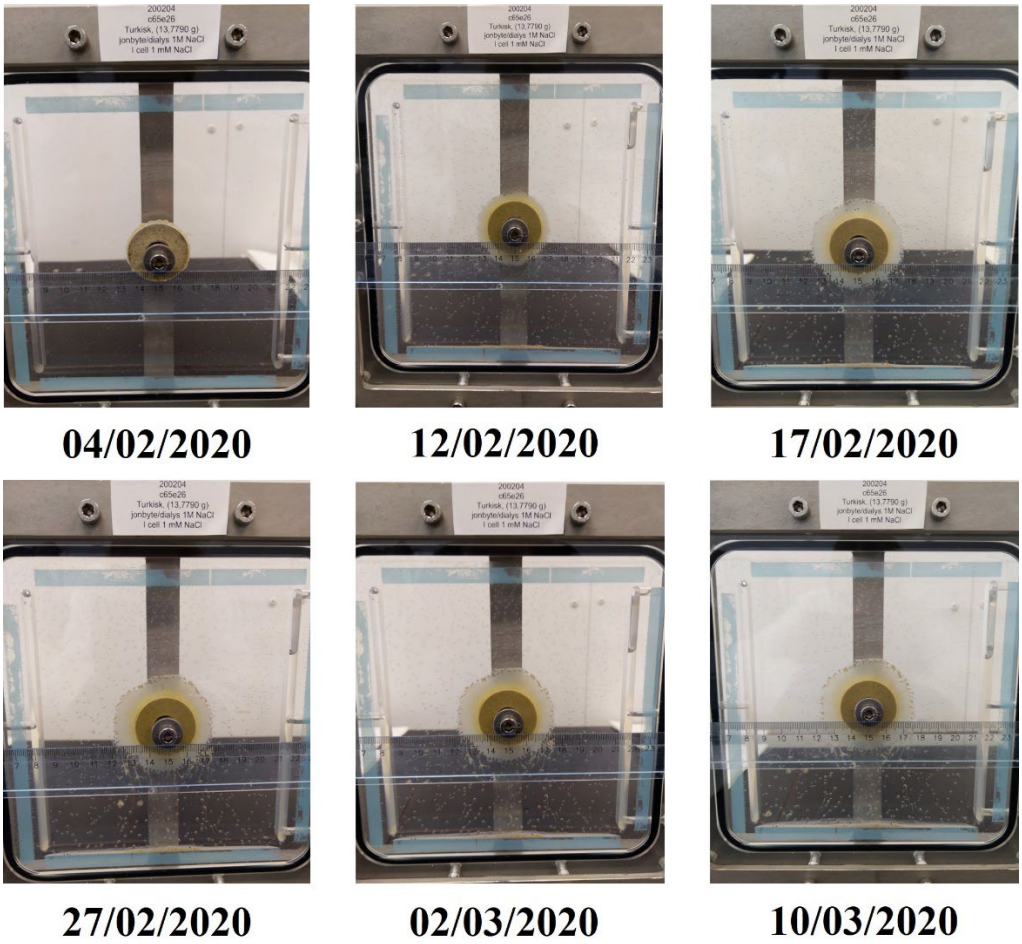

Figure A1- 27: *Turkish (35 days).*

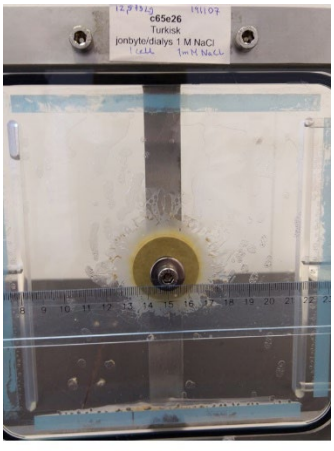

Figure A1- 28: *Turkish (74 days). Only one photo was taken at the termination of the experiment.*

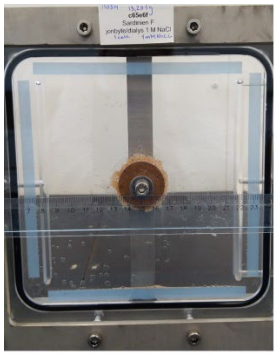

14/03/2019

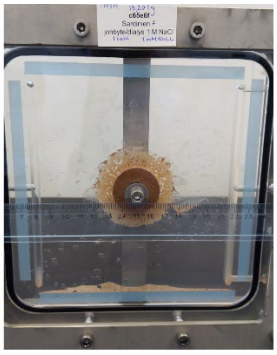

26/03/2019

03/04/2019

11/04/2019

Figure A1- 29: *Sardinian (28 days).*

27/01/2020

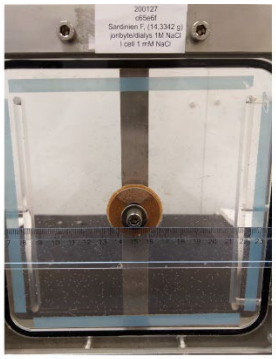

28/01/2020

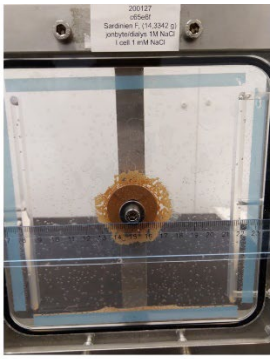

04/02/2020

12/02/2020

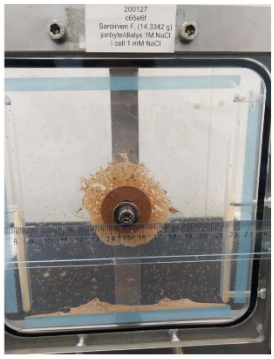

17/02/2020

27/02/2020

Figure A1- 30: *Sardinian (31 days).*

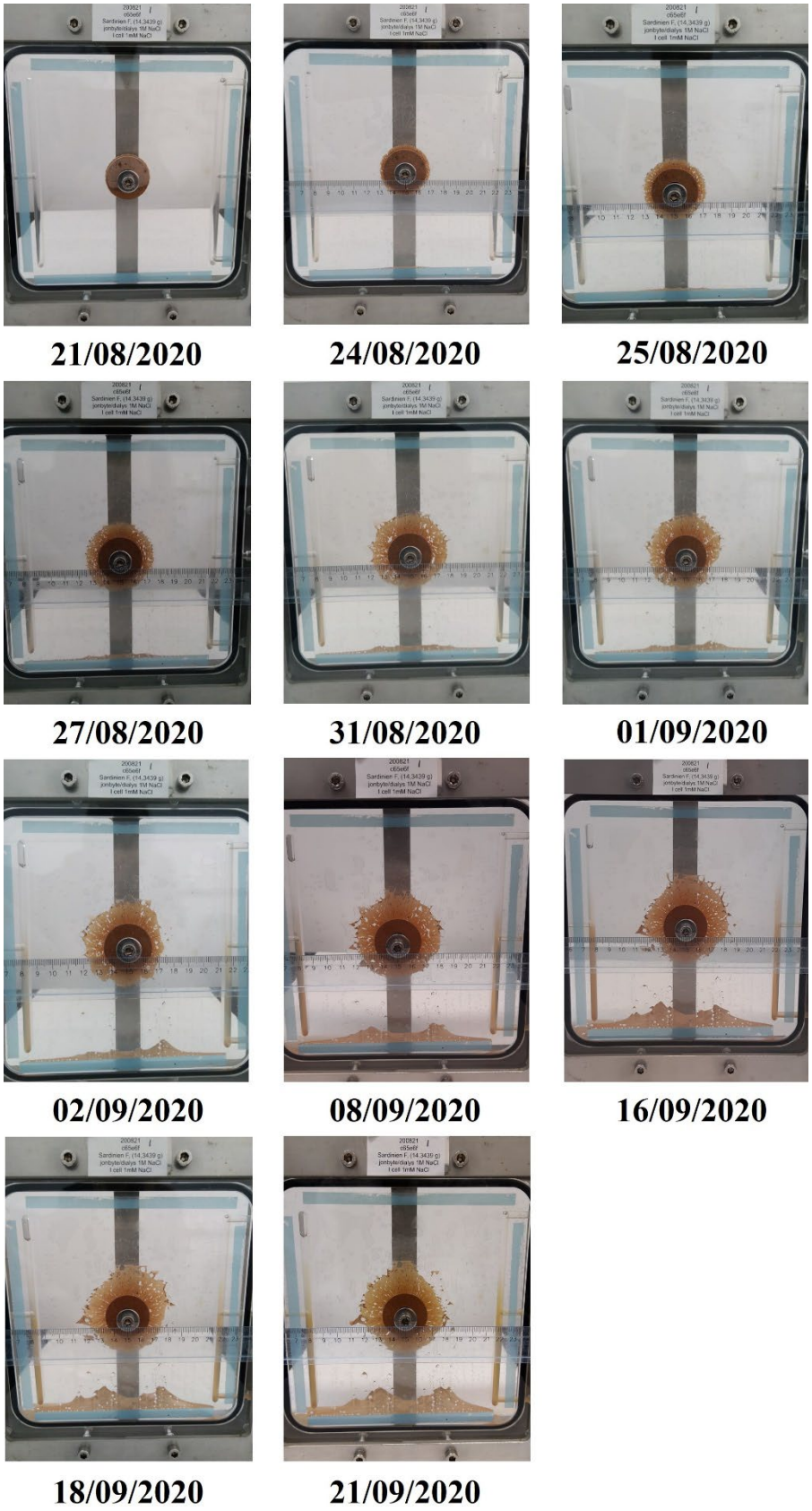

Figure A1- 31: *Sardinian (31 days).*

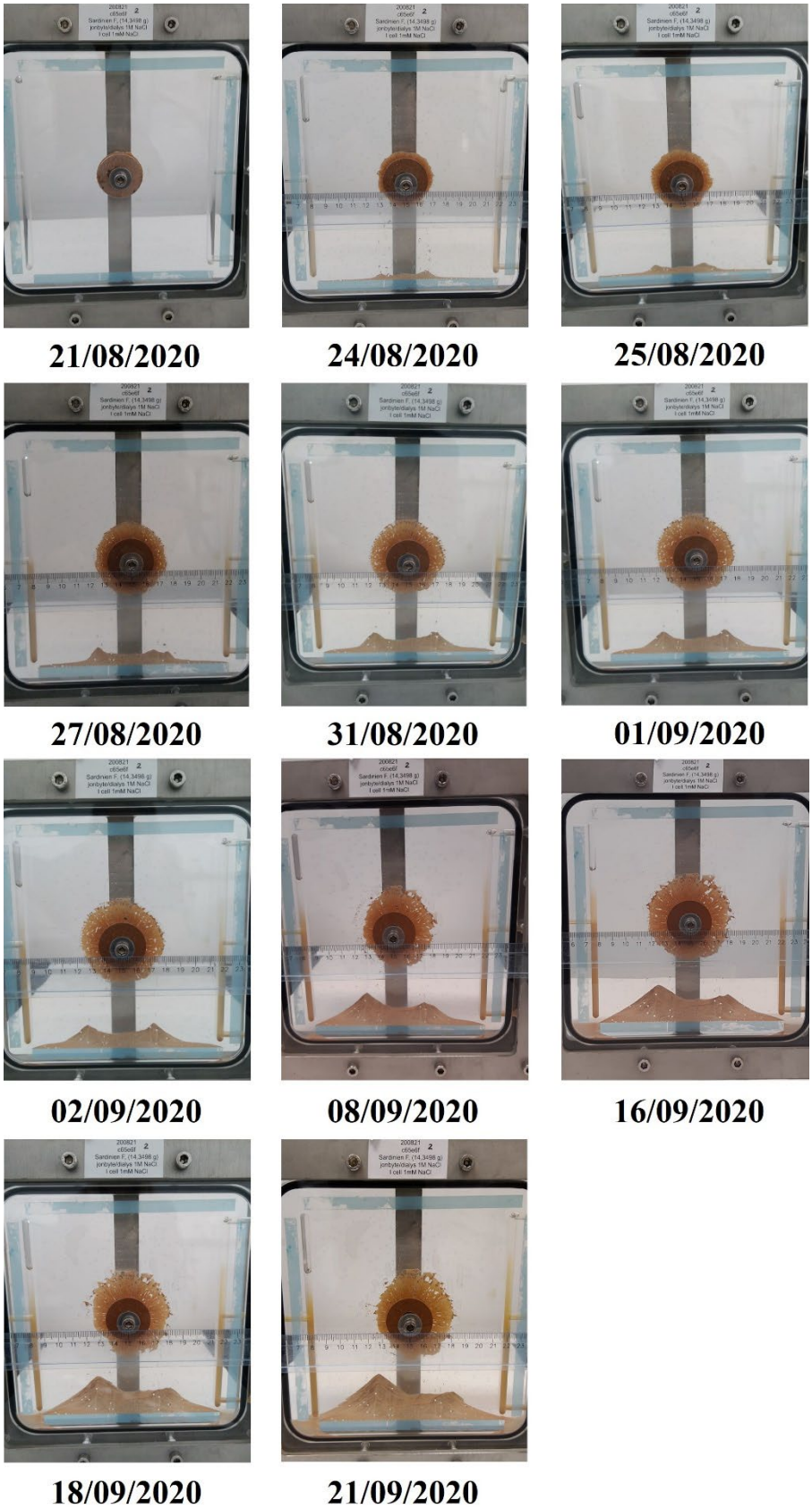

Figure A1- 32: *Sardinian (31 days).*

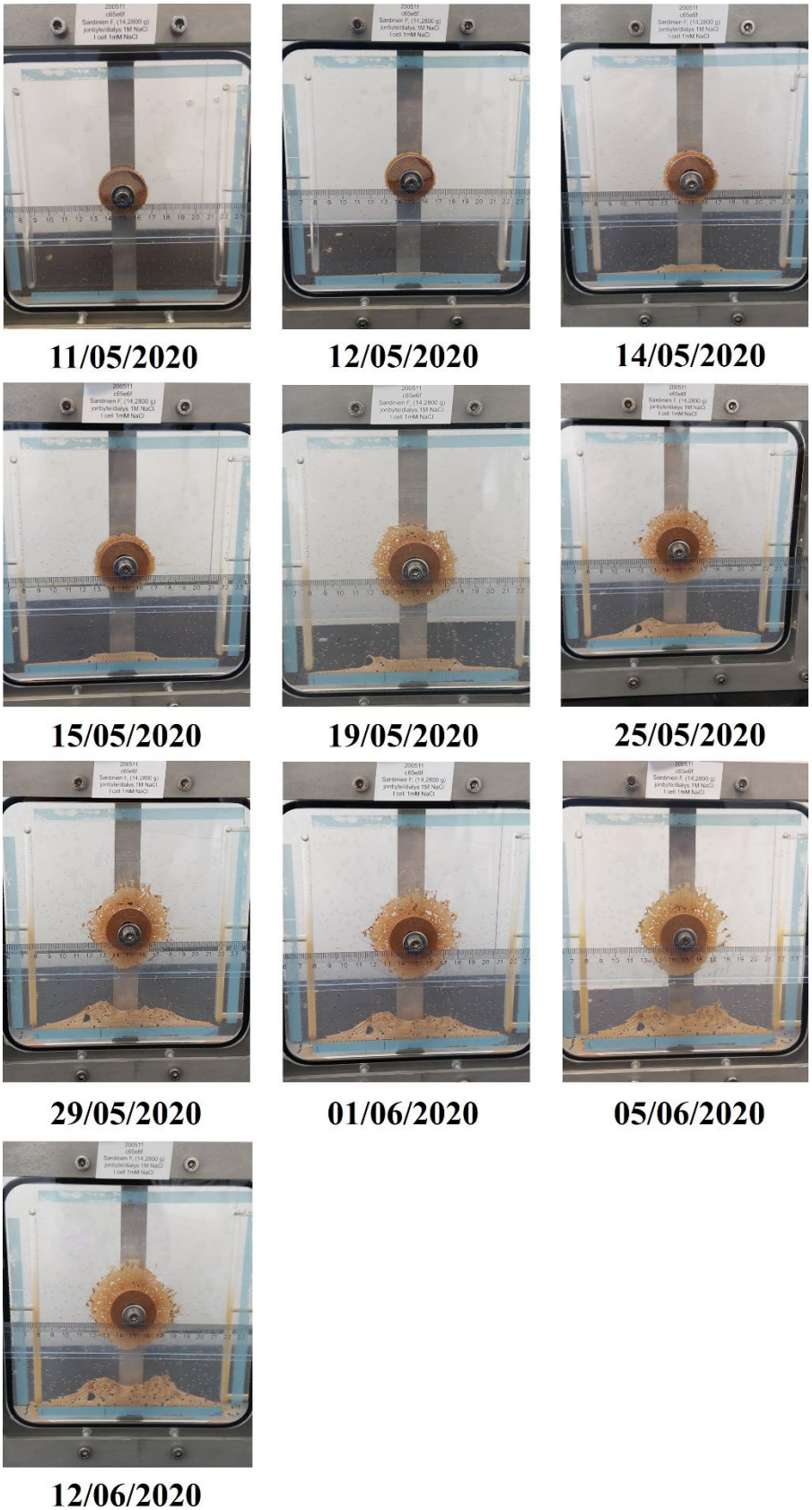

Figure A1- 33: *Sardinian (32 days).*

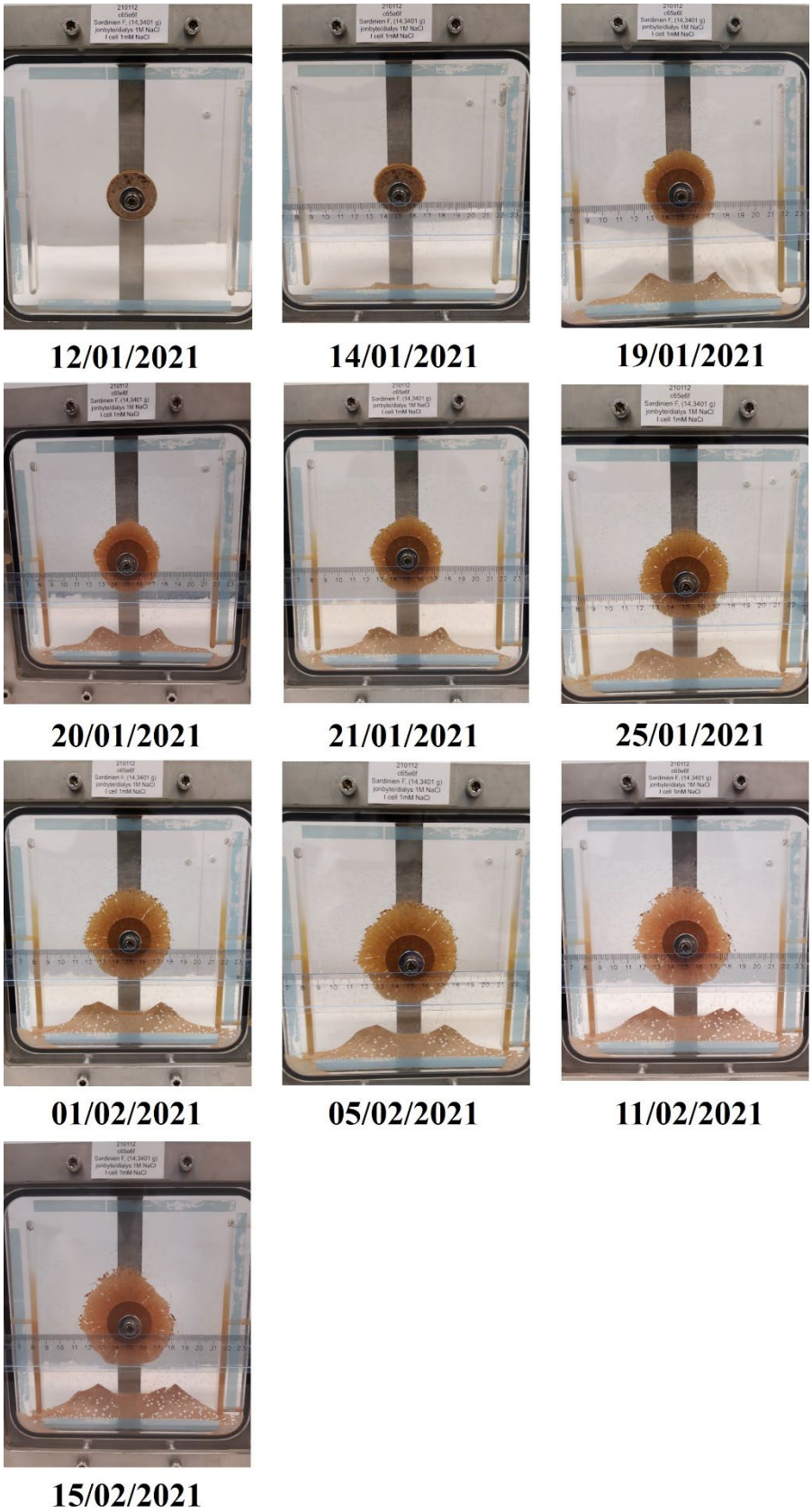

Figure A1- 34: *Sardinian (34 days).*

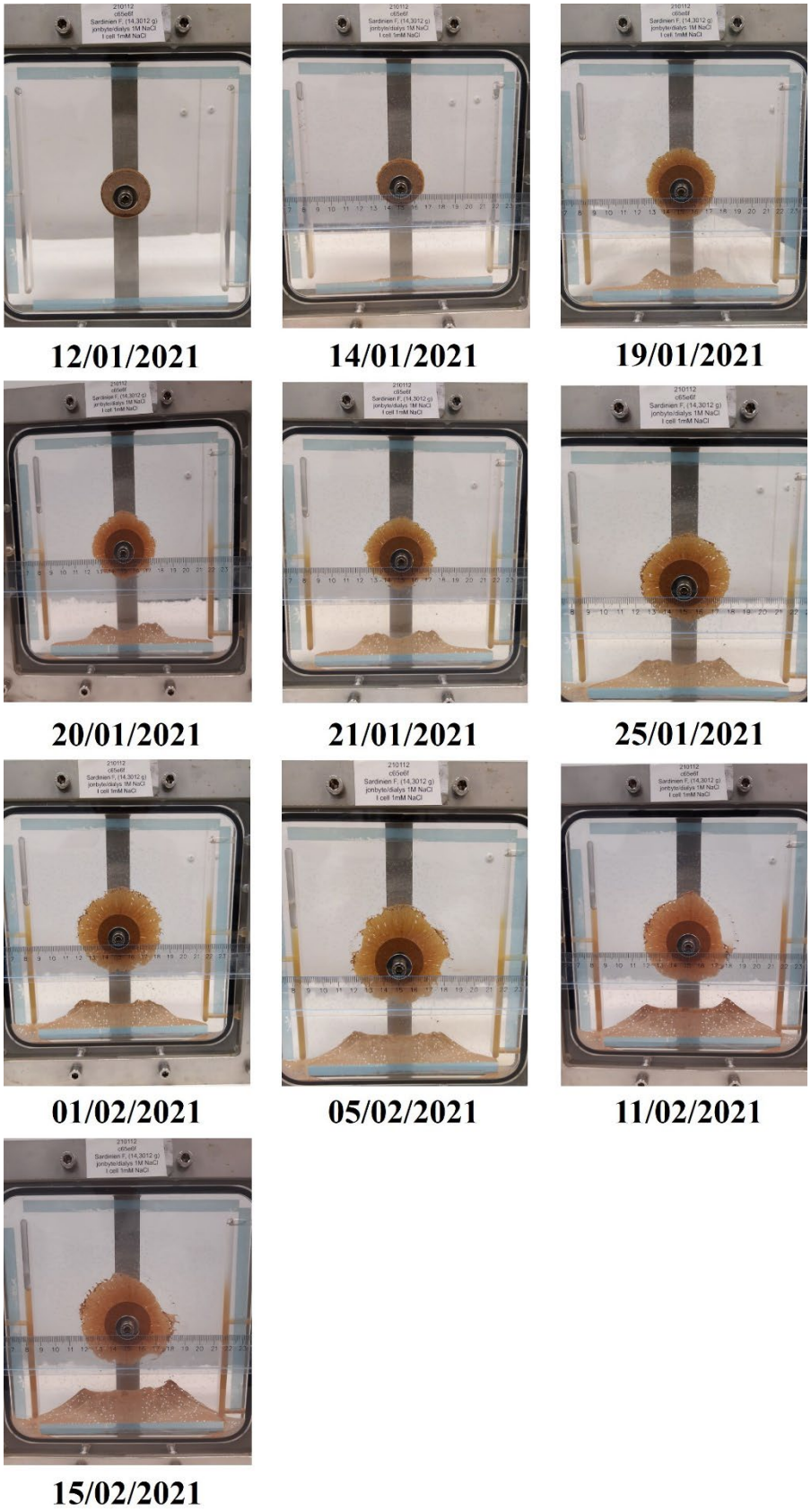

Figure A1- 35: *Sardinian (34 days).*

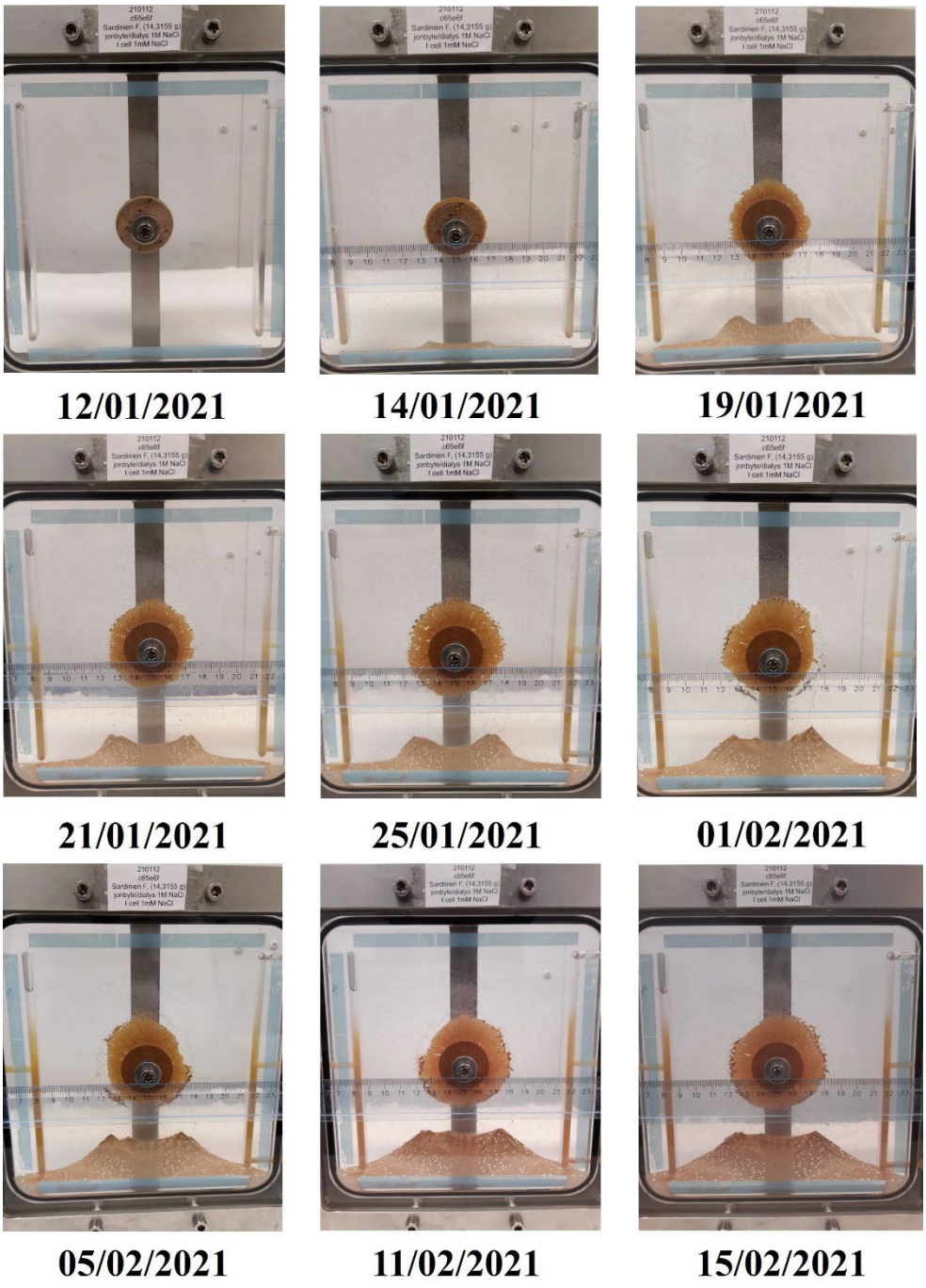

Figure A1- 36: *Sardinian (34 days).*

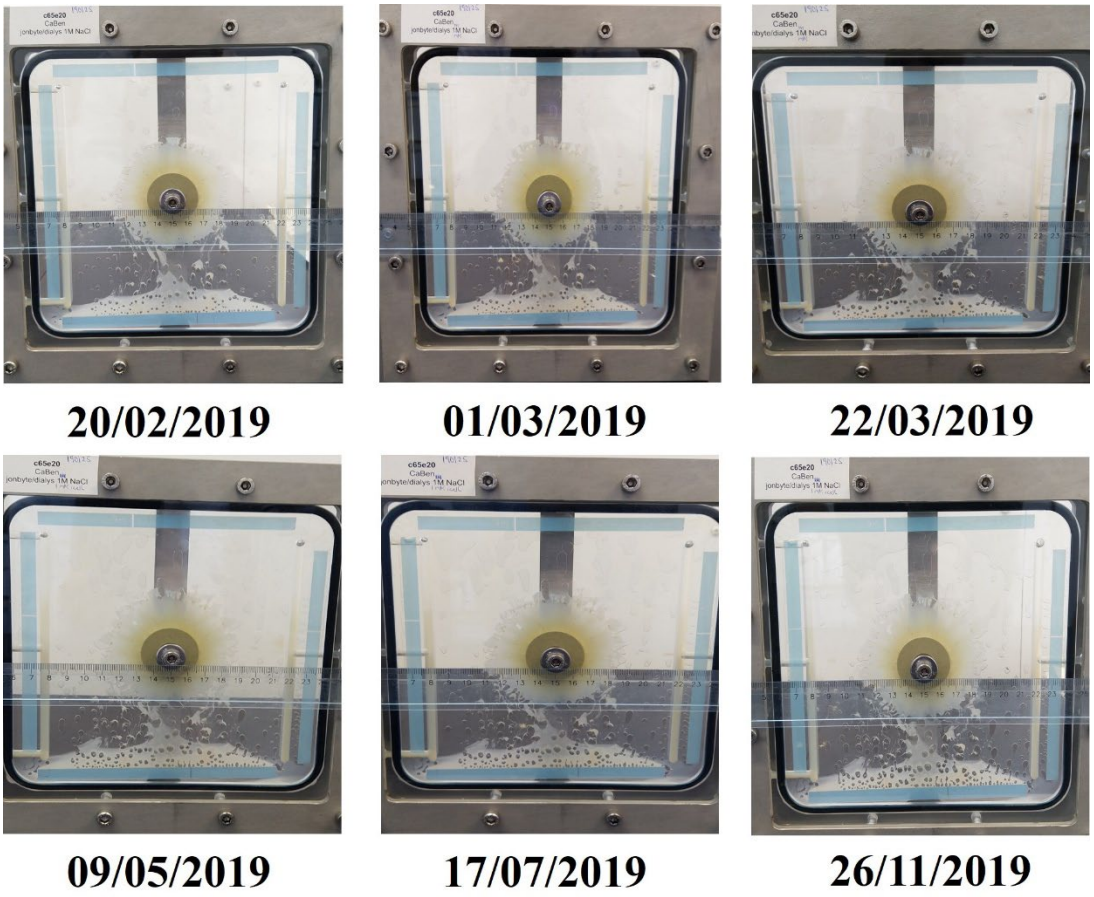

Figure A1- 37: *CaBen FLB (279 days).*

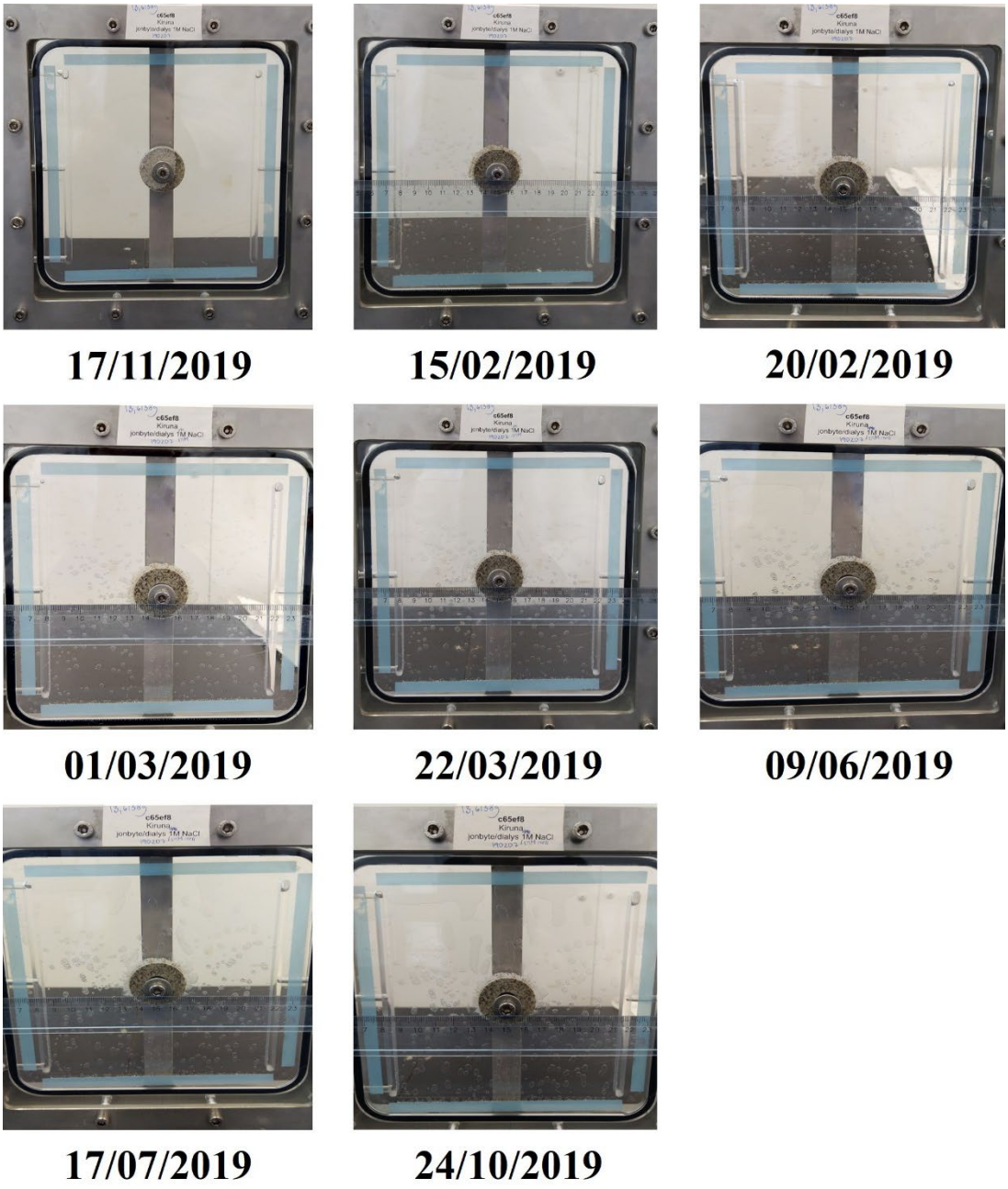

Figure A1- 38: *Kiruna (259 days).*

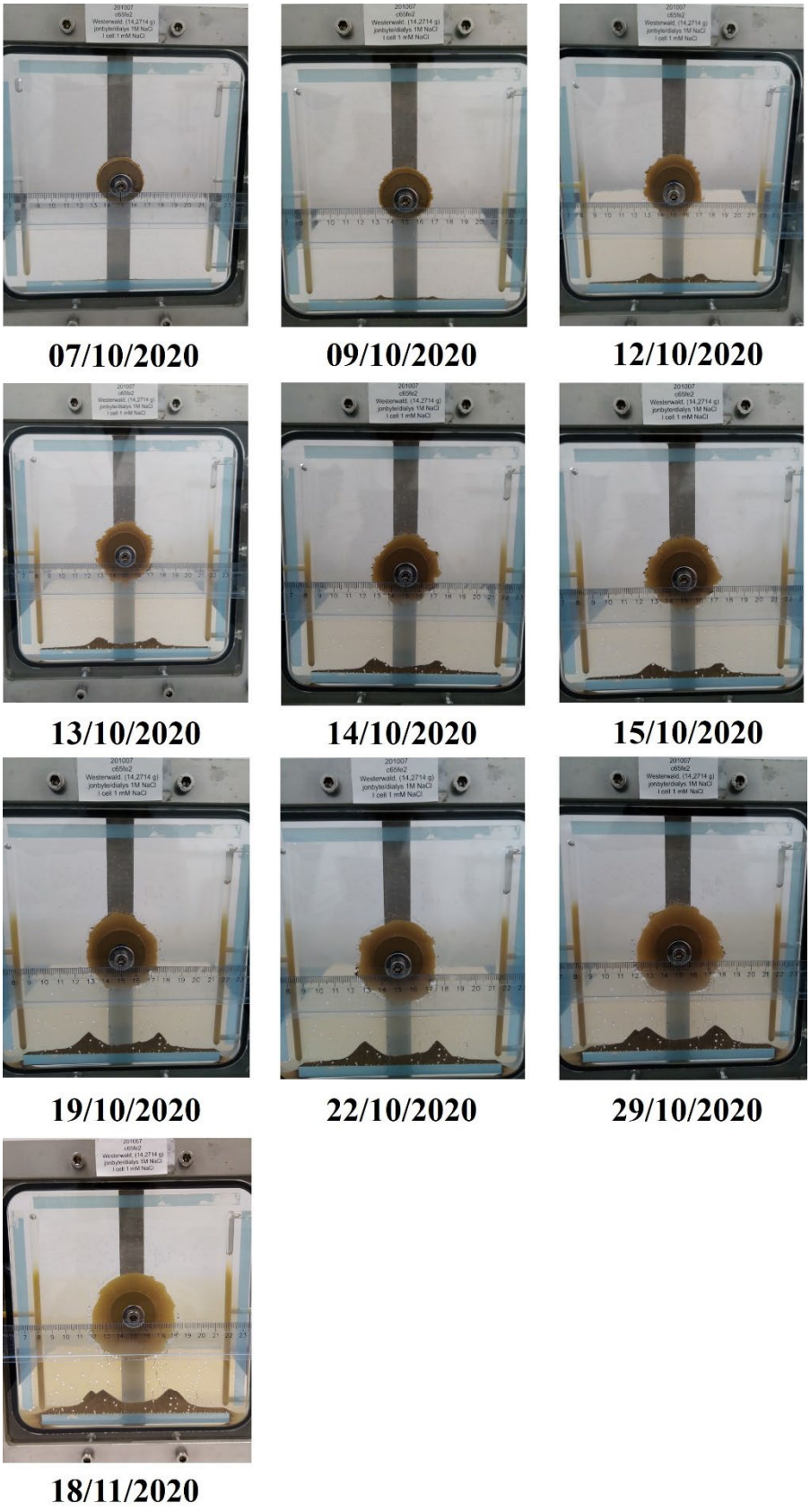

Figure A1- 39: *Westerwald (42 days).*

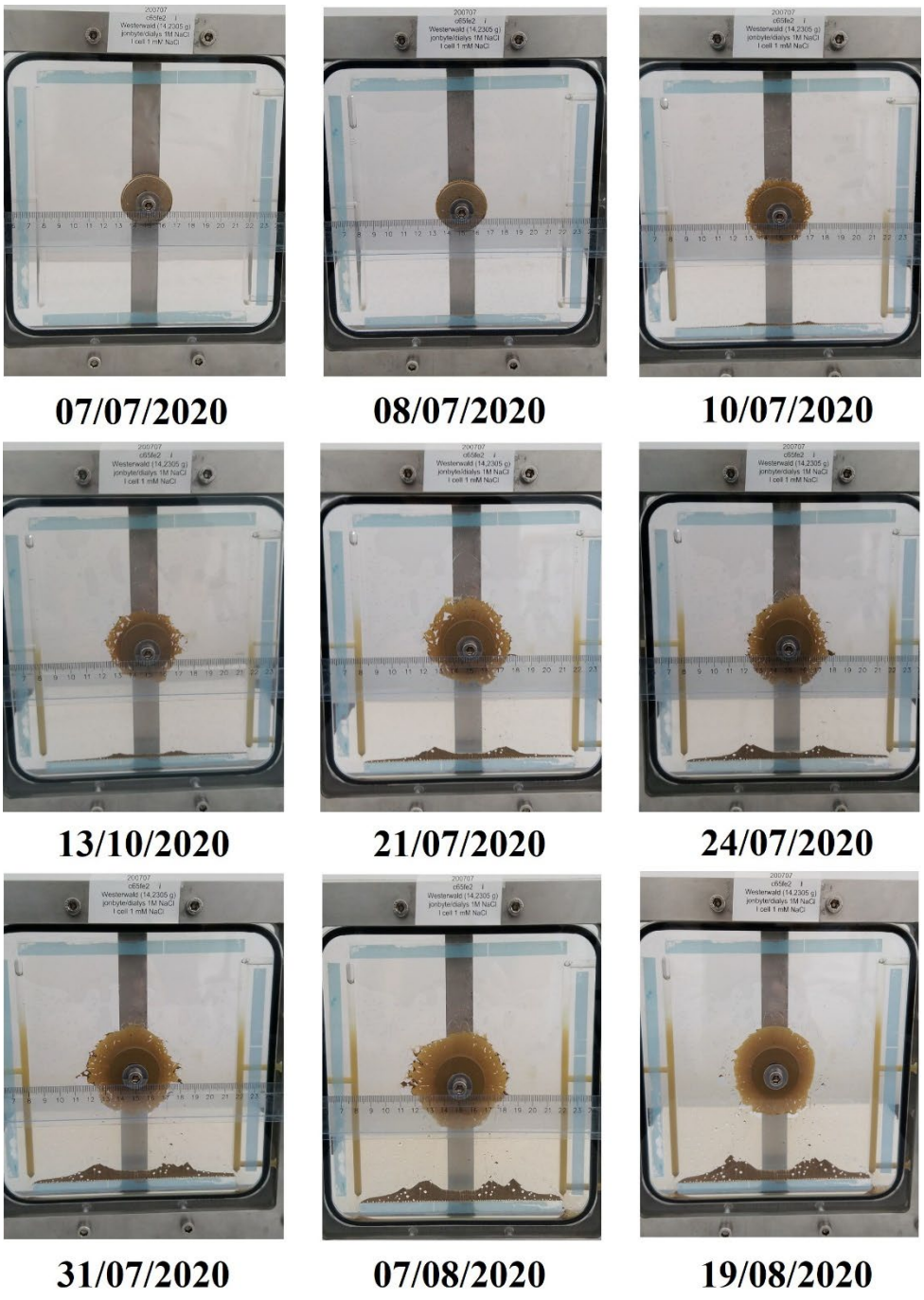

Figure A1- 40: *Westerwald (43 days).*

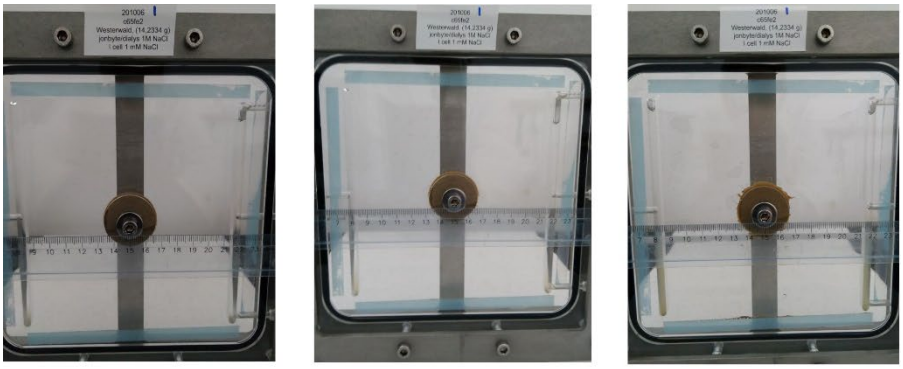

06/10/2020 08/10/2020 09/10/2020

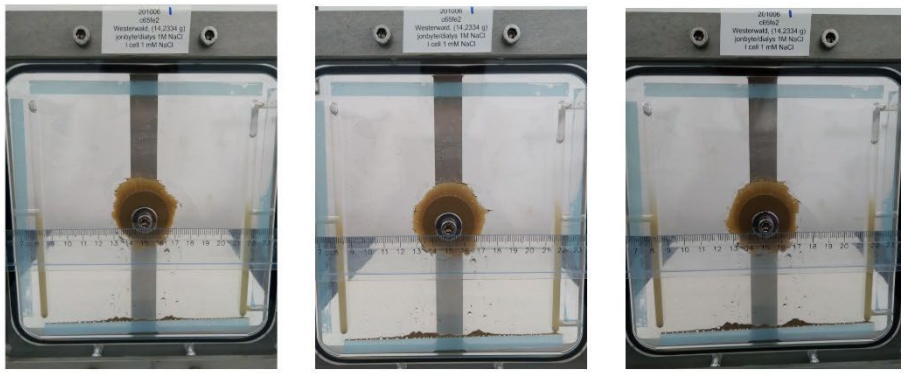

12/10/2020 13/10/2020 14/10/2020

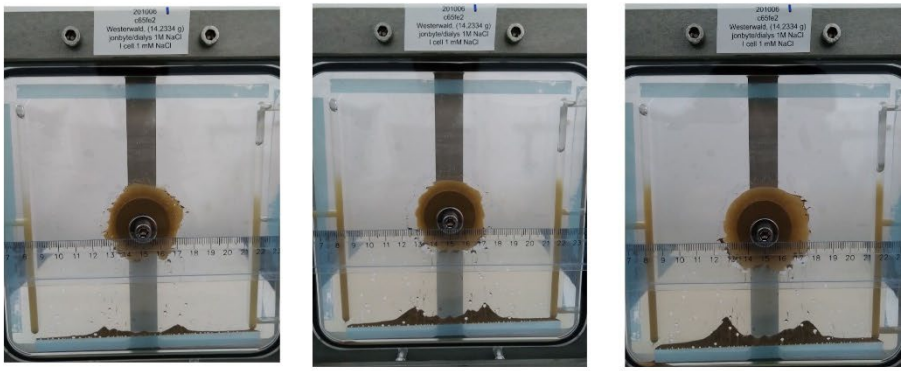

15/10/2020 19/10/2020 29/10/2020

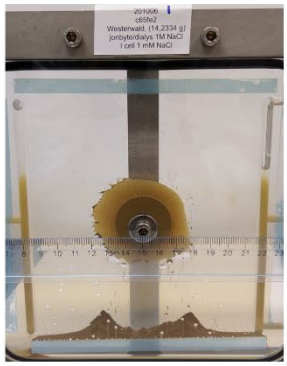

18/11/2020

Figure A1- 41: *Westerwald (43 days).*

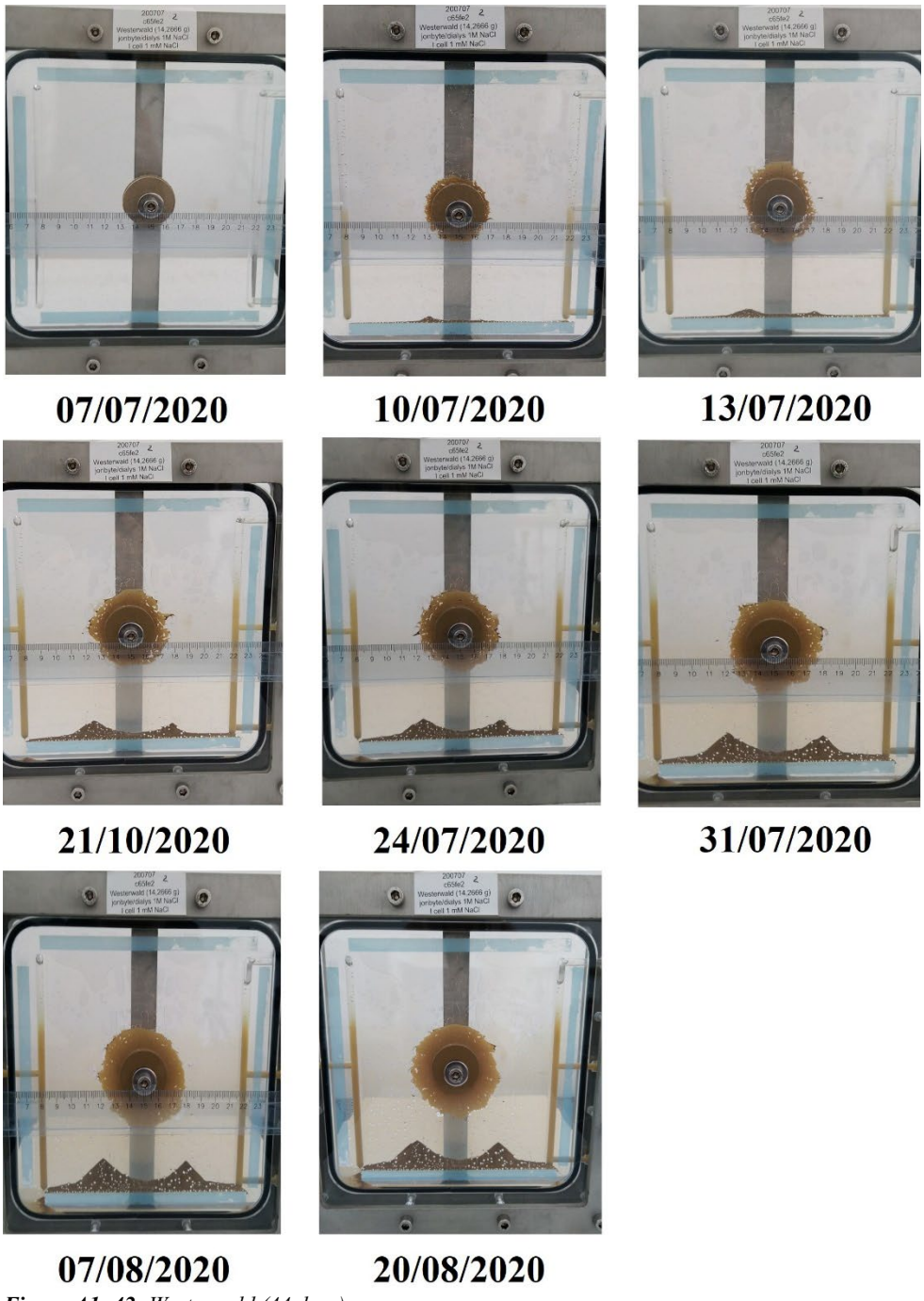

Figure A1- 42: *Westerwald (44 days).*

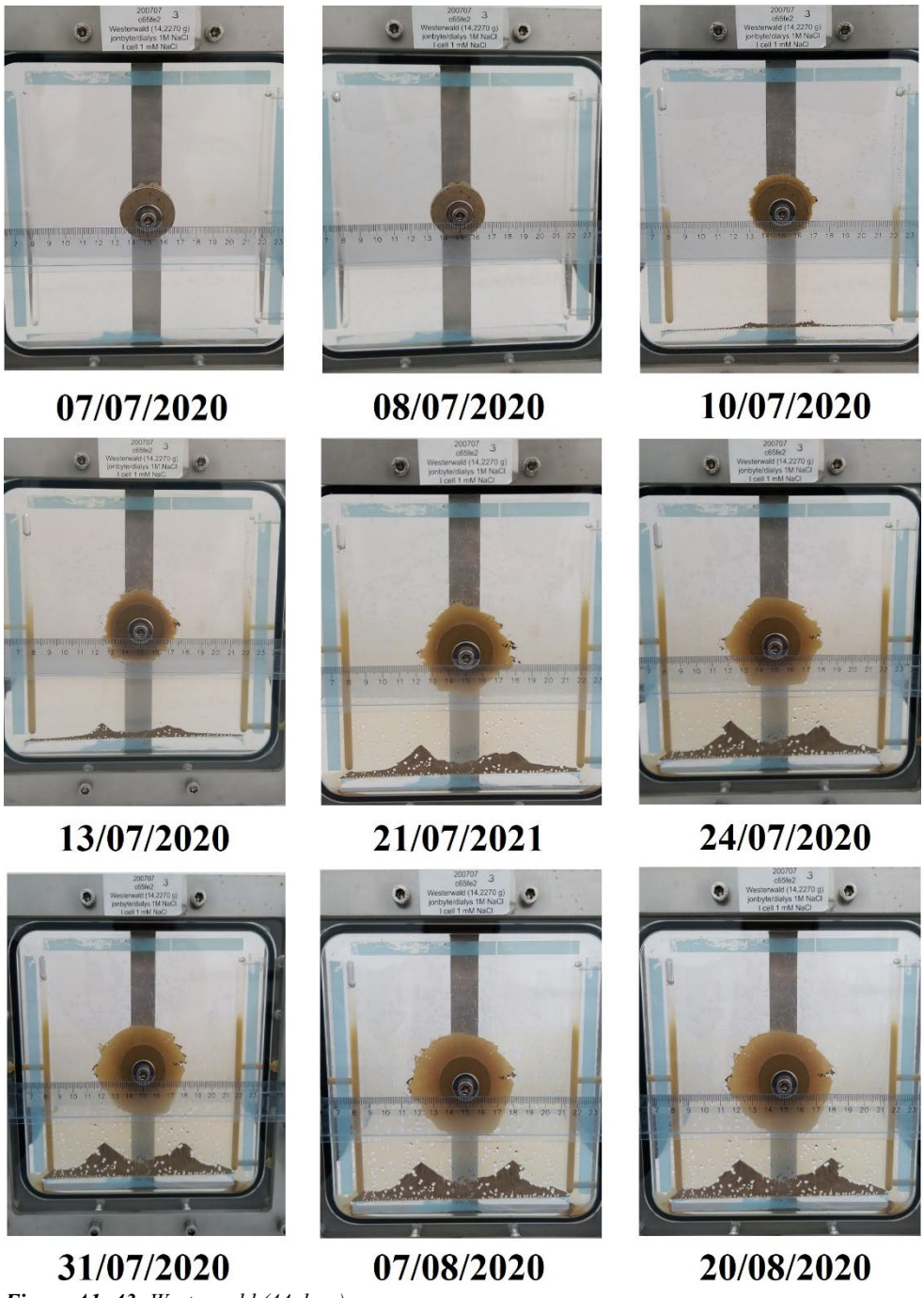

Figure A1- 43: *Westerwald (44 days).*